Bangor University

DOCTOR OF PHILOSOPHY

Signal processing for pulse-height spectroscopy

Thomas, Philip

Award date:
2019

Awarding institution:
Bangor University

[Link to publication](#)

SIGNAL PROCESSING FOR PULSE-HEIGHT SPECTROSCOPY

by

Philip Glyn Thomas

Thesis presented to the University of Wales
for the Degree of Doctor of Philosophy

October 1994
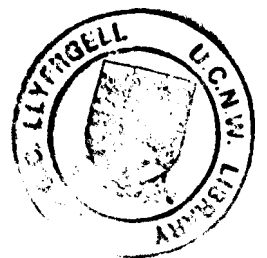
SIGNAL PROCESSING FOR PULSE-HEIGHT SPECTROSCOPY

P.G.Thomas

SUMMARY

The theory of analogue pulse shaping for nuclear pulse-height spectroscopy is reviewed, with the emphasis on time-variant filtering and the so-called 'Harwell' (or 'Kandiah') processor. An enhanced analogue pulse processor design, based on the same principle, is presented. The new design offers greater versatility and computer control. The application of digital signal processing to this field is reviewed and the design of a real-time digital pulse processor is developed. Noise index calculations for FIR digital filters are presented.

ACKNOWLEDGEMENTS

---

[1] AEA Technology is the trading name of the United Kingdom Atomic Energy Authority.

CONTENTS

CHAPTER 8 : A DIGITAL PULSE PROCESSOR

CHAPTER 1 : NUCLEAR RADIATION SPECTROSCOPY

1.1 : INTRODUCTION

Gamma ray spectroscopy is a technique that can be used to identify a radioactive isotope from the energies and intensities of the gamma rays that the isotope emits whilst undergoing radioactive decay. Such a signature can be used to determine the quantity and composition of radioactive material in a non-invasive way. This technique is widely used to quantify radioactive waste prior to disposal.

1.2 : INTERACTION OF GAMMA RAYS

Gamma rays belong to the family of ionising radiations produced by radioactive material; other members include X-rays, fast electrons, heavy charged particles and neutrons.

Gamma rays, like X-rays, are electromagnetic radiations and carry no charge. Gamma rays are generated when excited nuclei undergo transitions to lower energy states. X-rays are produced when excited orbital electrons fall to lower energy levels.

Electromagnetic radiations transfer their energy to the detection medium in one of three ways: The *photoelectric effect* occurs when an incoming photon transfers all of its energy to a detector atom. An electron is ejected, carrying all of the incident energy, minus its binding energy. This mechanism is predominant at incident energies up to several hundred KeV in materials with a high atomic number Z. (A high atomic number increases the probability of interaction.) At energies of several MeV, *pair production* becomes the dominant mechanism. The photon completely disappears, generating an electron-positron pair. These particles carry any energy excess to their creation in the form of kinetic energy. Again, high Z material is needed . At intermediate energies of several hundred KeV to several MeV, or in low Z material, *Compton scattering* occurs. Here, the photon collides with a detector electron, transfers part of its energy to the electron and is deflected through a scattering angle. The energy transferred to the electron can vary from almost nothing to a large fraction of the incident photon's energy. This gives rise to a continuum in the spectrum, as opposed to the monoenergetic peak generated by the photoelectric effect. It is obvious that the photoelectric effect is the desired mechanism for use in spectroscopy.

1.3 : SEMICONDUCTOR DIODES AS GAMMA-RAY DETECTORS

A semiconductor is an useful detection medium because it has a low ionisation energy that is fairly constant over a wide energy range. The number of carriers generated is much greater than in other materials, and the statistical fluctuation in this number is therefore lower as a fraction of the total. The variance is given by $F \times n$, where n is the mean number of carriers generated and F is the Fano factor, a correction introduced because the creation of each ion pair does not have constant probability, that is, the formation of individual charge carriers are not independent and a Poisson distribution does not apply. Fano factors ranging from 0.05 to 0.15 have been reported[1] for semiconductors. The large number of carriers generated also produces a stronger signal to compete with the system's electronic noise.

Semiconductor detectors are formed as reverse biased diodes. The depletion region becomes the active volume. In this arrangement, the steady state current flowing is low; only the minority carriers are assisted across the reverse biased junction plus any thermally generated electron-hole pairs. The carriers generated by the interaction of a photon with atoms in the depletion region are swept to the electrodes by the bias voltage.

A large active volume requires semiconductor material of high resistivity (i.e. low impurity concentration), so that a wide depletion region is created. Only Silicon and Germanium are generally available in such purity.

Germanium is the material used for gamma-ray detection. Its higher Z (32) makes interaction with the energies of gamma-rays more likely. It is also now available in hyper-pure form, and HPGe detectors are now prevalent in gamma-ray spectroscopy. A hyper-pure wafer of Ge with p+ and n+ contacts diffused into the upper and lower surfaces forms a diode which, under the influence of a large reverse bias, forms a detector with an active volume large enough to have good gamma-ray detection efficiency. In older detectors, Lithium ions were drifted into the naturally p-type Ge to form a compensated region of high resistivity. The main disadvantage of Ge is that its low energy gap ensures that the thermally generated leakage current is too high at room temperature, and cooling to liquid nitrogen temperature is always necessary.

Charge collection is not particularly fast, and is determined by the saturation drift velocity of electrons and holes (10^5 m/s at 77°K), if the electric field across the depletion region is high enough (10^5 V/m for electrons or 3×10^5 V/m for holes). At

2

this velocity, a charge generated 1cm from the electrode takes 100ns to reach that electrode. Large reverse bias voltages have to be applied to semi-conductor detectors to ensure that the saturation velocity is attained. (Large Germanium crystals often need up to 4000V of reverse bias.)

The charge collection time is dependent on the location of the photon interaction within the active volume. Electron-hole pairs generated mid-way between the electrodes will take less time to collect than ones generated close to an electrode (where one carrier has to travel the full distance between the electrodes). Signal charge can become trapped at trapping centres within the active volume; the subsequent de-trapping by thermal excitation has a slow component that also contributes to variable rise-time. Even longer rise-times can be caused by charge generated in regions where the electric field is weaker.

1.4 : PRE-AMPLIFIER NOISE

The signal from a semi-conductor detector needs to be conditioned by a low-noise pre-amplifier, located as close as possible to the detector, before it can be sent any distance to the electronic units that extract the information from that signal. The detector and pre-amplifier assembly is often referred to as the spectrometer.

The input amplifying device universally used is a low-noise field effect transistor. Its gain is assumed to be high enough to make the noise contributions of other components in the pre-amplifier negligible when referred to the input. Figure 1.4.1 shows the noise sources associated with the detector and the input FET.
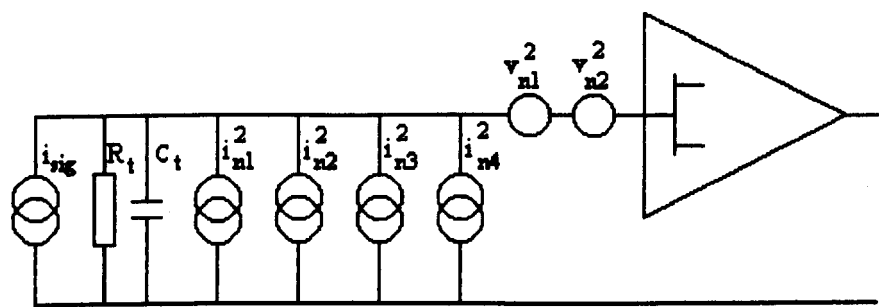
Fig 1.4.1

Resistance R_t represents the total shunt resistance at the amplifier input; the detector load resistor, through which the bias is applied, is the main component.

Capacitance C_t is the total shunt capacitance; it includes the detector capacitance C_d, the FET input capacitance C_i and any other strays.

Voltage noise generator v_{n1}^2 represents the flicker or $\frac{1}{f}$ noise component; it is usually ignored in analysis because its contribution cannot be influenced greatly by the choice of shaping.

$$v_{n1}^2 = \frac{A_f}{f} df \qquad (1.4.1)$$

The second voltage noise generator v_{n2}^2, represents the thermal noise generated in the FET channel. It can be shown[2,3] to be given by the expression:

$$v_{n2}^2 = \frac{4kTQ(Z)df}{gm} \qquad (1.4.2)$$

where k is Boltzmann's constant, T is the temperature, gm is the transconductance of the FET and Q(Z) is a function of gate bias and is typically between 0.60 and 0.67.

Current noise generators i_{n1}^2 and i_{n2}^2 represent the shot noise generated by the detector leakage current and the FET gate-source leakage current. The noise generated is given by:

$$i_{n1}^2 = 2qI_d df \qquad (1.4.3)$$

$$i_{n2}^2 = 2qI_{gs} df \qquad (1.4.4)$$

A third current noise source is the thermal noise associated with the shunt resistor. It is given by:

$$i_{n3}^2 = \frac{4kTdf}{R_t} \qquad (1.4.5)$$

Current noise generator i_{n4}^2 represents the coupling through the gate-source capacitance of some of the channel noise. It can be shown[4] to be:

$$i_{n4}^2 = \frac{4kTW^2C_{gs}^2F(Z)df}{gm} \qquad (1.4.6)$$

where F(Z) is another function of the gate bias, and $W = 2\pi f$. Typically F(Z) lies between 0.20 and 0.27.

The current noise generators collectively form a parallel noise generator. Alternatively, this can be labelled a step noise source, as the noise impulses are integrated by the input capacitance, and appear as noise steps at the output. Similarly, v_{n1}^2 and v_{n2}^2 can be combined into a series noise generator or a delta noise source because these input noise impulses also appear as output noise impulses. The simplified schematic is shown in Figure 1.4.2; the series voltage noise generator is shown as an equivalent current noise generator.
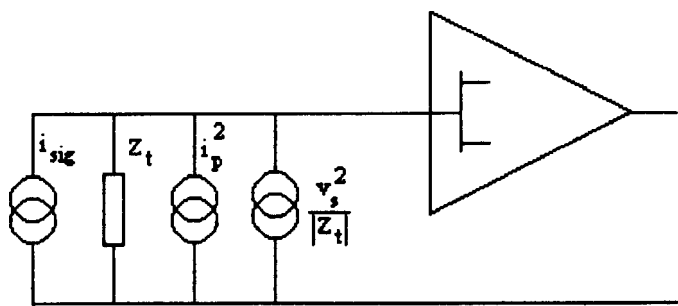
Fig 1.4.2

It is obvious that the signal to parallel noise ratio is independent of Z_t, but signal to series noise ratio will improve if Z_t is made large (i.e., R_t needs to be as large as possible and C_t needs to be as small as possible). The requirement of small C_t is the main reason for locating the pre-amplifier as close as possible to the detector, and is another reason for favouring a large reverse bias on the diode.

The effect of a fluctuating bias on the capacitance of the detector would make pulse-height spectroscopy difficult if the pre-amplifier was voltage sensitive. The voltage step produced would be proportional to the instantaneous capacitance. For this reason, a charge-sensitive configuration is always used. The feedback element is a small capacitance C_f. The Miller effect adds a capacitance of $(1+A)C_f$ in parallel with the detector capacitance and, if A is large, fluctuations in C_t will be swamped. The signal to series noise ratio need not suffer if $C_t \ll C_d + C_i$ and Z_t is not reduced significantly.
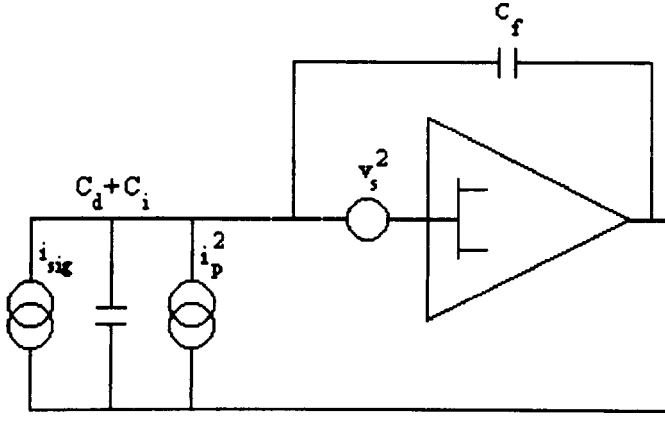
Fig 1.4.3

Figure 1.4.3 shows the charge amplifier configuration. The shunt resistance has been neglected, as its impedance is much greater than the impedance of the shunt capacitance at the frequencies of interest.

The noise at the output of the charge-amplifier can be seen to have the following components:

$$v_{no}^2 = v_s^2 \frac{(C_d + C_i + C_f)^2}{C_f^2} + \frac{i_p^2}{W^2 C_f^2} \qquad (1.4.7)$$

$$v_{no}^2 = \frac{2}{3} \frac{4kTdf}{gm} \frac{C_t^2}{C_f^2} + \frac{A_f df}{f} \frac{C_t^2}{C_f^2} + \frac{kTW^2 C_{gs}^2 df}{gmW^2 C_f^2} + \left(2qI_d + 2qI_{gs} + \frac{4kT}{R_t}\right) \frac{df}{W^2 C_f^2} \qquad (1.4.8)$$

This equation has the form:

$$\frac{v_{no}^2}{dW} = a^2 + \frac{b^2}{W^2} + \frac{c^2}{W} \qquad (1.4.9)$$

This is a description of the spectral density of the noise generated by a detector/charge amplifier. A noise corner is defined where the contribution of the a and b components are equal:

$$T_{nc} = \frac{1}{W_{nc}} = \frac{a}{b} \qquad (1.4.10)$$

1.5 : PRE-AMPLIFIER RESET MECHANISMS

A charge amplifier needs to be reset otherwise the charge will continue to be integrated until the amplifier saturates. The simplest method uses a feedback resistor R_f in parallel with the feedback capacitor C_f. The signal steps then decay with a time constant $C_f R_f$. A large valued resistor (typically $10^9 \Omega$) is needed to avoid adding excess parallel noise, and the time constant will usually be greater than $50\mu s$. This method is not suitable for the highest resolution work[5], because the resistor adds stray capacitance and adds significant parallel noise at higher frequencies, where its resistance can be much lower than at dc. The high frequency behaviour of high valued resistors can also make pole-zero compensation difficult. The method is also not ideal for the highest rates, as the charge-amplifier will eventually saturate due to the piling up of the pulse tails.

The problems associated with passive restoration can be overcome with pulsed reset techniques, where current of opposite polarity to the signal current is injected into the input whenever a reset is needed. The established pulsed reset methods are based on optical reset[6] or transistor reset[7] techniques.

Fig 1.5.1a

i_s = signal current
i_r = reset current

Fig 1.5.1b

7
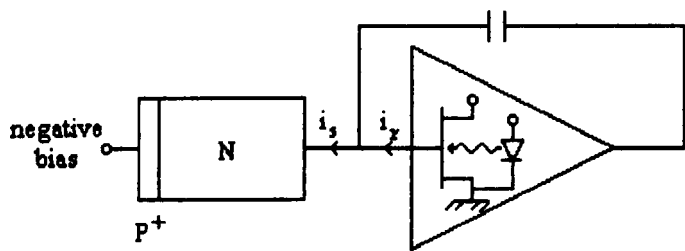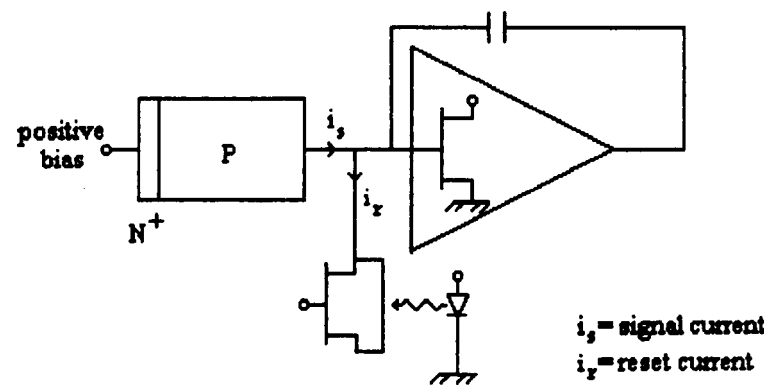
In the optical reset method, an LED is switched on, and it shines into the drain-gate diode of a FET. This diode is light-sensitive and an increased gate current flows. Figures 1.5.1a and 1.5.1b show the arrangement for n-type and p-type crystals.
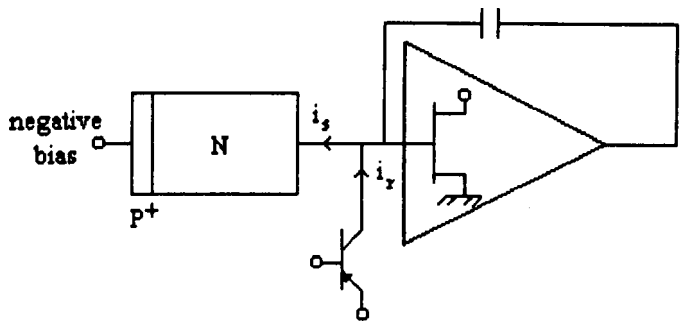
Fig 1.5.2a
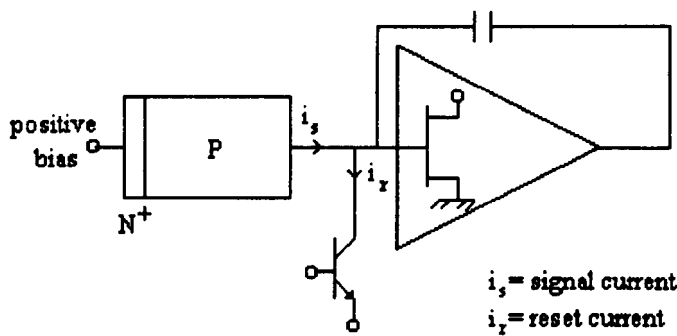
i_s = signal current
i_r = reset current

Fig 1.5.2b

Transistor reset involves forward biasing a transistor of appropriate polarity; its collector supplies the required current. Figures 1.5.2a and 1.5.2b show the two arrangements.

It should be noted that in the methods shown in figures 1.5.1b, 1.5.2a and 1.5.2b, significant input capacitance is added by the device supplying the reset current, and the noise performance may be degraded. (There are other, more exotic methods of pulsing a reset that makes use of special input devices that have injector diodes fabricated into the FET structure[8,9]. These methods minimise the extra input capacitance.)

The reset pulse can occur immediately after the signal pulse has been processed (pulse by pulse restore), or after a number of signal pulses have arrived and the charge-

amplifier is nearing saturation (limit restore). Because the detector leakage current is also integrated, pulsed reset systems also have to fire periodically to restore this charge.

1.6 : SPECTROSCOPY ELECTRONICS

The output of the spectrometer is processed by a number of electronic modules. A typical system might comprise a linear amplifier, an analogue-to-digital converter (ADC) and a multi-channel analyser (MCA) or single-channel analysers (SCA).

The function of the linear amplifier is developed in Chapter 2; it serves to amplify, filter and shape the spectrometer signal into a pulse suitable for use by the ADC.

The ADC converts the pulse height into a digital code that can be used by the MCA or SCA. An ADC resolution of at least 12bits is required to take advantage of the inherently good resolution of semi-conductor detectors. The conversion time of the ADC imposes a dead-time on the system which needs to be minimised if high throughput is a requirement.

Several types of ADCs have been used in spectroscopy electronics. The *linear ramp converter* (also known as the Wilkinson ADC) compares the input pulse amplitude with a linear ramp voltage, generated by charging a capacitor from a constant current source. During the time that the input pulse amplitude exceeds the ramp voltage, a linear gate is open, allowing high frequency clock pulses to be counted. The final count is proportional to the input pulse amplitude. Such an ADC is inherently linear but the conversion time is relatively long and is proportional to the input pulse height. *Successive approximation* and *flash* ADCs have also been used. These standard ADC techniques can offer faster fixed conversion times (1μs for 12bits) but the relatively poor differential linearity causes problems. For example, a differential non-linearity of ±½LSB means that some channels may be three times the width of others. Therefore, these ADCs are used with a linearity correction scheme such as the sliding scale principle proposed by Gatti[10]. Most of these ADCs include a peak stretcher circuit that holds the peak height of the input pulse constant for the duration of the conversion time.

In essence, a multi-channel analyser is a histogram memory. The ADC's output addresses one memory location, which then has its contents incremented by one. The

MCA's output, at the end of an acquisition time, is a histogram of the pulse amplitude distribution measured during that time. Often, the MCA will have a built-in ADC.

CHAPTER 2 : PULSE SHAPING

2.1 : INTRODUCTION

The charge amplifier in a spectroscopy system is followed by a 'pulse processor' that conditions the signal from the detector, making it suitable for input into a multi-channel analyser (MCA). The detector signal is amplified and shaped by the pulse processor. Amplification is relatively straight-forward; the main requirements are high linearity and , often, large dynamic range (see Section 4.9). Pulse shaping is a more complex consideration. A pulse-shaping arrangement must take into account its effect on resolution, the suitability of the pulse shape as an input into an MCA, and the ease of practical implementation of such a shaping circuitry.

Monoenergetic gamma-ray photons, on interacting with a detector system, generate a dispersion in the measured energy; a so-called monoenergetic peak will have a Gaussian distribution. The resolution of a particular system can be defined as the width of this Gaussian peak at half its maximum amplitude (Full Width Half Maximum or FWHM). This measure of resolution can be related to the noise V_n imposed on the average input voltage V in the following way:

$$\frac{E_{FWHM}}{E} = 2.36 \times \frac{V_n}{V} \tag{2.1.1}$$

where E is the energy of the photon in eV, and the FWHM is measured in eV.

Another measure of resolution is the 'equivalent noise charge' (ENC). This is the hypothetical charge, released in the detector, that would give an output pulse equivalent to V_n in amplitude. If a photon of energy E liberates a charge Q, then:

$$\frac{ENC}{Q} = \frac{V_n}{V}$$

$$ENC = \frac{Q \times E_{FWHM}}{E \times 2.36}$$

$$ENC = \frac{E_{FWHM}}{2.36 \times w} \tag{2.1.2}$$

where w is the eV/ion-pair measure of the ionisation energy, and ENC is measured in number of electrons.

The resolution is degraded by detector noise, electronic noise, pulse pile-up and ballistic deficit. An equivalent variance can be derived for all of these mechanisms and the overall variance is the sum of all of these individual contributions.

Detector noise has already been discussed; it is inherent in the charge generation mechanism. The variance of this noise source is given by:

$$\delta_d = \sqrt{F \times n} \times w$$

$$\delta_d^2 = FEw \qquad\qquad\qquad (2.1.3)$$

where F is the Fano Factor and n is the mean number of ion-pairs generated (E/w). The choice of detector materials with low F and w is the only way of reducing this noise source.

Pile-up is caused by overlapping signals. The pulse processor will have a resolving time for dealing with each detector pulse, and a second event within this resolving time causes an error in the measured pulse height. Two types of pile-up exist. In the first type, a second event can occur before the pulse height of the first event has been measured; in this case the pulse heights of both pulses are corrupted and a special provision must be made during live-time counting (see Section 4.11). In the second type of pile-up, a second event occurs after the measurement of the first event, but before the end of the resolving time; only the second event is considered invalid.

Pile-up obviously becomes a dominant mechanism for resolution degradation as the count-rate increases. Even at modest input rates, it becomes necessary to use pile-up rejection techniques to identify pile-up conditions, and prevent the resulting pulses from contributing to the spectrum.

Ballistic deficit is a measure of the loss of pulse height for a real detector event compared to the same charge appearing as an infinitesimally short impulse. Unfortunately, these real detector current pulse widths will vary with the position of the photon interaction, and the loss of pulse height is not constant. The output waveform can be calculated from the convolution of the system's impulse response and the shape of the detector pulse. It is fairly obvious that if the impulse response is long compared to the detector pulse, then the output will approximate the output caused by an impulse. It is also clear that if the impulse response has a flat top of a duration

greater than the total duration of the detector pulse, then the peak output will be independent of detector pulse shape. It has been observed[11] that most output pulse shapes having a continuous derivative exhibit similar ballistic deficit performance, but that pulse shapes with discontinuous derivatives are significantly worse.

The other mechanism for resolution degradation is *electronic noise*. The pulse processor should be designed so that its electronic noise, referred to the input, is negligible compared to the electronic noise at the detector/charge-amplifier output. Shaping for electronic noise reduction is therefore an exercise in reducing the contributions from the white, $\frac{1}{f}$ and $\frac{1}{f^2}$ noise sources derived in Section 1.4. In fact, it is well known[12] that the contribution of the $\frac{1}{f}$ noise source cannot be reduced significantly by the choice of shaping; this noise is reduced by the choice of suitable components. Its value is low if a JFET is used as the amplifying device.

For a fixed pulse shape, the amplitude S of the output signal will be proportional to the pulse duration T_m, because the filter is acting upon the signal step for that time. It can be written that:

$$S^2 \propto T_m^2 \tag{2.1.4}$$

Noise impulses occur during T_m with a Poisson Distribution. From statistical considerations, the variance of the delta noise at the output is proportional to the mean number of impulses in T_m, i.e.

$$\delta_d^2 \propto T_m \tag{2.1.5}$$

Random noise steps also occur during T_m. The variance of the step noise is therefore proportional to the mean number of steps in T_m. But the amplitude of each step at the end of the measurement time is also proportional to T_m. Therefore:

$$\delta_s^2 \propto T_m^3 \tag{2.1.6}$$

From Equations 2.1.4 and 2.1.5, it can be seen that the signal-to-delta-noise ratio is proportional to the time scale of the output pulse. Equations 2.1.4 and 2.1.6 indicate that signal-to-step-noise ratio is inversely proportional to this time scale. The optimum shaping time would be that value where the contributions from delta and step noise generators were equal (i.e. the noise corner). In practice, this value has been increasing

as technological advances reduce leakage currents and the influence of step noise, and the ideal value, from a signal-to-noise ratio consideration, is too long from a pile-up point-of-view. The challenge is to develop shapers that limit the delta noise contribution at reasonably short shaping times, whilst still retaining good immunity to ballistic deficit.

2.2 : MATCHED FILTERS

It is useful to derive the optimum filter for noise reduction; this gives a standard that can be used to compare other filters.
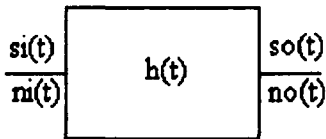
Fig 2.2.1

Figure 2.2.1 shows a linear system having an impulse response h(t). The optimum filter for noise reduction is that which maximises the signal to noise ratio at a specified measurement time.

$$SNR = \frac{s_o^2(t)}{E(n_o^2(t))} \qquad (2.2.1)$$

where E( ) is the expected value or mean. By convolution:

$$s_o(t) = \int_{-\infty}^{\infty} h(\beta) \times s_i(t - \beta)d\beta \qquad (2.2.2)$$

It can be shown[13] that the autocorrelation of the output noise is given by :

$$R_{no}(t_1, t_2) = \int_{-\infty}^{\infty} \int_{-\infty}^{\infty} R_{ni}(t_1 - \alpha, t_2 - \beta)h(\alpha)h^*(\beta)d\alpha d\beta$$

$$R_{no}(t, t) = \int_{-\infty}^{\infty} \int_{-\infty}^{\infty} R_{ni}(t - \alpha, t - \beta)h(\alpha)h^*(\beta)d\alpha d\beta \qquad (2.2.3)$$

If noise is stationary, its autocorrelation $R(\tau_1, \tau_2)$ depends only on τ, where $\tau = \tau_1 - \tau_2$, and the expression can be written $R(\tau)$.

$$R_{no}(t,t) = \int\limits_{-\infty}^{\infty}\int\limits_{-\infty}^{\infty} R_{ni}(\beta-\alpha)h(\alpha)h^{*}(\beta)d\alpha d\beta$$

but $\qquad R_{no}(t,t) = E(n_o^2(t))$

therefore $SNR = \dfrac{\left|\displaystyle\int\limits_{-\infty}^{\infty} h(\beta)s_i(t-\beta)d\beta\right|^2}{\displaystyle\int\limits_{-\infty}^{\infty}\int\limits_{-\infty}^{\infty} R_{ni}(\beta-\alpha)h(\alpha)h^{*}(\beta)d\alpha d\beta}$ $\qquad$ (2.2.4)

This will be a maximum[14] when

$$\int\limits_{-\infty}^{\infty} R_{ni}(\beta-\alpha)h(\alpha)d\alpha = ks_i(t-\beta) \qquad (2.2.5)$$

If $n_i(t)$ is a white noise source, then

$$R_{ni}(\beta-\alpha) = I\delta(\beta-\alpha) \qquad (2.2.6)$$

i.e., the autocorrelation function is an impulse of strength I. It can then be written that, for maximum SNR:

$$\int\limits_{-\infty}^{\infty} R_{ni}(\beta-\alpha)h(\alpha)d\alpha = Ih(\beta) = ks_i(t-\beta) \qquad (2.2.7)$$

The optimum impulse response looks like the input signal reversed in time, starting at some fixed measurement time t.

Before the matched filter theory can be applied to a spectroscopy amplifier, the noise must be made white. It has been shown in Section 1.4 that if the $\dfrac{1}{f}$ noise source is ignored, the noise generated in the spectrometer has a spectral density given by:

$$|H(W)|^2 = a^2 + \frac{b^2}{W^2}$$

$$|H(W)|^2 = a^2 \times \left(\frac{W^2 + W_{nc}^2}{W^2}\right) \qquad (2.2.8)$$

If this noise is passed through a pre-whitening filter having the response $\dfrac{jW}{W_{nc} + jW}$

then the output noise will have a modified spectral density given by:

$$\left|H'(W)\right|^2 = a^2 \times \left(\frac{W^2 + W_{nc}^2}{W^2}\right) \times \left(\frac{W^2}{W^2 + W_{nc}^2}\right)$$

$$\left|H'(W)\right|^2 = a^2 \qquad\qquad (2.2.9)$$

The pre-whitening filter is simply a CR differentiator, with a time constant $T_{nc} = CR$. The effect of this filter on the signal step, generates a waveform that looks like $\exp\left(\dfrac{-t}{T_{nc}}\right)$. The matched filter will therefore have an impulse response that has the form $\exp\left(\dfrac{t}{T_{nc}}\right)$. The convolution of these waveforms yields the output pulse shape; it is the so-called infinite cusp.
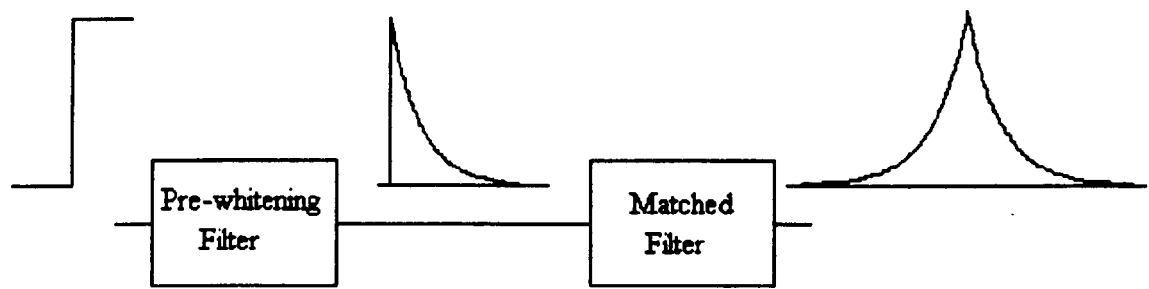
Fig 2.2.2

Figure 2.2.2 shows the waveforms generated by a step input; it is clear that the cusp is the step response of the combined filters.
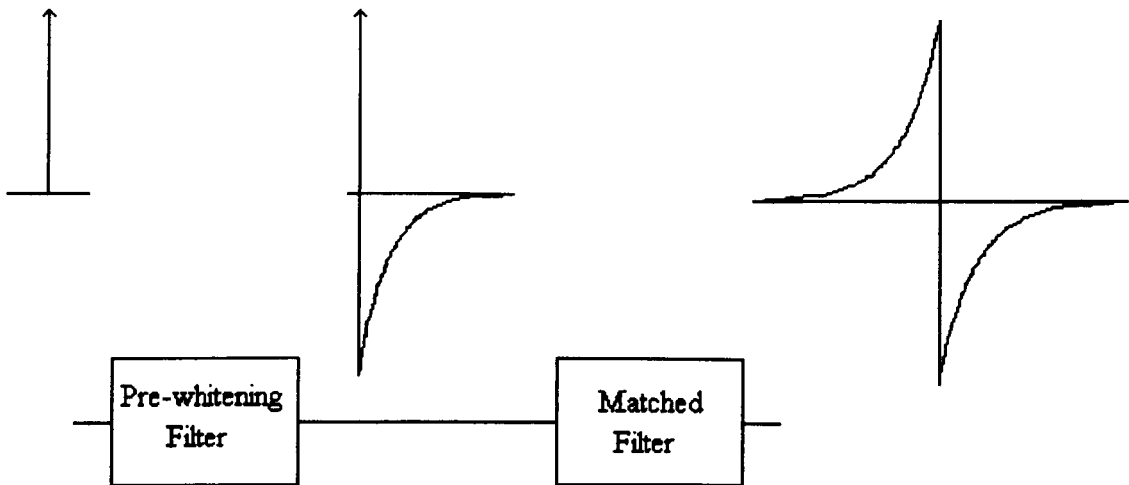
Fig 2.2.3

Figure 2.2.3 shows the waveforms generated by an impulse input. It can be seen that the overall impulse response of the combined filters is the first derivative of the step response , as would be expected.

The cusp cannot be realised in an analogue system, due to the matched filter section having an exponentially rising impulse response. In any case, the cusp waveform is of no practical use in analogue systems, because the response time is infinite; it is impossible to avoid pile-up. In fact when pulse shapes are normalised, the cusp is seen to have the worst trade-off between noise and resolving time[11]. Ballistic deficit would also be a problem due to the discontinuous derivative at the peak.

Again, it is to be noted that if the delta noise is increased (i.e. T_{nc} increased), then the optimum pulse duration is increased. If the step noise is increased (i.e. T_{nc} decreased), the optimum pulse duration is decreased.

2.3 : DELTA AND STEP NOISE INDICES

It is necessary to derive the noise variance at the output of the selected filter, given that we know the spectral density of the input noise source.

Campbell's theorem[15] states that the variance at the output of a filter, having an impulse response h(t), is given by the sum of the mean square contributions from all

preceding impulses, providing that the random process is stationary so that the variance is independent of the measuring time.

$$\sigma^2 = nq^2 \int_{-\infty}^{\infty} h^2(t)dt \qquad (2.3.1)$$

where n is the mean rate of impulses and q is the impulse strength. If Parseval's theorem is applied:

$$\sigma^2 = 2nq^2 \int_0^{\infty} |H(W)|^2 df \qquad (2.3.2)$$

But $2nq^2$ represents the single sided spectral density W_i of the input noise. For illustration, nq could represent a shot noise current I_s, where the spectral density is $2I_sq$. In our charge-amplifier arrangement, the impulse strength is amplified by the factor $\dfrac{C_t}{C_f}$, and the impulse noise at the output is given by:

$$\sigma_i^2 = \frac{W_i C_t^2}{2C_f^2} \int_{-\infty}^{\infty} h_i^2(t)dt \qquad (2.3.3)$$

Random steps also contribute to the output variance. By similar arguments, it can be written that:

$$\sigma_s^2 = \frac{W_s}{2C_f^2} \int_{-\infty}^{\infty} h_s^{2}(t)dt \qquad (2.3.4)$$

where $h_s(t)$ is the step response; $h_i(t)$ will be its derivative.

W_i and W_s were derived in Section 1.4 as v_s^2 and i_p^2, and the total variance at the output is given by the expression:

$$\sigma^2 = \frac{v_i^2}{2} \frac{C_t^2}{C_f^2} \int_{-\infty}^{\infty} h_i^2(t)dt + \frac{i_p^2}{2C_f^2} \int_{-\infty}^{\infty} h_s^{2}(t)dt \qquad (2.3.5)$$

The following simplifications will be made: The $\dfrac{1}{f}$ noise generator v_{n1}^2 will be ignored for the reasons discussed in Section 2.2. The noise generator i_{n4}^2, representing the channel noise coupled through the FET gate-source capacitance, will also be ignored; its value will be less than 10% of the total 'a' noise if C_{gs} is

approximately C_d for maximum SNR[16]. Delta noise can then be equated with 'b' noise.

The delta noise generator can be represented by:

$$v_s^2 = 4kTR_n \tag{2.3.6}$$

$$\text{where } R_n = \frac{2}{3g_m}$$

The step noise generator is re-defined as:

$$i_p^2 = 2qI_n \tag{2.3.7}$$

$$\text{where } I_n = \left(I_d + I_{gs} + \frac{4kT}{R_t 2q} \right)$$

The total variance at the output is now given by:

$$\sigma^2 = 2kTR_n \frac{C_t^2}{C_f^2} \int_{-\infty}^{\infty} h_i'^2(t)dt + \frac{I_n q}{C_f^2} \int_{-\infty}^{\infty} h_s^2(t)dt \tag{2.3.8}$$

A signal charge q, entering the system, will produce a peak signal amplitude of :

$$v_{peak} = h_{peak} \frac{q}{C_f} \tag{2.3.9}$$

The variance σ^2 can be normalised to an equivalent noise charge if it is divided by the square of v_{peak}.

$$ENC^2 = \frac{2kTR_n C_t^2}{q^2} \frac{\int_{-\infty}^{\infty} h_i'^2(t)dt}{h_{peak}^2} + \frac{I_n}{q} \frac{\int_{-\infty}^{\infty} h_s^2(t)dt}{h_{peak}^2} \tag{2.3.10}$$

The expressions

$$\frac{\int_{-\infty}^{\infty} h_i'^2(t)dt}{h_{peak}^2} \quad \text{and} \quad \frac{\int_{-\infty}^{\infty} h_s^2(t)dt}{h_{peak}^2} \tag{2.3.11}$$

are labelled delta noise index and step noise index.

We are interested in knowing what is the effect of previous noise impulses at a given time when the amplitude of a signal is being measured. A 'Weighting Function' or 'Residual Function' R(t) can be defined which specifies the contribution at the measurement time of noise steps occurring time t before the measurement time. It can be shown[17] that the total mean square step noise at T_m is given by:

$$n \int_0^\infty [R(t)]^2 \, dt \qquad (2.3.12)$$

where n is the mean rate of unit amplitude steps. This expression derives from Campbell's theorem, with the provision that, in a causal system, noise steps that occur after the measurement time cannot contribute to the measured noise variance; the integral is therefore limited to positive values of t.

A step noise index is defined as:

$$N_s^2 = \frac{\int_0^\infty [R(t)]^2 \, dt}{S^2} \qquad (2.3.13)$$

where S^2 is the peak response for an unit amplitude step signal. It follows that there is a similar delta noise index defined by:

$$N_d^2 = \frac{\int_0^\infty [R'(t)]^2 \, dt}{S^2} \qquad (2.3.14)$$

where $R'(t)$ is the first derivative of the weighting function

These indices are derived for unit amplitude steps and impulses. When considering ENC, the expressions become:

$$ENC^2 = \frac{2kTR_s C_i^2}{q^2} N_d^2 + \frac{I_s}{q} N_s^2 \qquad (2.3.15)$$

The noise indices have now been derived in terms of the step response $h_s(t)$ and its derivative, and also in terms of the weighting function R(t) and its derivative. In fact, the step response (output pulse shape) and the weighting function are identical for a

time invariant system (see Figure 2.2.4). The reason for using the weighting function becomes apparent when a time variant system is considered (see Figure 2.2.5).
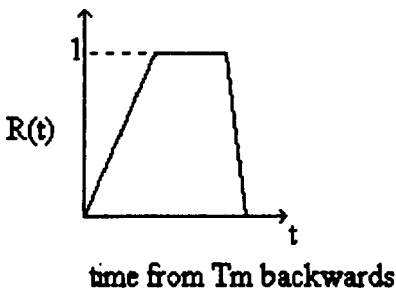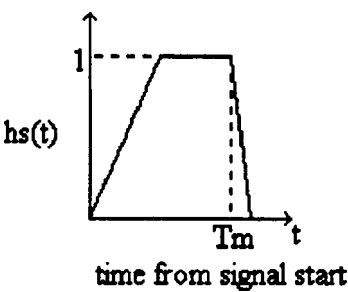

time from signal start

time from Tm backwards

Fig 2.2.4

Figure 2.2.4 shows the output hs(t) of a time-invariant trapezoidal shaper, with the amplitude being measured at some time Tm. The weighting function is calculated by considering the response at Tm of noise steps occurring at various times before Tm. The weighting function and the step response are seen to be identical.

input to gated integrator — time from signal start

output from gated integrator $h_s(t)$ — time from signal start — T_m — T_i — T

$R(t)$ — time from T_m backwards — T_i — T — T
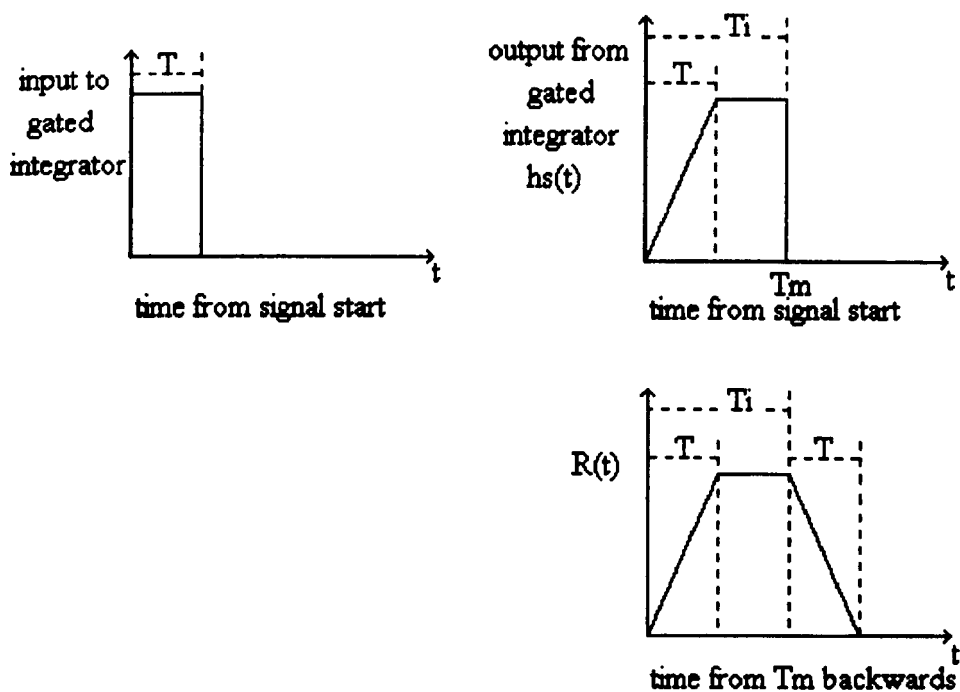
Fig 2.2.5

In Figure 2.2.5, the output $h_s(t)$ of a time-variant trapezoidal filter is shown. The time-variant element is an integrator, gated to integrate for a time T_i from the start of a signal pulse. A time-invariant element is assumed to generate the rectangular pulse. When the weighting function is considered in this case, it can be seen that it differs from the step response.

In a time-variant system, system response is not constant with time; it varies in synchronisation with the time arrival of a valid signal. We cannot therefore integrate over all time the step response $h_s(t)$ to calculate the step noise index, as the response for a particular noise step is related to its time relationship with the signal.. We need to use the weighting function.

Weighting functions allow us to intuitively predict noise performance. The step noise contribution will be increased if the area under the function is increased; this is what happens if the output pulse time-scale is increased. The delta noise contribution will increase if the steepness of the sides is increased; this happens when the time scale is decreased. It might be correctly guessed that delta noise was a minimum when the weighting function was symmetrical because of the quadratic addition of the slopes. The insertion of a flat top for ballistic deficit protection, without increasing the time-scale, will obviously increase the area and step noise, and will also cause the sides to be steeper and increase the delta noise.

It should be noted that:

$$N_s^2 = k_1 T_F \qquad (2.3.16)$$

$$N_d^2 = \frac{k_2}{T_F} \qquad (2.3.17)$$

where T_F is related to the timescale of the weighting function. The scaling factor T_F can be chosen arbitrarily to be, e.g., time-to-peak, pulse width, pulse width at a given fraction of the pulse height; constants k_1 and k_2 will be modified accordingly.

The equation for ENC can be re-written to give:

$$ENC^2 = \frac{2kTR_n C_t^2}{q^2 T_F} N_{d1}^2 + \frac{I_n T_F}{q} N_{s1}^2 \qquad (2.3.18)$$

The optimum value of T_F is that which gives the smallest value of ENC, i.e.:

$$\frac{2kTR_n C_t^2}{q^2 T_F} N_{d1}^2 = \frac{I_n T_F}{q} N_{s1}^2$$

$$T_F = \sqrt{\frac{2kTR_n C_t^2}{qI_n} \frac{N_{d1}}{N_{s1}}}$$

$$T_F = T_{nc} \frac{N_{d1}}{N_{s1}} \qquad (2.3.19)$$

It is useful to define an index P given by:

$$P = \sqrt{N_d^2 \times N_s^2} \qquad (2.3.20)$$

This index is a measure of the goodness of a filter when there is equal contribution from delta and step noise. It is independent of the filter time scale; its value is fixed by the shape of the weighting function. It can be shown[18] that the P index for the infinite cusp filter is 1.00. This measure of goodness does not take into account pile-up, ballistic deficit, or operation at sub-optimal shaping times.

CHAPTER 3 : ANALOGUE PULSE SHAPING

3.1 : TIME-INVARIANT VERSUS TIME-VARIANT SHAPING

The simplest pulse shaping arrangement comprises a CR "differentiator" followed by an RC "integrator", as shown in Figure 3.1.1. The differentiator serves to limit the time scale of the charge-amplifier pulse, reducing pile-up and overloading. The integrator acts as a low pass filter. It can be shown[19] that the maximum SNR is obtained when T1 = T2 (where T1 is the differentiator time-constant and T2 is the integrator time-constant). This condition is also a good compromise in that T1 > T2 gives a quicker return to baseline, but T1 < T2 produces a shape less sensitive to ballistic deficit. The waveform shape is shown in Figure 3.1.2.
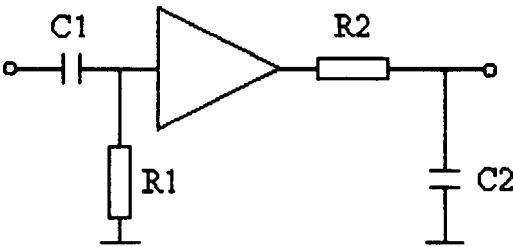
Fig 3.1.1

Extra RC integrators can be added to make the pulse shape become approximately Gaussian. The approximation becomes better as the number of integrators (n) is increased. In practice, the improvement for n > 7 is not worth the circuit complexity.
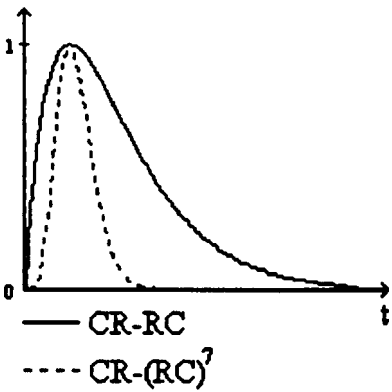
Fig 3.1.2

Intuitively, the better SNR can be explained by a more symmetrical shape leading to less delta noise (see Figure 3.1.2). The waveforms from these $(CR) - (RC)^n$ shapers are defined by:

$$V_o(t) = \left(\frac{t}{\tau_o}\right)^n \times \exp\left(n\left(1 - \frac{t}{\tau_o}\right)\right) \qquad (3.1.1)$$

where τ_0 is the peaking time. Goulding[17] derives the noise indices for the following shapers:

Shaper	N_d^2	N_s^2	P
CR - RC	$1.85/\tau_0$	$1.85\tau_0$	1.85
CR - $(RC)^4$	$2.04/\tau_0$	$0.90\tau_0$	1.35
CR - $(RC)^7$	$2.53/\tau_0$	$0.67\tau_0$	1.30

It should be noticed that τ_0 can be made longer as n increases for the same overall pulse width.

A second CR differentiator generates a bipolar pulse. Konrad[20] derives the figures of merit for these shapers:

Shaper	P
$(CR)^2 - RC$	2.02
$(CR)^2 - (RC)^4$	1.90

The noise performance is poor, and ballistic deficit immunity will also be worse than that of an unipolar pulse of the same overall width. The advantage of a bipolar shape is that, with area balance between negative and positive lobes, it can be transmitted through an AC coupled system without a baseline shift. Unipolar shapers usually need a baseline restoration circuit to limit this baseline shift at moderate count rates. At the highest counting rates, bipolar shaping becomes necessary. Bipolar shaping is often used for timing applications, as the zero cross-over time is independent of pulse height.

Modern spectroscopy amplifiers do not use CR - $(RC)^n$ filters, as better shaping can be obtained with fewer stages if a CR differentiator is followed by a lower number of active integrator stages.[21] This structure depends on the integrators supplying pairs of complex poles. A typical single complex pole pair stage is shown in Figure 3.1.3.
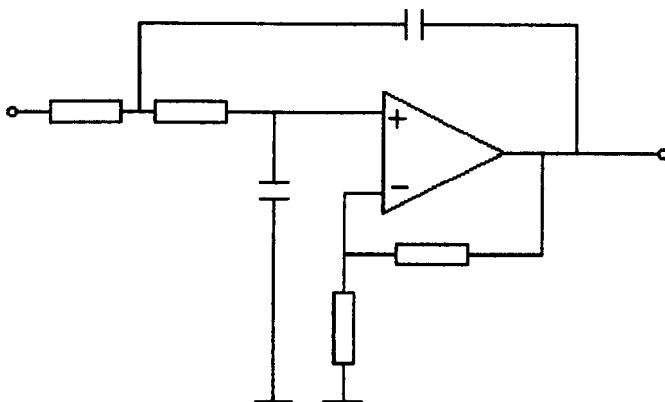
Fig 3.1.3

Goulding[17] derived the noise indices of a time-invariant symmetrical triangular waveform. This shape would be expected to have a good SNR, as it approximates a cusp with finite resolving time.

$$N_s^2 = 0.67\tau_O$$
$$N_d^2 = 2/\tau_O$$
$$P = 1.16$$

The P index is seen to be much better than for $CR - (RC)^n$ shapers and the waveform returns to the baseline much quicker. The disadvantage is a poor immunity to ballistic deficit due to the discontinuous derivative at the peak.

Triangular pulse shaping was originally generated by integrating the output of a double delay line shaper. Such a shaper is shown in Figure 3.1.4. The first delay line stage produces a rectangular waveform, making use of the fact that the step waveform undergoes a polarity reversal on reflection at the grounded end of the delay line. The second stage generates a bipolar pulse by the same principle. This bipolar shape, integrated in a true integrator, generates the triangular waveform. Unfortunately, delay lines are not ideal circuit elements. They can be bulky, they can cause gain to be very temperature sensitive, and imperfections make perfect termination and complete cancellation with the input step impossible. Another major drawback is the difficulty in changing the shaping time.
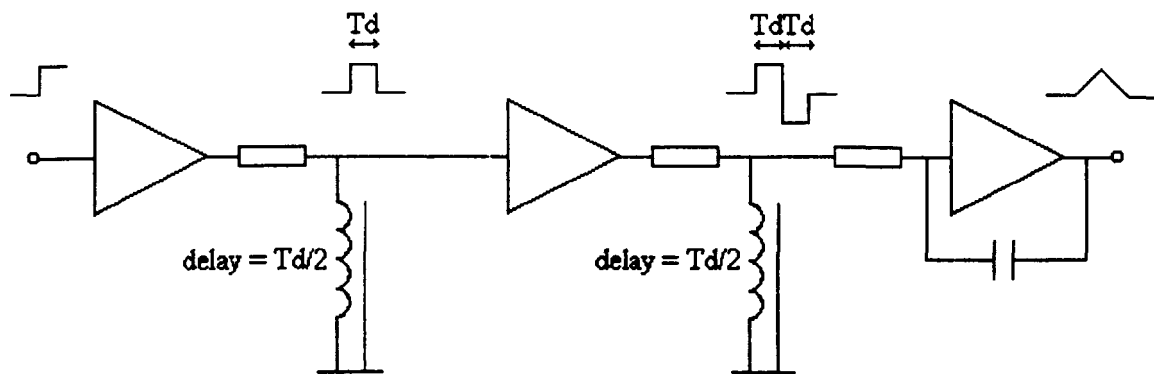
Fig 3.1.4

Modern amplifiers employing triangular shaping use an arrangement whereby the outputs of several low pass filters having complex poles are weighted and summed to produce the required output waveform, as shown in Figure 3.1.5.
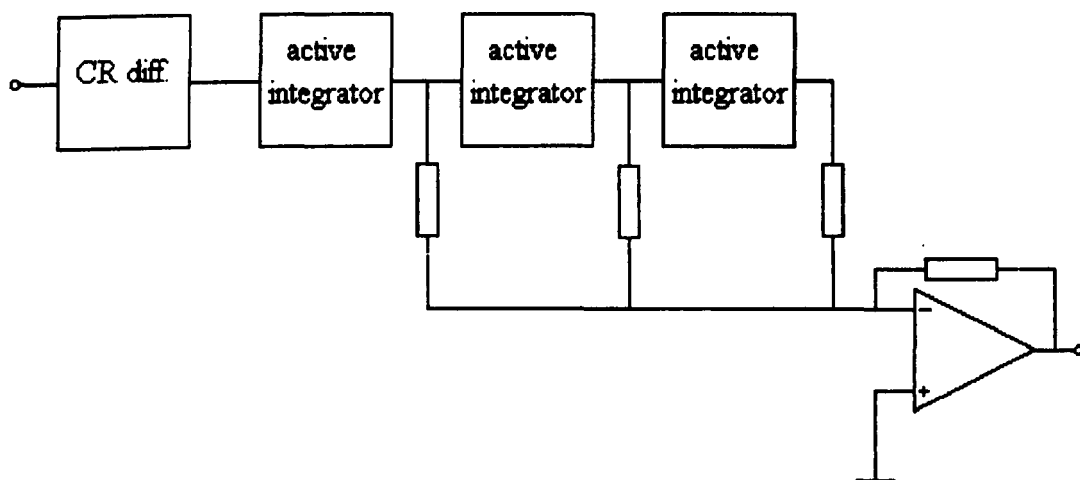
Fig 3.1.5

The low pass sections may be the components of an overall CR - $(RC)^n$ filter[22], $sine^n$ filter[11] or other. The quasi-triangular shape may have a rounded top, which is advantageous from a ballistic deficit consideration, but it may also have a slightly rounded tail that will impair the pile-up performance.

When large Ge detectors are used, it is usually necessary to have a flat top as wide as the variation in detector collection times; otherwise ballistic deficit is unacceptable. The triangle becomes trapezoidal at the expense of some impairment in noise reduction (see Section 2.2). Goulding[17]derives the indices for a time-invariant trapezoid (see Figure 3.1.6) as:

27

$$N_s^2 = T_2 + \frac{T_1}{3} + \frac{T_3}{3}$$ (3.1.2)

$$N_d^2 = \frac{1}{T_1} + \frac{1}{T_3}$$ (3.1.3)

It is illustrative to compare the weighting function of this time-invariant filter with that of the time-variant equivalent. The weighting functions can be identical, but for the time-variant case, the output pulse duration is much shorter and higher counting rates are possible. Alternatively, if the output pulse durations are made equal, the weighting function will be modified to give less delta noise (less steep sides) and more step noise (greater area). This is useful when shaping times shorter than optimum are used and delta noise is dominant.

Fig 3.1.6

The time-variant trapezoid can be generated by feeding a rectangular pulse into an integrator, gated to integrate for a time T_I that is greater than the width of the rectangle by a factor T_F, the width of the flat top. At the end of the gating period, the integrator is reset, losing all memory of the previous event. Modern amplifiers can

avoid the use of delay lines by using the technique of summing the weighted intermediate outputs of a semi-Gaussian shaper to generate an approximation to the rectangular waveform[23,24].
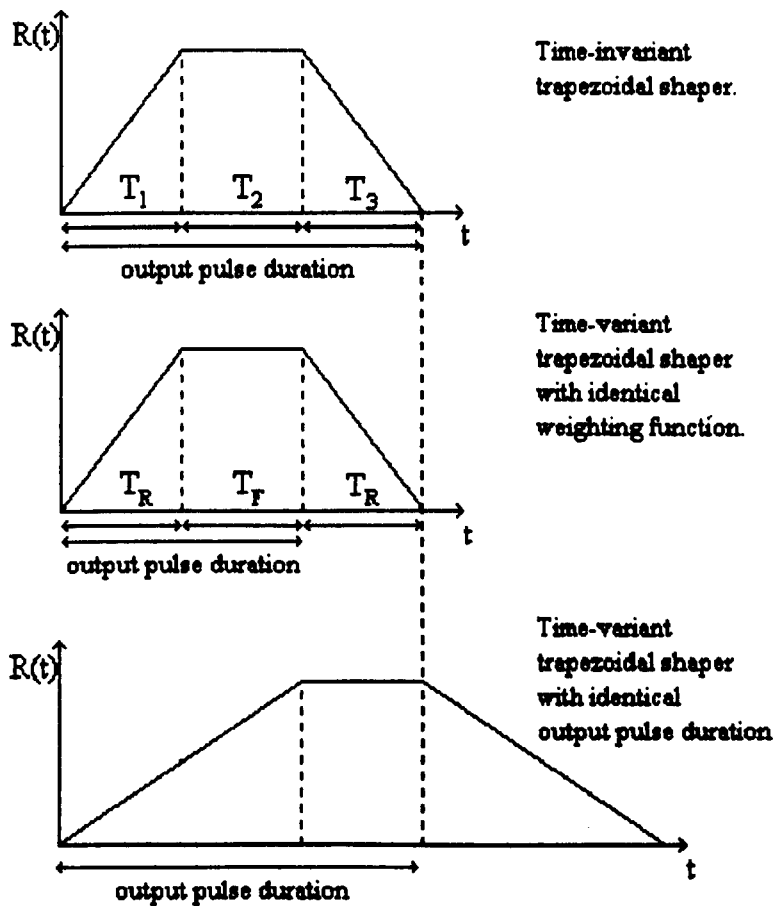
Earlier attempts to approximate the trapezoidal pulse shape used the semi-Gaussian signal as the input of the gated integrator. As the integrator time is greater than the semi-Gaussian pulse width by the factor T_F, counting-rate performance will not be changed significantly by the addition of the gated integrator[25,26]. Goulding gives the noise indices of a CR - $(RC)^7$ shaper with gated integrator as:

$$N_s^2 = 2.07\tau_0$$
$$N_d^2 = 1.47/\tau_0$$
$$P = 1.74$$

The overall figure of merit is seen to be degraded when compared with that of the same semi-Gaussian shaper used without the gated integrator. The delta noise index, however, is much better, and the shaping method is therefore useful at short shaping, especially as the immunity to ballistic deficit is so much better. Put another way, for the same delta noise index, a gated integrator on the output of a semi-Gaussian shaper allows the use of a shorter shaping time, and throughput is therefore better.

3.2 : HARWELL TIME-VARIANT SHAPERS

A different type of time-variant filter was developed at the Atomic Energy Research Establishment, Harwell. Kandiah's original idea was to replace the passive RC integrator in a typical CR - RC system with a gated active integrator[27], the idea being that there would be a better discrimination against noise pulse occurring before the signal. Deighton's mathematical analysis of the system[28] proved that the noise performance was indeed better. The optimum ENC was found to be 0.808 times the optimum ENC of a CR - RC system. The optimum system parameters were given by:

$$T = T_1 = 1.3 \, T_0$$

where T is the integration time, T_1 is the CR time constant and T_0 is the noise corner.

Deighton went on to analyse the effect of having an amplifier of finite bandwidth (3dB point at a frequency of $\dfrac{1}{T_2}$ preceding the CR differentiator, and of having the differentiator time-constant switched from a small value to an infinitely large value

during the integration time. The optimum ENC was now 0.748 times the optimum ENC of the CR - RC system, and the requisite conditions were:

$$T_2 = 1.05 \, T_0$$
$$T_1 = 0 \text{ switched to } \infty \text{ during } T$$
$$T = 2.10 \, T_0$$

The figure of merit P is related to the SNR[29] by:

$$ENC = \sqrt{P} \times ENC_{cusp}$$

$$\text{or } SNR = \frac{1}{\sqrt{P}} \times SNR_{cusp}$$

$$\text{therefore } ENC_{har} = ENC_{rccr} \times 0.748$$

$$ENC_{har} = \sqrt{1.847} \times ENC_{cusp} \times 0.748$$

$$ENC_{har} = 1.017 \times ENC_{cusp} \qquad (3.2.1)$$

The SNR is only 1.7% worse than that of a cusp. In a later paper, however, Deighton[30] pointed out that the ballistic deficit immunity of this virtually ideal noise filter was very poor, worse in fact than for the cusp filter.

Kandiah's team developed a practical circuit employing these ideas[31,32,33] with the added refinement that T_2 was switched to a low value immediately after the processing of a pulse, in order to speed up the decay of residual voltages in the system, shortening the dead-time before another pulse could be accepted. The system is shown in Figure 3.2.1.
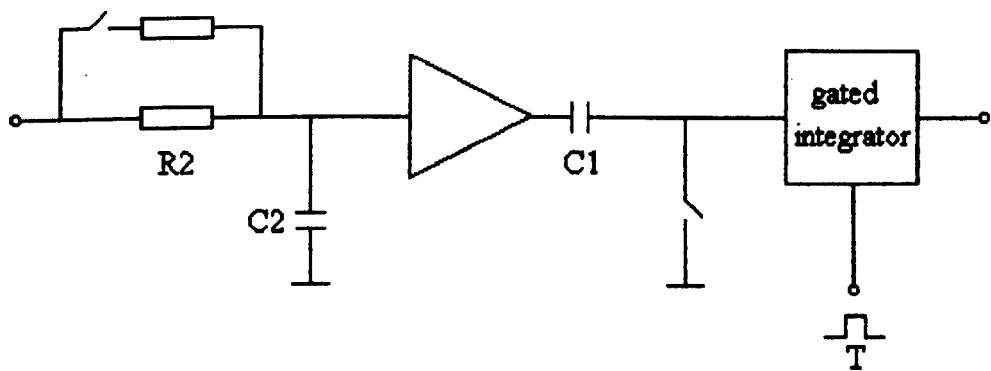

Fig 3.2.1

30

Intuitively, decreasing T_2 might be expected to increase the noise in the system by virtue of increased bandwidth. The increased noise would decay after restoration of T_2 , but following pulses occurring immediately after this restoration might be expected to suffer from an increased non-stationary noise. Deighton[34] analysed the circuit and developed the weighting function shown in Figure 3.2.2, where T represents the integration time of the gated integrator, T_d represents the time that T_2 is reduced to T_2' or $\dfrac{T_2}{m}$ and T_x represents the time between restoration of integrator RC to T_2 and the arrival of a second event.

R(t)

T T_x T_d t
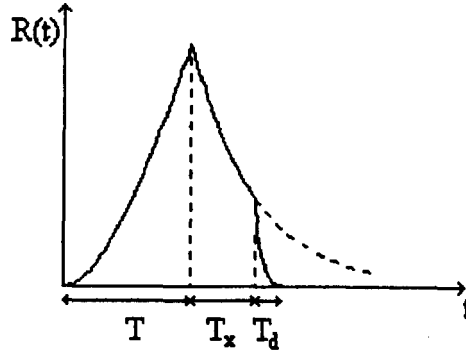
Fig 3.2.2

It can be seen that the weighting function varies with the time of arrival of an event. If T_x is long, the weighting function will resemble that of a filter where T_2 is not switched (dotted line). When T_x is short, it can be deduced from the shape of the weighting function that there will be an increase in the delta noise index. Deighton's calculation derives an expression for the delta noise.

$$ENC_d^2 = \frac{kT_aR_nC^2}{q^2T_2}\left[\frac{u^2-2+2(u+1)e^{-u}}{\left(u-1+e^{-u}\right)^2}+\left((m-1)e^{-2\frac{T_x}{T_2}}\right)\right] \qquad (3.2.2)$$

where the second term in the brackets represents the extra noise due to the switching of T_2. The increased noise can be limited by imposing a minimum T_{xo} on the system, i.e. extend the dead time after processing from T_d to $T_d + T_{xo}$. Deighton went on to derive the mean effective noise for a given count rate n, assuming pulses to occur with a known statistical distribution from T_{xo} to ∞ after the restoration of T_2.

$$ENC_d^2 = \frac{kT_aR_nC^2}{q^2T_2}\left[\frac{u^2-2+2(u+1)e^{-u}}{\left(u-1+e^{-u}\right)^2}+\left((m-1)e^{-2\frac{T_{xo}}{T_2}}\right)\frac{nT_2}{nT_2+2}\right] \qquad (3.2.3)$$

31

The pulse acceptance rate is lowered by the extra protection time T_{xo} and at a high rate is given by:

$$\frac{n_a}{n} \approx \exp\left(-n\left(T + T_d + T_{xo}\right)\right) \qquad (3.2.4)$$

where n_a is the acceptance rate. An effective dead time for the system is therefore given by $T + T_d + T_{xo}$.

Harwell went on to develop processors optimised for X-ray work[35] (NM8840) and for γ-ray applications[36] (NM8841). In these instruments, the problem of ballistic deficit immunity was solved by the use of a series switch[37] that was opened before the arrival of an event, and only closed after a delay set to be longer than any collection time in the detector. Figure 3.2.3 shows the circuit schematic and Figure 3.2.4 shows the circuit waveforms.

Filter   Baseline Restorer   Gated Integrator
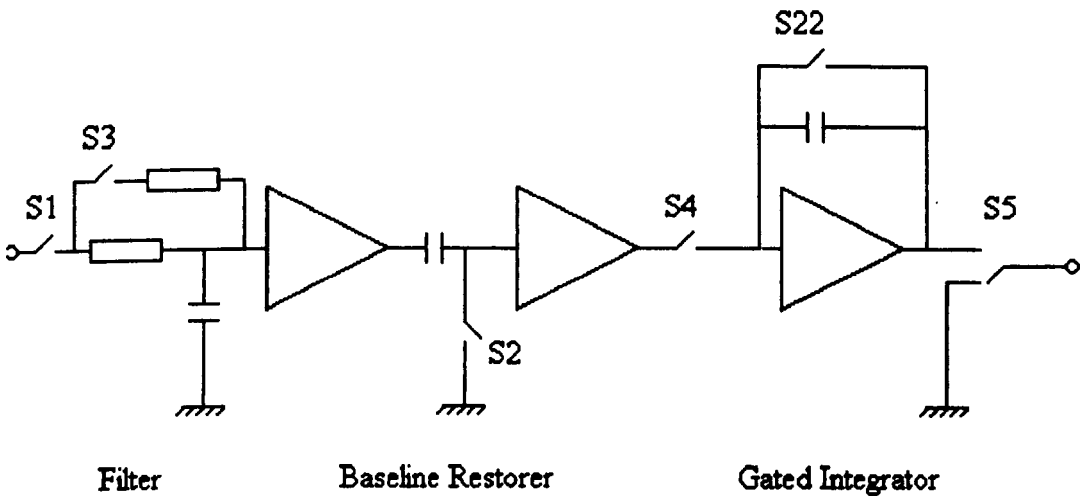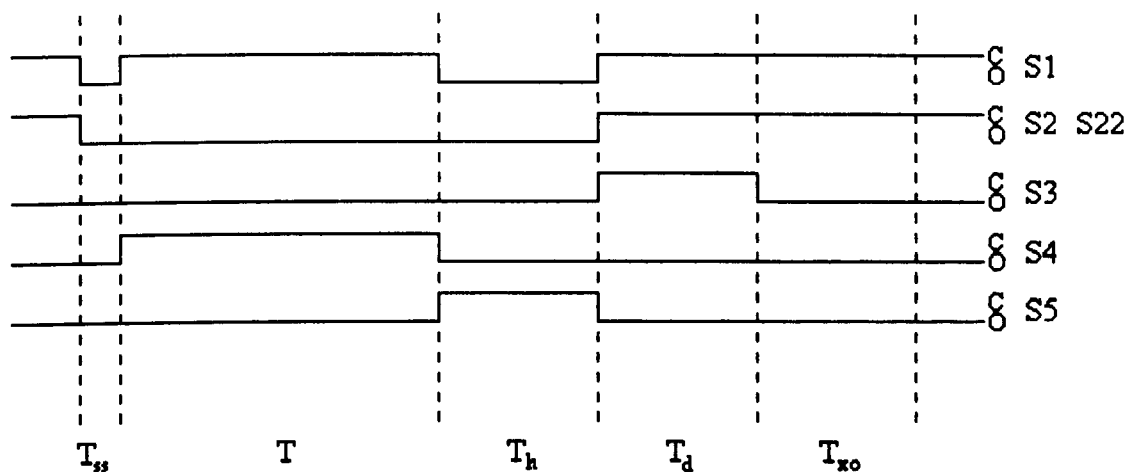
Fig 3.2.3

Fig 3.2.4

The weighting function is modified by the series switch as shown in Figure 3.2.5. Delta noise will not be affected by the flat top but the acceptance rate will suffer a little.
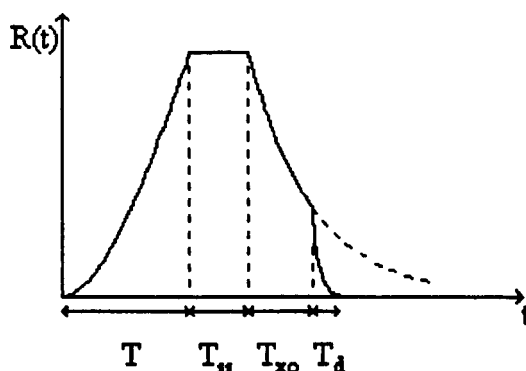
Fig 3.2.5

In all these systems, step noise is not taken into much consideration, its value being so low at the shaping times of interest. White[38] took this a stage further when he proposed to eliminate the gated integrator from the Harwell design in order to simplify the circuit. The weighting function is seen to be modified as shown in Figure 3.2.6. The increased step noise index caused by the increased area was considered to be unimportant.

33
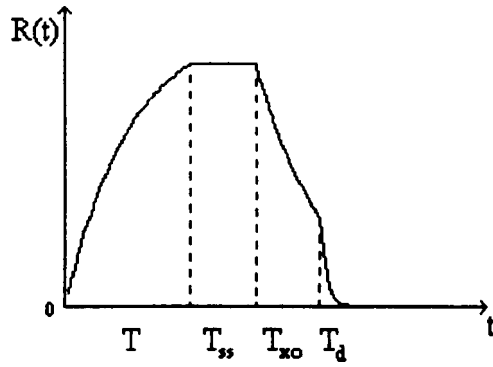
Fig 3.2.6

For our application, an useful indicator of the goodness of a particular filter might be the product $N_d^2.T_D$, where T_D is the dead time of the system. This index was first proposed by Goulding[18] and has also been used by Husimi[25], it combines the data throughput property of the filter with its ability to reduce the dominant noise. For the filters discussed above, the following figures apply:

	Filter	N_d^2	T_D	$N_d^2.T_D$
A)	CR-RC	$1.85/T_O$	$11.0\,T_O$	20.4
B)	CR-(RC)^4	$2.04/T_O$	$5.1\,T_O$	10.4
C)	CR-(RC)^7	$2.53/T_O$	$4.1\,T_O$	10.4
D)	Triangular	$2.00/T_O$	$3.0\,T_O$	6.0
E)	CR-(RC)^7 + Gated Integrator	$1.47/T_O$	$6.2\,T_O$	9.1
F)	Rectangular + Gated Integrator	$2.00/T_r$	$2.0\,T_r$	4.0
G)	Harwell	$2.18/T$	$1.9\,T$	4.0

where T_O is the peaking time, T_r is the width of the rectangular function and T is the gating time.

It has been assumed that the dead time in filters A-F is determined by the pile-up rejector. In filters A-D (time-invariant) such a rejector demands that a valid pulse does not occur within $T_A + T_B$ of the start of another pulse, where T_A is the time from the start of the event to the measuring-time, and T_B is the time from the measuring-time to the end of the event. It also demands that the valid pulse is not followed by another within T_A. The dead-time is therefore set at $2T_A + T_B$. For a gated integrator system (E-F), T_B is effectively zero as the integrator is reset immediately after the measuring-

time. T_B for filters A-C is taken as the time it takes the signal to decay to less than 0.1% of the peak value.

For filters E-G, no flat-top has been incorporated in the dead-time calculations as it is a fixed time overhead. The gating time of filter E is assumed to last $3.1T_O$ (until the semi-Gaussian input decays to 0.1% of its peak value), the gating time of filter F is the duration of the input pulse, and the gating time of the Harwell filter is twice the circuit time-constant T_2. The dead-time of the Harwell filter has been taken to be $T + T_d + T_{xo}$, with T_{xo} set to T_2 and T_d set to $0.7T_2$, as used by Deighton. If a short shaping-time of $0.5\mu s$ is assumed for the Harwell processor, the delta noise index will only increase to 2.20 at 10^5 pps and 2.32 at 10^6 pps (see Equation 3.2.3). It is clear that the Harwell processor scores highly when this indicator of goodness is considered.

The selection of $T = 2T_2$ is optimum when equal contributions from delta noise and step noise are considered. In our sub-optimal case other values of μ, the ratio of T to T_2 might be better. Equation 3.2.3 yields the following results:

μ	N_d^2	T_D	$N_d^2.T_D$
0.5	1.53/T	4.40 T	6.7
1	1.74/T	2.70 T	4.7
2	2.18/T	1.85 T	4.0
4	3.11/T	1.43 T	4.4

It can be seen that $T = 2T_2$ is still the best selection under our new criterion.

3.3 : NOISE INDEX CALCULATIONS

From Figure 3.2.5, R(t) in the interval T is defined by:

$$R(t) = \int (1 - e^{-t/T_2}) dt$$

$$R(t) = t + T_2(e^{-t/T_2} - 1) \tag{3.3.1}$$

In the interval T_{ss}, R(t) is defined by:

$$R(t) = T + T_2(e^{-T/T_2} - 1) \tag{3.3.2}$$

In the interval T_{xo}, R(t) is defined by:

$$R(t) = (T + T_2(e^{-T/T_2} - 1))e^{-t/T_2} \qquad (3.3.3)$$

Finally, in the interval T_d, R(t) is defined by:

$$R(t) = ((T + T_2(e^{-T/T_2} - 1))e^{-T_{xo}/T_2})e^{-tm/T_2} \qquad (3.3.4)$$

N_s^2 can now be calculated:

$$N_s^2 \times S^2 = \int_0^T \left(t + T_2(e^{-t/T_2} - 1)\right)^2 dt + \int_0^{T_{ss}} \left(T + T_2(e^{-T/T_2} - 1)\right)^2 dt$$

$$+ \int_0^{T_{xo}} \left((T + T_2(e^{-T/T_2} - 1))e^{-t/T_2}\right)^2 dt + \int_0^{T_d} \left((T + T_2(e^{-T/T_2} - 1))e^{-T_{xo}/T_2}e^{-tm/T_2}\right)^2 dt$$

$$N_s^2 \times S^2 = T_2^3 \left(\frac{u^3}{3} - u^2 + u - 2ue^{-u} - \frac{e^{-2u}}{2} + \frac{1}{2}\right) + T_2^2 \left(u + e^{-u} - 1\right)^2 T_{ss}$$

$$+ T_2^2 \left(u + e^{-u} - 1\right)^2 \frac{T_2}{2}\left(1 - e^{-2T_{xo}/T_2}\right) + T_2^2 \left((u + e^{-u} - 1)e^{-T_{xo}/T_2}\right)^2 \frac{T_2}{2m}\left(1 - e^{-2mT_d/T_2}\right)$$

$$(3.3.5)$$

where $u = \dfrac{T}{T_2}$. Dividing by S^2, the square of the maximum amplitude, gives the final result:

$$N_s^2 = \frac{T_2 \left(\dfrac{u^3}{3} - u^2 + u - 2ue^{-u} - \dfrac{e^{-2u}}{2} + \dfrac{1}{2}\right)}{\left(u + e^{-u} - 1\right)^2} + T_{ss} + \frac{T_2}{2}(1 - e^{-2T_{xo}/T_2}) + e^{-2T_{xo}/T_2}\frac{T_2}{2m}\left(1 - e^{-2mT_d/T_2}\right)$$

$$(3.3.6)$$

Similarly for the delta noise index:

$$N_d^2 \times S^2 = \int_0^T \left(1 - e^{-t/T_2}\right)^2 dt + \int_0^{T_{ss}} \left(\frac{-Se^{-t/T_2}}{T_2}\right)^2 dt + \int_0^{T_d} \left(\frac{-mS}{T_2}e^{-T_{xo}/T_2}e^{-mt/T_2}\right)^2 dt$$

$$N_d^2 \times S^2 = T_2 \left(u + 2e^{-u} - \frac{e^{-2u}}{2} - \frac{3}{2}\right) + \frac{S^2}{2T_2}(1 - e^{-2T_{xo}/T_2}) + \frac{mS^2}{2T_2}e^{-2T_{xo}/T_2}\left(1 - e^{-2mT_d/T_2}\right)$$

$$(3.3.7)$$

Dividing by S^2 gives the final result:

$$N_d^2 = \frac{\left(u + 2e^{-u} - \dfrac{e^{-2u}}{2} - \dfrac{3}{2}\right)}{T_2\left(u + e^{-u} - 1\right)^2} + \frac{\left(1 - e^{-2T_{xo}/T_2}\right)}{2T_2} + \frac{m e^{-2T_{xo}/T_2}}{2T_2}\left(1 - e^{-2mT_d/T_2}\right) \qquad (3.3.8)$$

If $\exp\left(\dfrac{-2mT_d}{T_2}\right)$ is assumed to be approximately zero, N_d^2 can be re-written as:

$$N_d^2 = \frac{u^2 - 2 + 2(u+1)e^{-u}}{2T_2\left(u - 1 + e^{-u}\right)^2} + \frac{(m-1)e^{-2T_{xo}/T_2}}{2T_2} \qquad (3.3.9)$$

This is the equation used by Deighton to calculate the increased noise due to switching T_2 (see Equation 3.2.2 above).

If the Gated Integrator is left out then, during T, R(t) is defined by $1 - e^{-t/T_2}$ and $R'(t)$ is defined by $\dfrac{e^{-t/T_2}}{T_2}$. Following the procedure shown above:

$$N_s^2 = \frac{T_2\left(u - \dfrac{3}{2} + 2e^{-u} - \dfrac{e^{-2u}}{2}\right)}{\left(1 - e^{-u}\right)^2} + T_{ss} + \frac{T_2}{2}\left(1 - e^{-2T_{xo}/T_2}\right) + \frac{T_2}{2m}e^{-2T_{xo}/T_2}\left(1 - e^{-2mT_d/T_2}\right)$$

$$(3.3.10)$$

$$N_d^2 = \frac{\left(1 + e^{-u}\right)}{2T_2\left(1 - e^{-u}\right)} + \frac{\left(1 - e^{-2T_{xo}/T_2}\right)}{2T_2} + \frac{m e^{-2T_{xo}/T_2}}{2T_2}\left(1 - e^{-2mT_d/T_2}\right) \qquad (3.3.11)$$

3.4 : THE USE OF A GATED INTEGRATOR

Figures 3.4.1 and 3.4.2 show plots of $\sqrt{N_d^2 \times T}$ and $\sqrt{\dfrac{N_s^2}{T}}$ versus u, the ratio of T to T_2. It has been assumed that the effect of switching T_2 is negligible at the processing times of interest and the effect of the series switch has been ignored too.

Fig 3.4.1

Ndl
delta noise index
without gated
integrator

Nd2
delta noise index
with gated
integrator

Fig 3.4.2

Ns1
step noise index
without gated
integrator

Ns2
step noise index
with gated
integrator
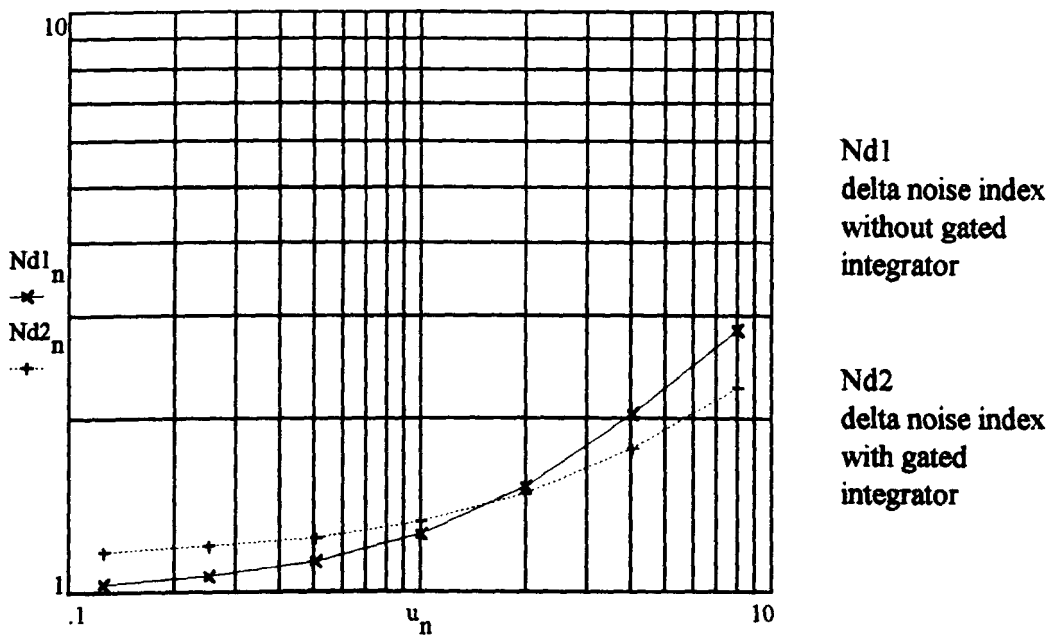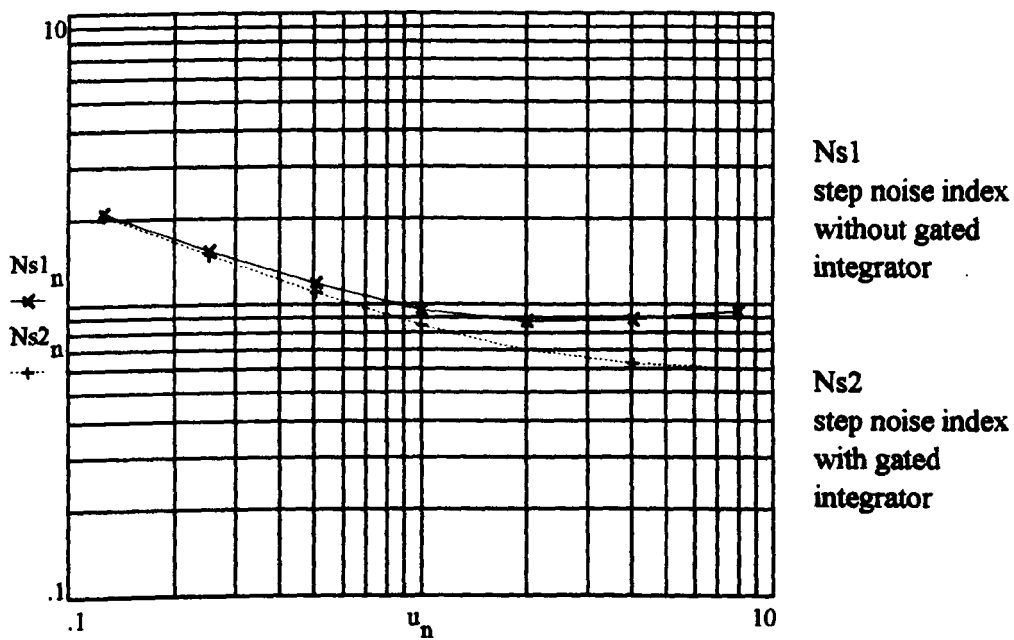
Figure 3.4.3 shows the plot of $P = \sqrt{N_d^2 \times N_s^2}$.

38
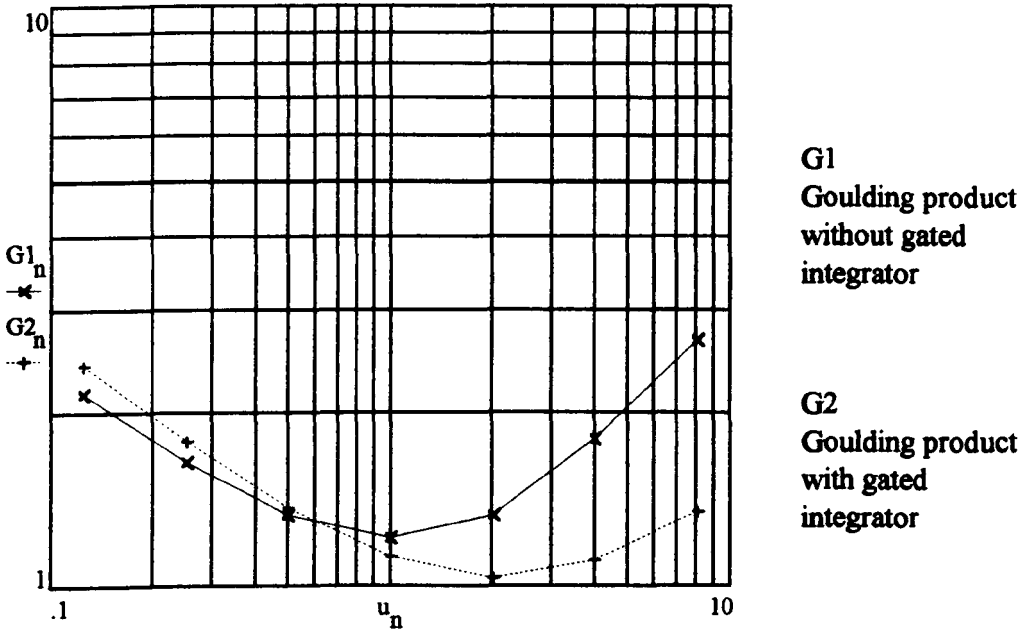
Fig 3.4.3

It can be seen that, for a Harwell processor with a gated integrator, the optimum value of u is 2 (where P = 1.03). If the gated integrator is omitted, the optimum value of u is seen to be 1 (where P = 1.21).

The step and delta noise indices calculated above can be used to derive the ENC figures as shown below:

$$ENC^2 = K_1 N_s^2 T + K_2 \frac{N_d^2}{T}$$

where $K_1 = \dfrac{I_g}{q}$ and $K_2 = 2kT_a R_n \dfrac{C^2}{q^2}$ and $T_o = \sqrt{\dfrac{K_2}{K_1}}$

ENC1
without gated
integrator

ENC2
with gated
integrator

$\text{ENC1}_{3,m}$
$\rightarrow$
$\text{ENC2}_{4,m}$
$\cdots + \cdots$

100

10

.1

k_m

100
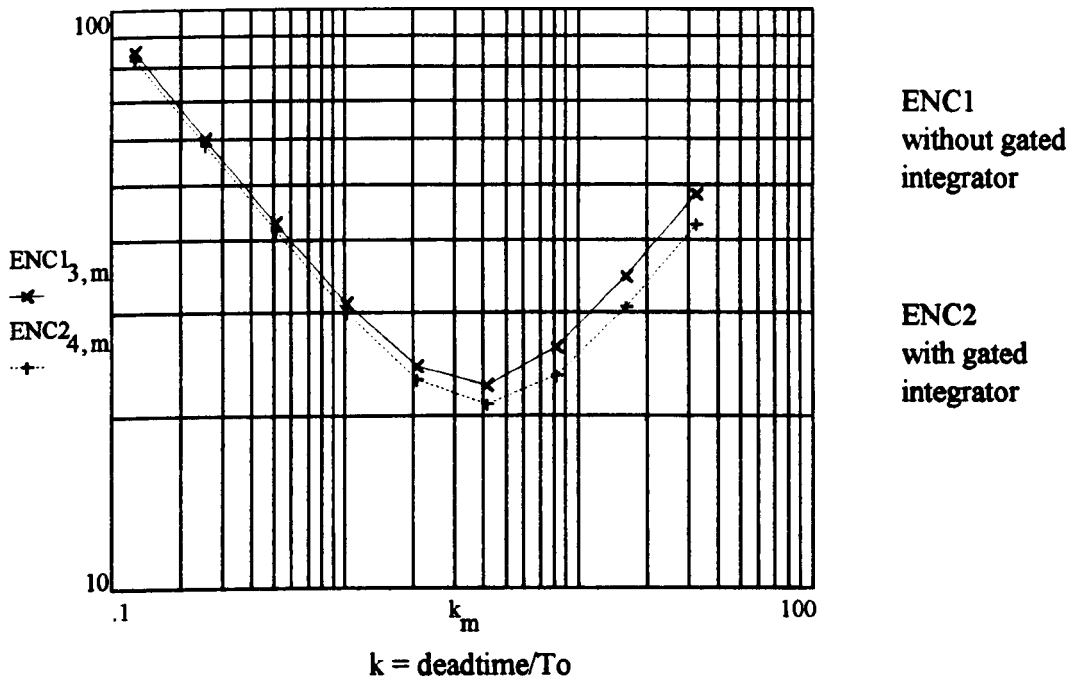
k = deadtime/To

Fig 3.4.3

Figure 3.4.3 shows how the ENC varies as the deadtime of the processor is changed. The deadtime has been taken as $T + \dfrac{1.7T}{u}$. The ratio u is set to 2 for the filter with gated integrator but is set to 1 for the filter without. The following parameters have been used for the calculation of ENC:

$I_g = 10^{-11}$

$T_a = 150$

$R_n = 120$

$C = 6 \times 10^{-12}$

It is clear that there is an advantage in using a gated integrator, even at processing times that are shorter than the optimum value.

CHAPTER 4 : THE DESIGN OF AN ANALOGUE PULSE PROCESSOR

4.1 : INTRODUCTION

In Section 3.2, it was shown that the Harwell processor seemed to be ideally suited to spectroscopy applications where high throughput rates and good resolution were required. However, most modern high performance amplifiers (e.g. Canberra 2025, Ortec 672 or Tennelec 244) tend to offer triangular shaping for demanding applications. When high throughput is required, semi-Gaussian filters with gated integrators are available (e.g. Canberra 2024 or Ortec 673).

Several factors have contributed to limiting the commercial exploitation of the Harwell processor. It has always been necessary to use a compatible spectrometer, having a rather limited range of noise-corners, and using a prompt-reset charge-amplifier of well specified sensitivity. Conventional, resistor-restored charge-amplifiers could not be accommodated because of the baseline shift during the processing time. Limit-restore charge-amplifiers have been used in the past but, because the system is virtually direct-coupled, the limited dynamic range caused energy dependant losses. For the same reason, only a limited gain range was possible. The numbers of selectable processing times was limited too, because several capacitors had to be switched in the passive and active integrators and also in the timing circuits defining the processing, restoration and protection times.

Several features of the Harwell processor were difficult to implement practically. In particular, the design of a gated integrator increased the cost and complexity of the unit. Implementations included discrete designs employing 20-30 transistors, or the use of custom designed plug-in amplifier modules that had wide bandwidth and low input currents, but suffered from high power consumption. Stringent demands were made on the design of a good linear gate in terms of DC stability, gate duration stability and synchronisation with a valid event. The implementation of the switches in the analogue paths, requiring fast switching of voltages floating at signal levels, caused problems too. Solutions included the use of double-emitter transistors and diode bridges with rather complex driving circuits.

One aim of the research work described here, was the development of a high performance versatile analogue pulse processor. The remaining sections of this chapter describe how modern electronic components and innovative circuit techniques were used to overcome the limitations associated with the Harwell processor.

Figure 4.1.1 is a block diagram of the analogue circuit developed. The unit has the time-variant integrating and differentiating time-constants and the gated integrator associated with the Harwell processor. The unit's versatility, however, is enhanced by the development of a pole-zero compensator that allows passively restored charge-amplifiers to be used, by the availability of a wide selection of gain setting and by the provision of a wide choice of processing times. The ability to control system parameters from a remote computer is another important enhancement. The processor was designed as a NIM (Nuclear Instrument Module) standard unit[39].
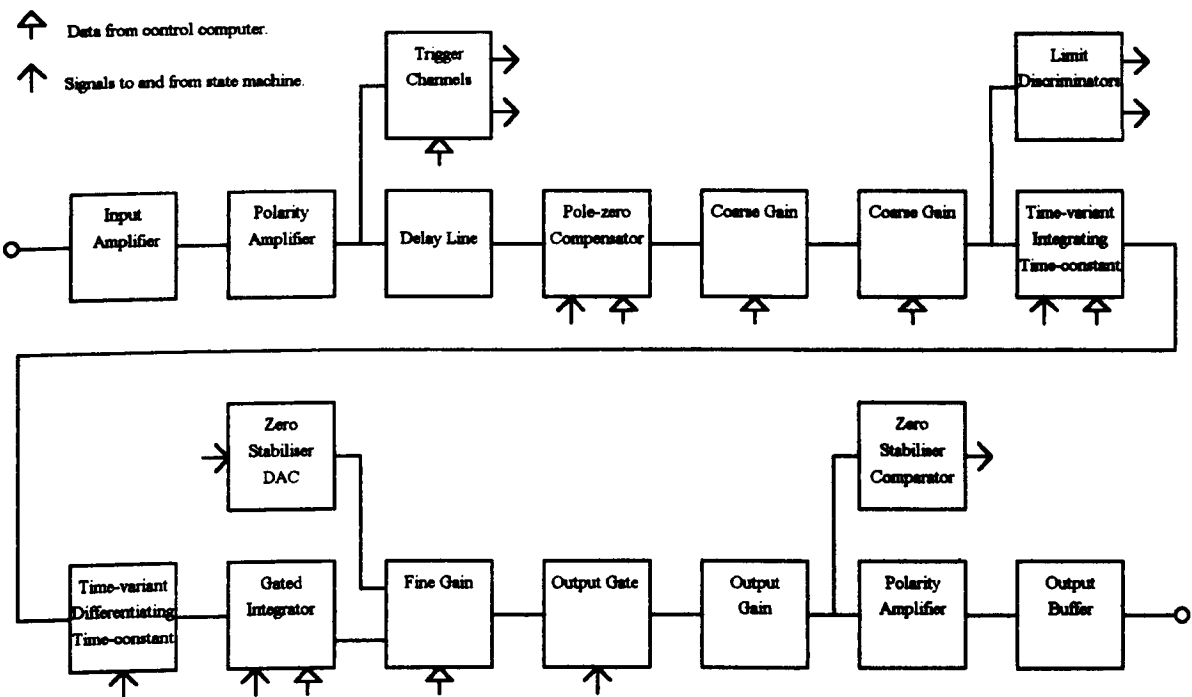
Fig 4.1.1

4.2 : BASELINE RESTORE CIRCUIT

The switched time-constant 'differentiator' in the processing circuit is referred to here as a baseline restorer, but this nomenclature has to be qualified.

Baseline restore (BLR) circuits were originally developed to maintain a constant baseline in AC coupled amplifiers handling unipolar shaped pulses. The AC coupling caused the baseline to shift with input rate, and this was highly undesirable in a pulse-height analysis system. One type of baseline restoration, known as gated passive restoration, is shown in Figure 4.2.1.

Fig 4.2.1

The gate is open during a valid pulse so that the BLR circuit does not affect the output pulse shape, but the baseline is differentiated by the time-constant C_bR_b. It can be shown[40] that C_bR_b needs to be greater than the autocorrelation time of the noise, otherwise the noise frozen on the capacitor when the gate is opened is comparable to the 'live' noise measured at the 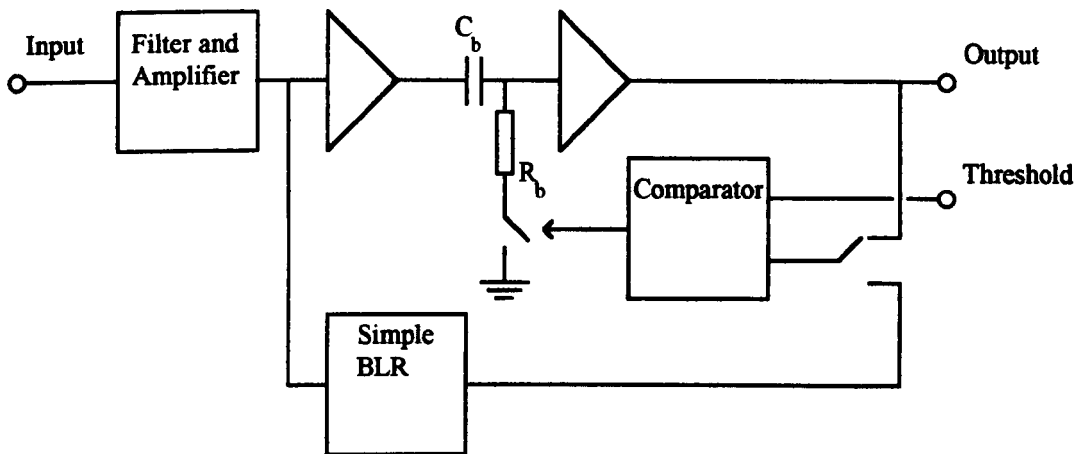peaking time. However, as pulse rates increase, the effectiveness of the BLR diminishes, as there is less time for the circuit to restore the baseline before the next event, unless C_bR_b is reduced. It is usually the case that these circuits have a time constant that is varied with input pulse rate. (At the highest rates, effective baseline restoration is not possible and bipolar shaping has to be used, as discussed in Section 3.1.) An added benefit of having a baseline restorer is that low frequency fluctuations are removed from the output.

Fig 4.2.2

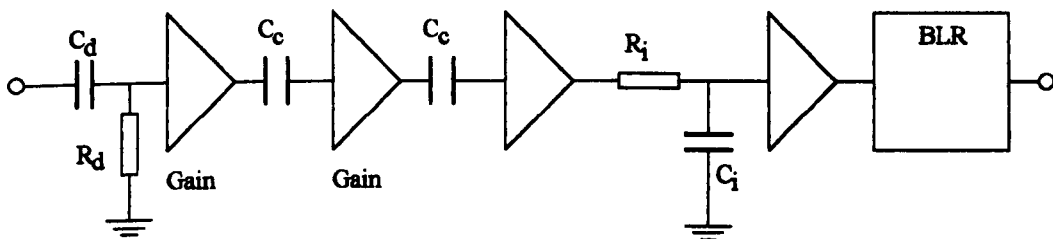Figure 4.2.2 shows a conventional time-invariant pulse shaping system. The differentiating time constant C_dR_d provides high-pass filtering of the input signal and eliminates the effect of the long tail of the charge-amplifier's output pulse. The AC coupling capacitors C_c alleviate the problems of DC coupling amplifier stages, but cause baseline shifts that have to be removed by the BLR circuit at the output.
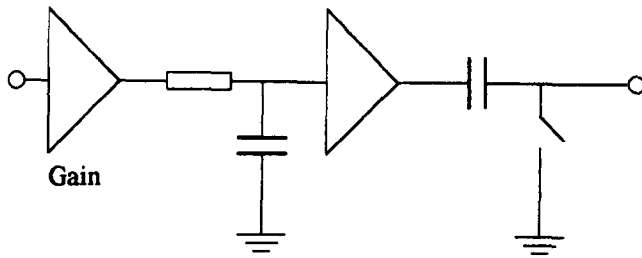
Fig 4.2.3

The time-constants in the Harwell processor is shown in Figure 4.2.3. The system is essentially DC coupled and baseline shifting with input rate does not happen. However with a DC coupled system, a small offset at the input is magnified to give a large offset in the output baseline. Such offsets can arise, for example, from small fluctuations in the charge amplifier's baseline due to the integration of leakage currents. The switched time-constant differentiator acts to remove this spurious DC level from the output signal, whilst providing high pass filtering of the signal too. If the charge-amplifier is a limit restore type, the function of the input differentiator of the time-invariant system is also replicated in that the residual effect of previous pulses is removed from the output.

To implement the switched time-constant differentiator, a high quality fast switch is needed. A diode bridge could be used, but it was decided that a more compact solution was required. The problems in using an analogue switch are caused by the finite switch on-resistance and the charge injected by the opening or closing of the switch. For example, if the 4316 analogue switch is considered (it has, perhaps, the best specification for this function), R_{on} is typically 50 to 60 ohms, and the injected charge will be of the order of 10pC. The capacitance C_b required to absorb this charge with a negligible voltage step of 0.5mV (less than 1 channel in 8192 for a 5V MCA) will be 10nF. The restoration time constant of $C_b R_{on}$ is then too long at 0.5μs. If a short processing time of 0.5μs is used, the dead-time (T_d and T_{xo}) after the closure of the BLR switch might only be 0.5μs. If we assume that seven time-constants are required for the baseline to have been restored to an insignificant level, it can be seen that this time-constant needs to be in the region of 50nS.
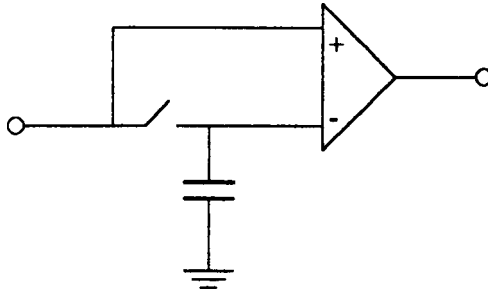
Fig 4.2.4

In an attempt to avoid using analogue switches, the possibility of using Track and Hold (T&H) integrated circuits to implement the BLR was investigated. The basic idea is developed from the fact that the voltage measured is that appearing across the switch in a switch/capacitor series arrangement. The structure shown in Figure 4.2.4 is therefore another form of the BLR circuit, but the switch/capacitor arrangement is now that of a T&H circuit. The speed and accuracy requirements of the T&H circuit are exacting, and two of the most promising devices (Comlinear CLC940 and Analog Devices AD9100) proved unsuitable due to the noise generated in 'hold' mode for one device, and an input level dependent droop rate in the other.
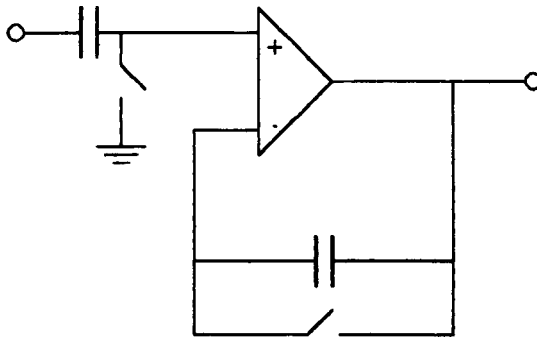
Fig 4.2.5

The effect of charge injection can be compensated by the arrangement shown in Figure 4.2.5. A similar switch is opened and closed simultaneously with the BLR switch, and the injected charge is integrated in a similar capacitor; a differential amplifier subtracts the error from the output. It has been shown[41] that the voltage step can be reduced by a factor of twenty by the charge compensation method. This allows a capacitor of 1000pF to be used, and the discharging time-constant is acceptable.

Smaller capacitors could be discharged by the bias currents of the differential amplifier and, ideally, an FET input device is used. The Elantec EL2006 has proved to be an useful device in this function.

4.3 : PROCESSING TIME REQUIREMENTS

A versatile amplifier needs to have a wide range of shaping times available. The optimum shaping for a semi-conductor surface barrier detector would be typically $0.5\mu s$. For HPGe detectors, the optimum shaping might be $2\mu s$, with shorter times used at high rates. Silicon detectors used for high resolution X-ray spectrometry might use shaping times greater than $10\mu s$. When considering other types of detectors, scintillation detectors having large parallel noise would need short shaping, whilst gas proportional counters, having large series noise and slow rise-times, would need longer shaping times in the region of $2\mu s$ to $10\mu s$.

It was decided to implement a selection of eight processing times namely 0.5, 1, 2, 4, 8, 16, 32 and $64\mu s$.
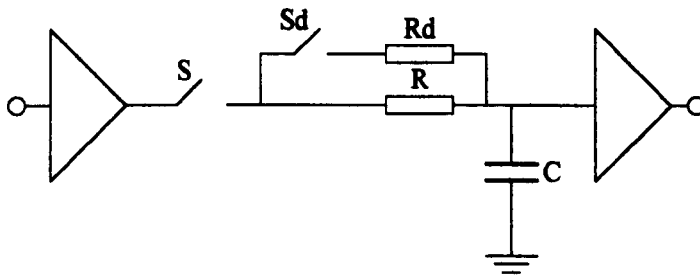
Fig 4.3.1

The filter section to be implemented is shown in Figure 4.3.1. The charging time-constant RC, will be selectable between 0.25 and $32\mu s$, whilst the discharging time-constant needs to be approximately 1/10th of RC.

The arrangement shown in Figure 4.3.1 is not an ideal one in which to use FET analogue switches due to the difficulties of switching the FET hard-on and hard-off, given that the source and drain are floating at signal levels ranging over several volts. CMOS switches are useful in that any signal level between the supply rails can be accommodated. However, the on-resistance can vary significantly with signal level.

This effect gets worse as the supply voltage is reduced. Unfortunately, the lowest supply voltage commensurate with the signal levels is required to limit charge injection, which is caused by the drive waveform coupling into the FET channel through the gate-channel capacitance.
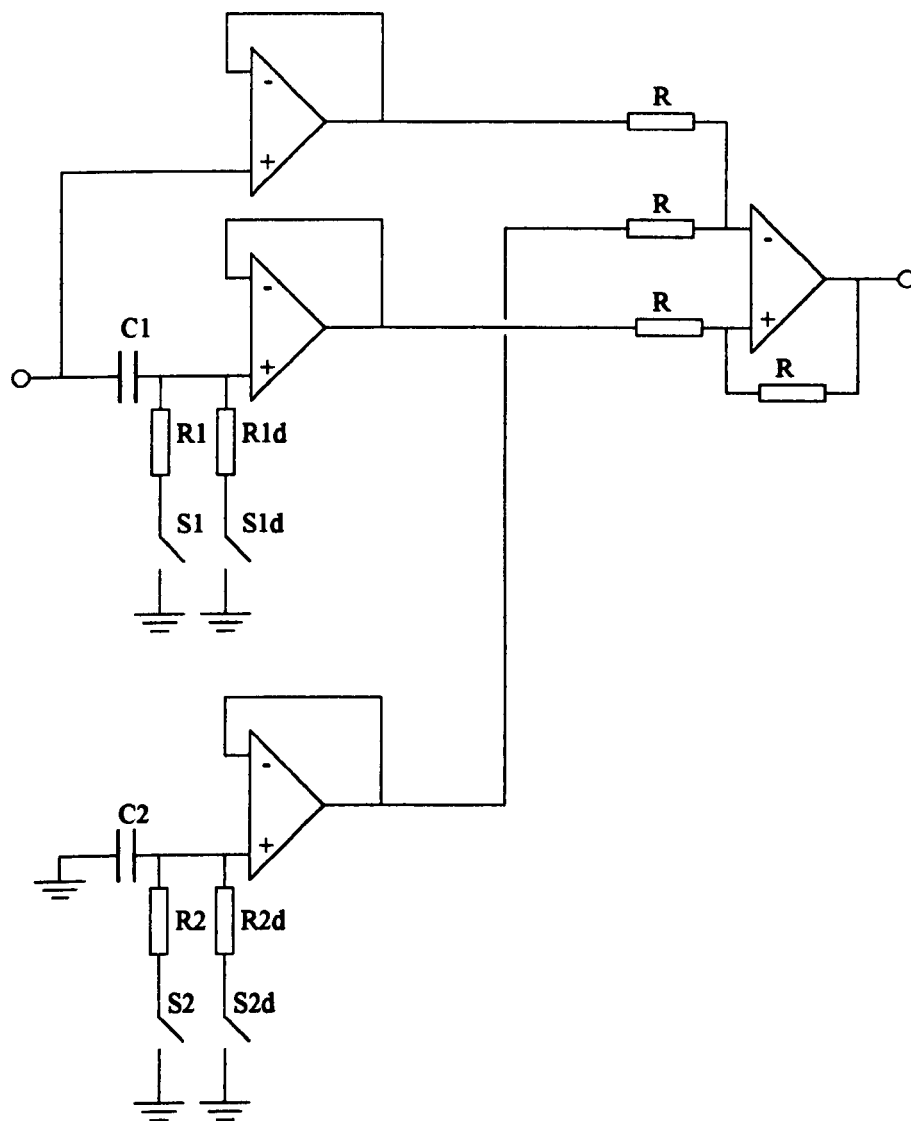
Fig 4.3.2

These problems can be alleviated by re-arranging the filter as shown in Figure 4.3.2[45]. Now the closed FET switch only passes signals close to ground potential. It can be seen that when the switches S_1 and S_{1d} open, any signal at the input is applied to both inverting and non-inverting inputs of the differential amplifier and the output point does not move; this is equivalent to opening S in Figure 4.3.1. When S_1 is closed, the differential amplifier outputs the voltage developed across the capacitor C_1 in a series combination with R_1; the analogy in Figure 4.3.1 is the closure of S. When the shorter discharging time constant is required, S_1 is opened and S_{1d} is closed, a function implemented by closing S and S_d in Figure 4.3.1.

47

The paralleled arrangement C_2, R_2, S_2 etc., is used to generate charge compensation as discussed in Section 4.2, switches S_2 and S_{2d} opening and closing in unison with S_1 and S_{1d}.

By making the discharging time-constant 1/8th of the charging time-constant, the number of resistor-switch combinations can be reduced, some being used for charging at one set processing time and for discharging at another.

For the shorter time constants, it is necessary to parallel two and four analogue switches to achieve the required series resistance.

4.4 : GATED INTEGRATOR

The basic structure of the gated integrator is shown in Figure 4.4.1.
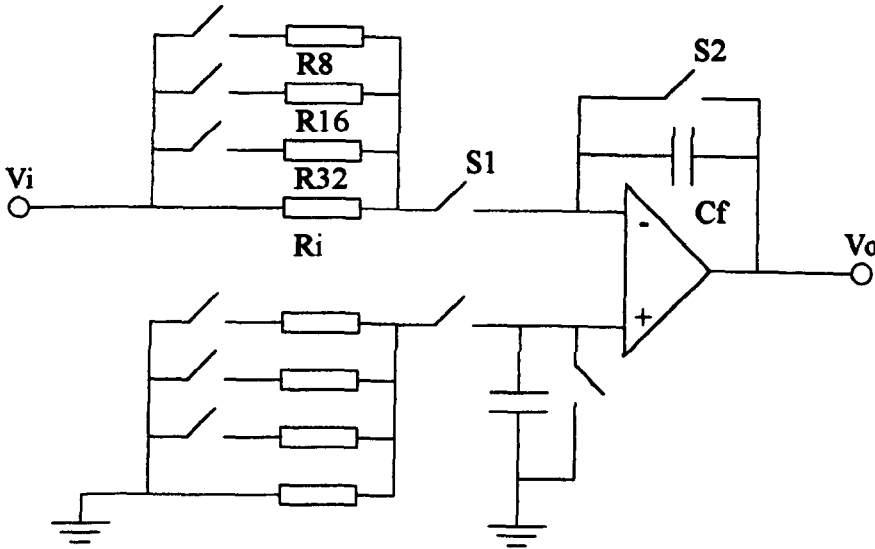
Fig 4.4.1

The output is given by :

$$V_o = \frac{1}{R_S C_F} \int_0^T V_i dt$$

where R_S is the parallel combination of R_i and one of R_{32}, R_{16}, R_8 etc., selected by the choice of processing time to maintain a constant gain (see Section 4.9).

Switch S_1 is a CMOS switch that allows the integration of V_i during the processing time T. With one end connected to the virtual earth, there are no driving problems

associated with this arrangement. Switch S_2 resets the integrator after the output pulse has been sampled by the MCA. In fact, the integrator is then held in the reset state until just before the arrival of the next pulse; this eliminates the integration of the op-amp bias current in-between pulses. The op-amp needs to have an FET input stage to reduce these bias currents, and the Elantec EL2006 is a good choice.

As in the circuits described in Sections 4.2 and 4.3, there is a balance circuit connected to the non-inverting input that injects a charge into the dummy capacitor to offset the analogue switch charge injection.

4.5 : POLE-ZERO COMPENSATION

When the theory of pulse shaping was discussed in Section 3.1, it was assumed that the signal from the charge-amplifier was a voltage step produced by the integration of an impulse of charge on the input capacitor. Figure 4.5.1 shows this arrangement for a simple CR-RC shaper.
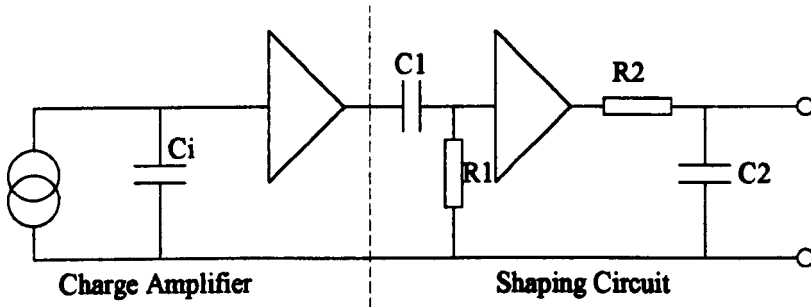
Fig 4.5.1

The Laplace transform of the output waveform is given by :

$$V_o = \frac{T_1}{C_i(1+ST_1)(1+ST_2)} \qquad (4.5.1)$$

This is the uni-polar semi-Gaussian shape expected. Many charge-amplifiers, however, have charge feedback via a resistor. Figure 4.5.2 shows the modified circuit.
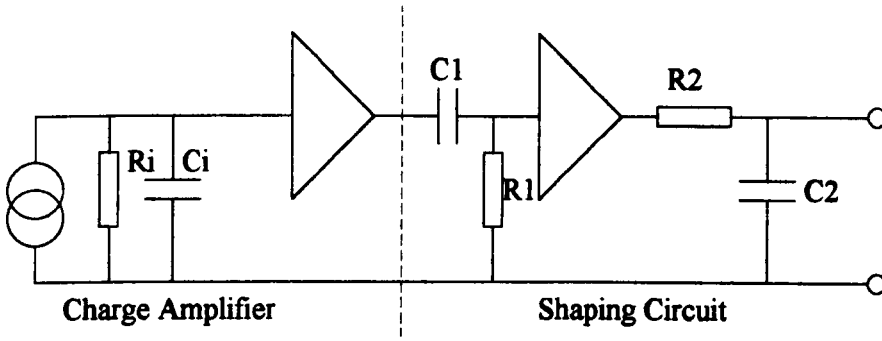
Fig 4.5.2

The output waveform is now given by :

$$V_o = \frac{ST_i T_1}{C_i(1+ST_i)(1+ST_1)(1+ST_2)}$$
(4.5.2)

This waveform is not unipolar; it has a negative undershoot that can last for a long time, particularly when a large overloading pulse arrives. Baseline restorers may not completely remove this source of error, e.g. the conventional gated BLR described in Section 4.2 cannot remove the slope of the undershoot during the next pulse when the differentiating action is suspended.

Nowlin and Blankenship[42] devised a method of pole-zero compensation whereby the pole of the input circuit at $-\dfrac{1}{T_i}$ is cancelled by a zero in the differentiator. The modified differentiator is shown in Figure 4.5.3.
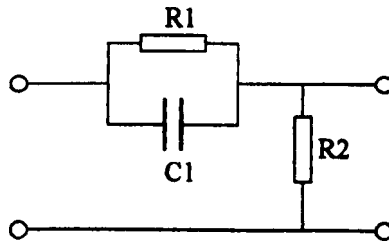
Fig 4.5.3

The transfer function is given by :

$$H(s) = \frac{s+a}{s+b}$$

50

where $a = \dfrac{1}{R_1 C_1}$ and $b = \dfrac{1}{C_1}\left[\dfrac{1}{R_1} + \dfrac{1}{R_2}\right]$ \hfill (4.5.3)

If the component values can be modified to give :

$$a = \frac{1}{T_i} \text{ and } b = \frac{1}{T_1} \hfill (4.5.4)$$

then the transfer function is given by :

$$H(s) = \frac{s + \dfrac{1}{T_i}}{s + \dfrac{1}{T_1}} \hfill (4.5.5)$$

The output waveform is now given by :

$$V_o(s) = \frac{T_i}{C_i(1 + sT_i)} \times \frac{s + \dfrac{1}{T_i}}{s + \dfrac{1}{T_1}} \times \frac{1}{(1 + sT_2)}$$

$$V_o(s) = \frac{T_1}{C_i(1 + sT_1)(1 + sT_2)} \hfill (4.5.6)$$

The waveform is unipolar again, and is identical to the waveform produced by passing a voltage step through the simple CR section.

Limit restore or pulse-by-pulse restore charge amplifiers have always been used with the Harwell time-variant processors. A new type of pole-zero compensator is needed to generate the staircase type waveform, favoured by the processor, from resistor restored charge amplifiers.
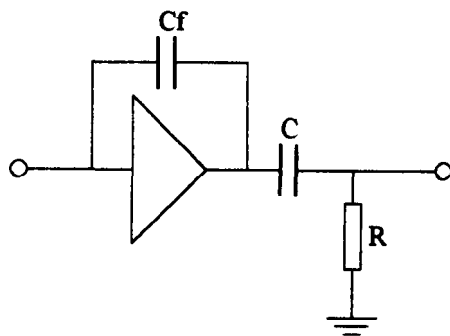
Fig 4.5.4

Figure 4.5.4 shows the equivalent circuit of the resistor restored charge-amplifier. The differentiator at the output, having the transfer function $\dfrac{sCR}{1+sCR}$, represents the unwanted function that must be eliminated. Figure 4.5.5 illustrates a compensation scheme[46].
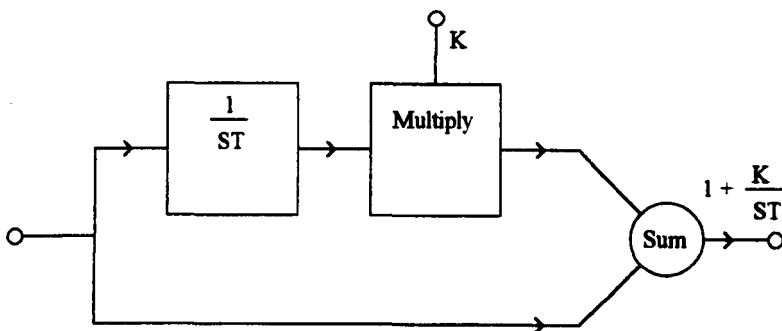
Fig 4.5.5

The overall transfer function can be seen to be :

$$H(s) = \frac{\dfrac{sT}{K}+1}{\dfrac{sT}{K}} \tag{4.5.7}$$

If $\dfrac{T}{K} = CR$, then the compensation will be perfect. The function $\dfrac{1}{sT}$ can be implemented with an op-amp integrator (see Figure 4.5.6) where $T = C_i R_i$. A practical implementation of the pole-zero circuit is shown in Figure 4.5.7.
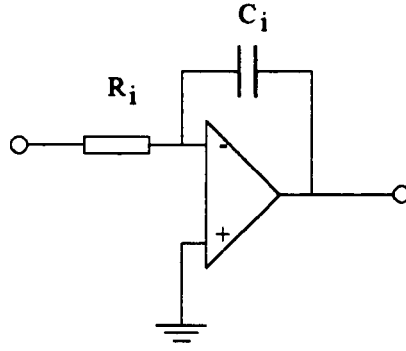
Fig 4.5.6
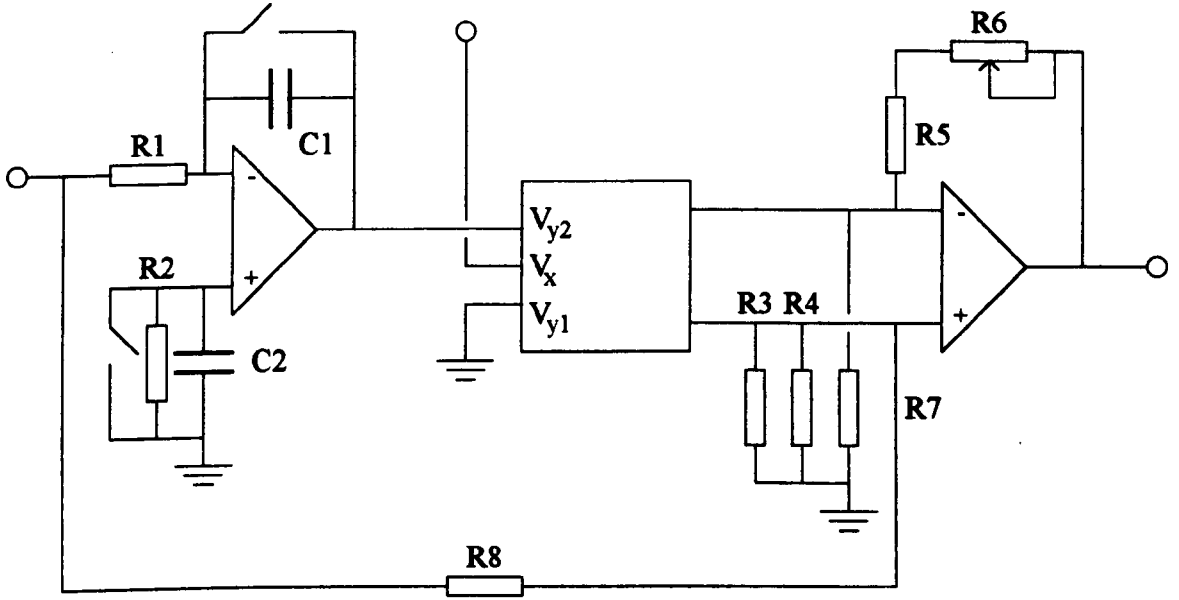
Fig 4.5.7

The op-amp integrator is similar to the one used in the gated integrator (see Section 4.4). The analogue multiplier is similar to the circuit used for setting the system's fine gain (see Section 4.9); the output voltage is given by :

$$V_o = \frac{V_x}{2}\left(V_{y1} - V_{y2}\right)$$

$$V_o = \frac{-V_x V_{y2}}{2} \qquad (4.5.8)$$

To this multiplier output voltage, an attenuated version of the original signal is added via R_8. The value of this series resistance determines the attenuation (in conjunction with the fixed values of R_3, R_4, R_5, R_6 and R_7).

53

If $R_1C_1 = 60\mu s$ and $V_x = 0V$ to $3V$, then the charge amplifier decay times that can be compensated range from 40μs (K=1.5) to ∞ (K=0). In fact, the range is limited by the maximum signal allowed at the input of the multiplier.

If the attenuation of the pole-zero circuit is set to 8, and the minimum coarse gain is set to 8, the maximum signal level at the output of the pole-zero circuit is approximately 250mV before the processor gets overloaded. With the multiplier input levels limited to +/- 2V, the minimum value of K allowed is therefore 0.125. This limits the maximum charge amplifier decay time-constant to 480μs. Modern charge amplifiers, particularly ones designed for high rates , tend to have decay time-constants set to less than 100μs.

The integrator needs to be reset periodically to avoid saturation. In this scheme the reset pulse is applied during T_h immediately after the processing time. Typical waveforms are shown in Figure 4.5.8.

It can be seen that there is a residual offset voltage after resetting the integrator. This offset is removed by the BLR. It is the flatness of this baseline that allows the tailed pulses to be processed without error. In the absence of the pole-zero circuit, the slope of the baseline during a pile-up acts to subtract a variable amount from the height of the pulse being processed, leading to low energy tailing.

One disadvantage of this pole-zero compensating scheme is that the output of the circuit is restored to a voltage that is only a little lower than the gross height of the previous pulse. The input rate at which the processor overloads is therefore lower.

waveform into pole-zero circuit

Fig 4.5.8a

waveform generated by pole-zero circuit integrator

Fig 4.5.8b

pole-zero circuit output waveform
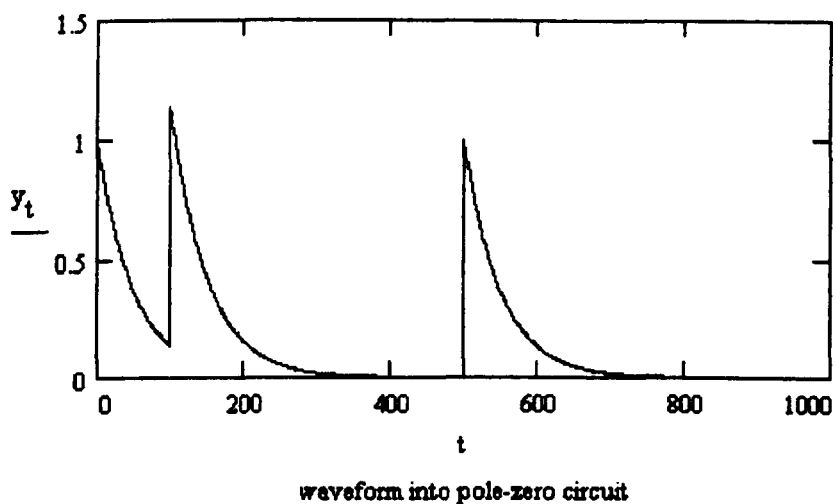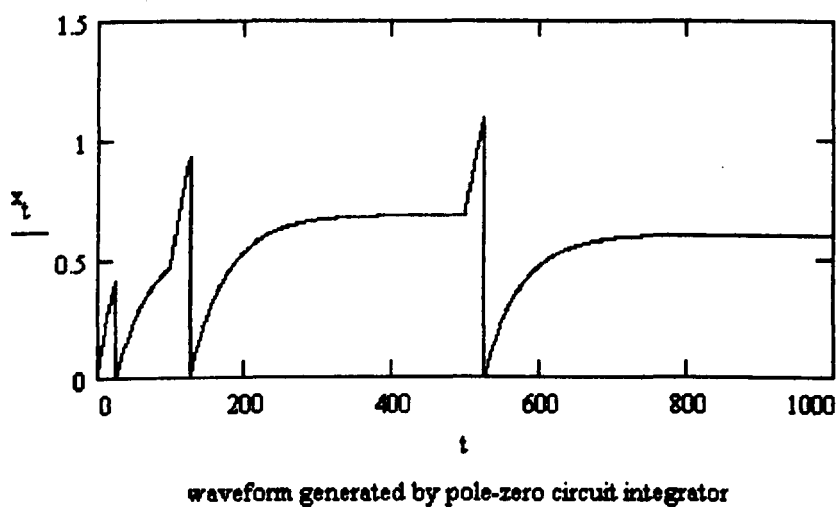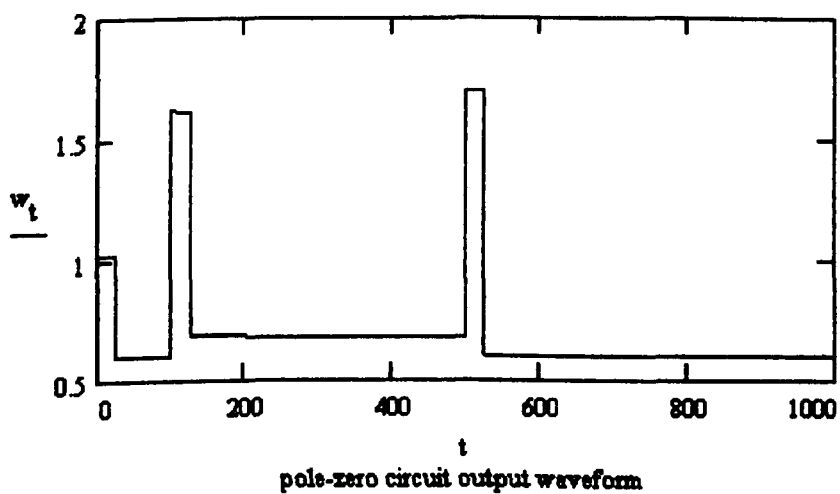
Fig 4.5.8c

4.6 : ZERO STABILISER CIRCUIT

It is important that the zero level of this essentially DC coupled system is maintained. One cause of variable baseline at the output might be the temperature dependent offsets of the components following the BLR. The other major cause can be described as charge-amplifier output slew, caused by the integration of FET leakage currents. This causes the charge amplifier baseline to ramp linearly until the processors' limit discriminators fire to initiate a charge-amplifier reset. Detector pulses are imposed on the sawtooth baseline, and a component of the baseline slope is added to the measured pulse height. The effect is not insignificant when room temperature FETs are used.

These offset errors can be minimised by periodically initiating a full processing cycle in the absence of a valid pulse. The output pulse height is then a measure of the system's zero energy level. Figure 4.6.1 shows how the zero stabiliser is arranged.
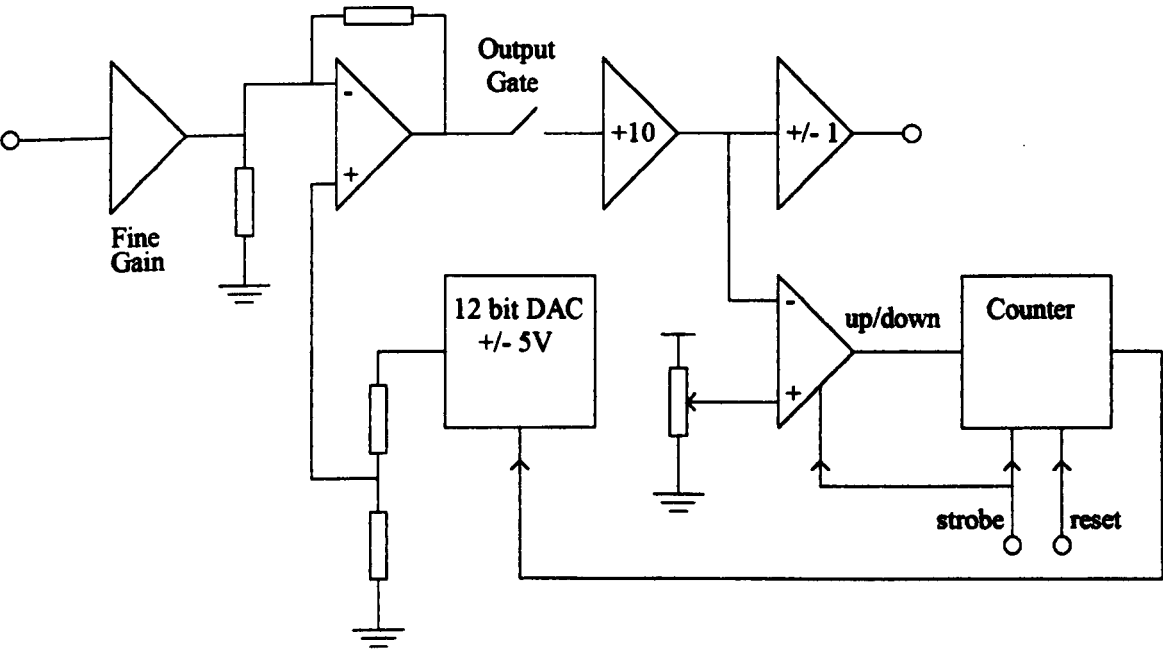
Fig 4.6.1

When the output gate is closed, the discriminator is enabled by the zero strobe. Depending on whether the output level of the processor is above or below the pre-set pedestal level, an up or down signal is generated that is used by a 12bit counter clocked on the back edge of the zero strobe. This counter, driving a DAC, controls an offset voltage added at the output of the fine gain stage. The output baseline can be changed by +/- 1.5V; this is equivalent to 0.7mV/bit for the DAC.

A divide by 2048 counter counts 1MHz clock pulses and generates a request for zero stabilisation every 2mS. When the processor becomes free, it enters the zero stabilising cycle, resetting this counter. The cycle will be aborted if a valid event occurs before the end of the processing time.

This system will output the zero event as a pulse for storage in a MCA. The resolution of this line is an useful indication of the electronic noise of the system and can be used to check system integrity. In the event that such a line is not required, the zero strobe signal, routed to an external connector, can be used to inhibit the MCA.

4.7 : TRIGGER CIRCUITS

This time-variant system needs advanced warning that an event is about to happen, so that switches in the signal path can be activated just before the signal's arrival. The way in which this is done is shown in Figure 4.7.1.
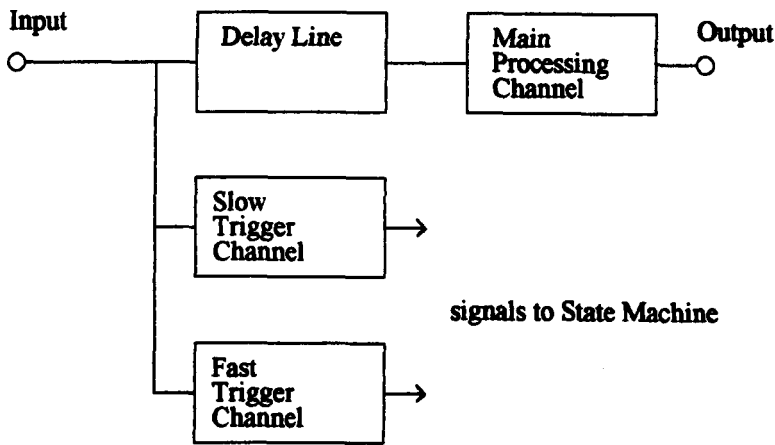
Fig 4.7.1

Independent signal shaping channels are used to decide if a signal is present. The state-machine, acting on signals from these trigger channels, has time to activate switches because the signal has to pass through a delay line on its way to the main processing channel.

The trigger channels are conventional time-invariant shapers. In this circuit, $(CR)^2$-RC shaping is used with CR time-constants of 200nS in the slow channel and 20nS in the fast channel. Figure 4.7.2 shows the arrangement of one channel. An eight bit DAC controls the threshold, set just above noise triggers.

Fig 4.7.2
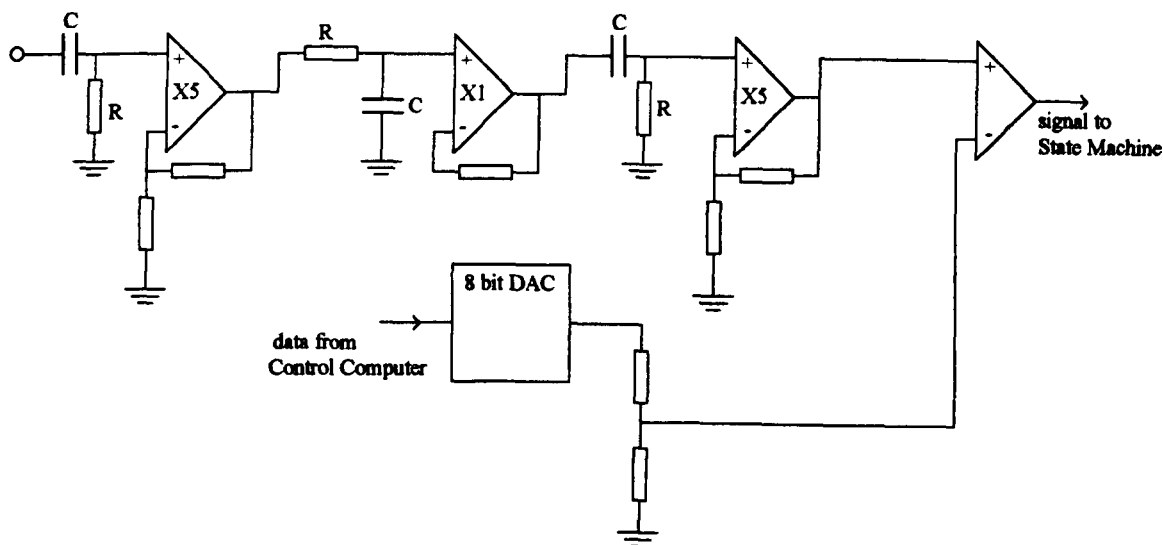
Of the two channels, the fast shaping has greater resolving time and can distinguish events that are closer together. The slow channel has a narrower bandwidth and therefore lower noise; the discriminator threshold can be lowered so that small amplitude signals can be detected. The state-machine uses the slow channel to initiate processing and either channel to detect pile-up.

4.8 : BANDWIDTH REQUIREMENTS

The Harwell pulse processing system might be represented by the simplified structure shown in Figure 4.8.1. It is useful to consider the effect of a finite input amplifier bandwidth, and how the output of the system is affected.
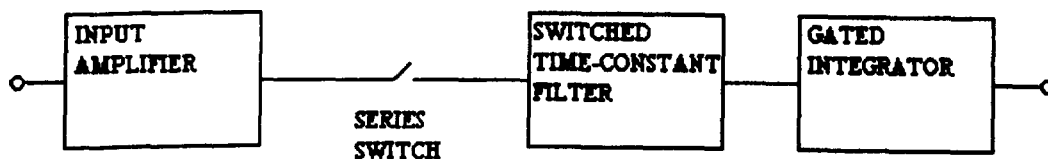
Fig 4.8.1

In Appendix 1, the error in the final amplitude of the gated integrator pulse is calculated for input amplifier bandwidths of 32MHz, 16MHz and 6.4MHz. The input signal rise-time is assumed to equal the series-switch time of 500nS. The charging time-constant of the filter is set to $1\mu S$ or 250nS, with the corresponding processing time set to $2\mu S$ or 500ns. Figures 4.8.2a and 4.8.2b show how the error settles to a final value.
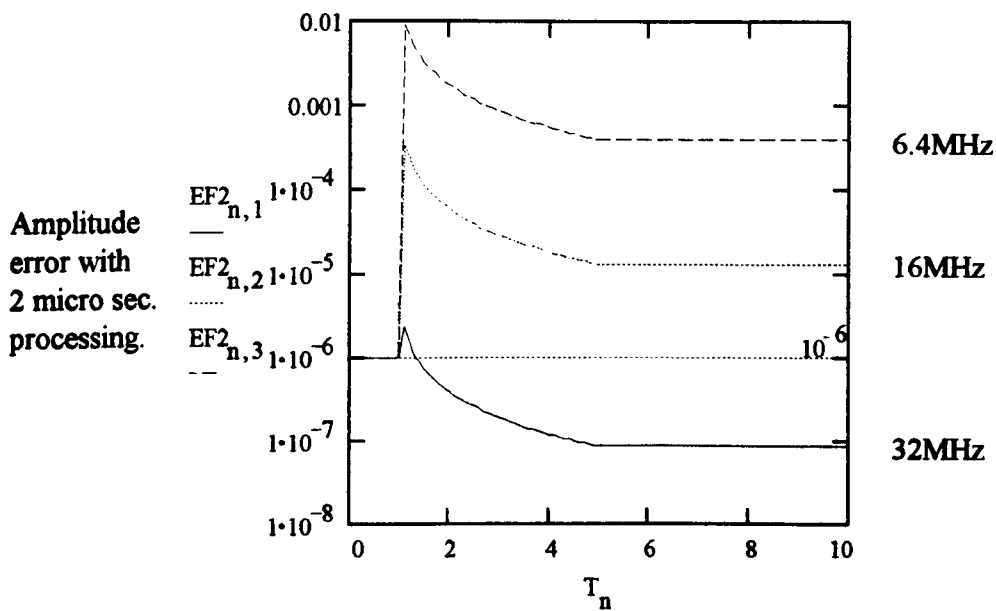
Amplitude error with 2 micro sec. processing.

$EF2_{n,1}$ ——
$EF2_{n,2}$ ·······
$EF2_{n,3}$ – –

Time measured in relation to collection time.

Fig 4.8.2a

Amplitude error with 250 nano sec. processing.

$EF1_{n,1}$ ——
$EF1_{n,2}$ ·······
$EF1_{n,3}$ – –
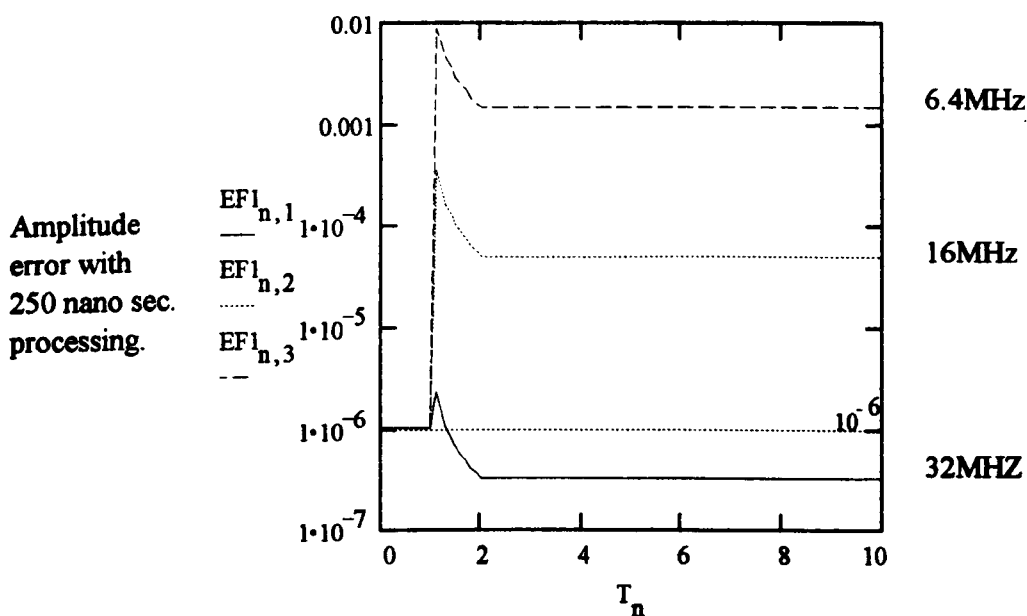
Time measured in relation to collection time.

Fig 4.8.2b

It can be seen that a shorter processing time causes greater errors, and that a bandwidth of 16MHz is required if the final error is not to exceed 0.01% (less than one channel in an 8K Multi-channel Analyser).

For a number n of RC sections in series, the overall rise-time t_{ro} is related to the individual rise-time t_r by the approximation $t_{ro} \approx \sqrt{n} \times t_r$, and t_r is related to 3dB

59

frequency by the approximation $t_r \times f_h \approx 0.35$[43]. It can be deduced that the bandwidth requirement of an individual amplifier in our system is given by:

$$f_h \approx f_{ho} \times \sqrt{n}$$

(4.8.1)

For six amplifier rings in the input stage, each amplifier should have a bandwidth of 40MHz. Implementing such wideband amplifiers, having variable closed-loop gains proved difficult in the past.

In the last few years, a number of wideband current-feedback amplifiers have been made available by companies such as Comlinear and Elantec. The performance of these devices make them indispensable as analogue building blocks in the design of a modern 'Harwell' processor.
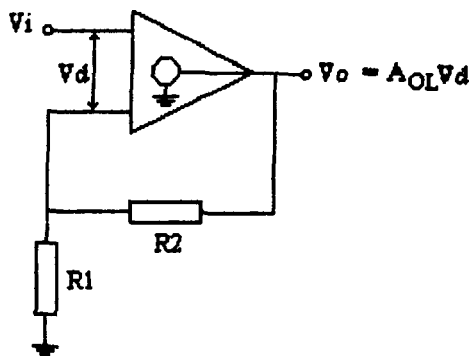
Fig 4.8.3

For the conventional amplifier shown in Figure 4.8.3, the closed loop gain is given by:

$$A_{CL}(jf) = \left(1 + \frac{R_2}{R_1}\right) \times \left(\frac{1}{1 + \frac{1}{T(jf)}}\right)$$

(4.8.2)

where T(jf) is the loop gain, given by:

$$T(jf) = \beta \times A_{OL}(jf)$$

(4.8.3)

where β is the feedback fraction, given by:

$$\beta = \frac{R_1}{R_1 + R_2}$$

(4.8.4)

and $A_{OL}(jf)$ is the open loop gain given by:

$$A_{OL}(jf) = \frac{A_{OL}}{1 + \dfrac{jf}{f_{OL}}}$$

(4.8.5)

These equations can be manipulated to give the result:

$$A_{CL}(jf) = \frac{1 + \dfrac{R_2}{R_1}}{1 + \dfrac{jf}{f_{CL}}}$$

(4.8.6)

$$\text{where } f_{CL} = \frac{f_{OL} \times A_{OL}}{1 + \dfrac{R_2}{R_1}}$$

It can be seen that as the closed loop gain is increased, the closed loop gain bandwidth is decreased. A graphical illustration is shown in Figure 4.8.4.
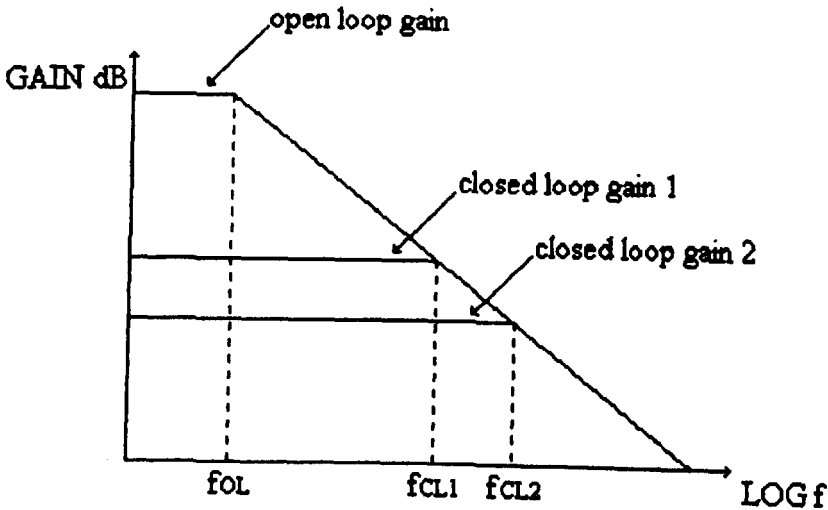
Fig 4.8.4

The situation for current feedback amplifiers is quite different. Figure 4.8.5 shows that V_o is given by $Z(jf)I_n$, where $Z(jf)$ is the transimpedance gain of the amplifier and I_n is the current flowing out of the negative terminal to maintain zero volts across the amplifier input terminals.

61

$$I_n = \frac{V_i}{R_1} - \frac{V_o - V_i}{R_2}$$

$$I_n = \frac{V_i(R_1 + R_2)}{R_1 \times R_2} - \frac{V_o}{R_2} \tag{4.8.7}$$

This equation can be manipulated to give :

$$A_{CL} = \left(1 + \frac{R_2}{R_1}\right) \times \left(\frac{1}{1 + \frac{1}{T(jf)}}\right) \tag{4.8.8}$$

Again, T(jf) is the loop gain, but now it is given by:

$$T(jf) = \frac{Z(jf)}{R_2} \tag{4.8.9}$$

where Z(jf) is the frequency dependent transimpedance gain given by[44]:

$$Z(jf) = \frac{Z}{1 + \frac{jf}{f_z}} \tag{4.8.10}$$

The closed loop gain can be shown to be:

$$A_{CL}(jf) = \frac{1 + \frac{R_2}{R_1}}{1 + \frac{jf}{f_{CL}}} \tag{4.8.11}$$

$$\text{where } f_{CL} = \frac{f_z \times Z}{R_2}$$

It is seen that the closed loop bandwidth is determined by the value of the feedback resistor and not by the value of the closed loop gain. Current feedback amplifiers allow the bandwidth to be maintained as the gain is increased. The penalty is that a feedback resistor of optimised value has to be used.
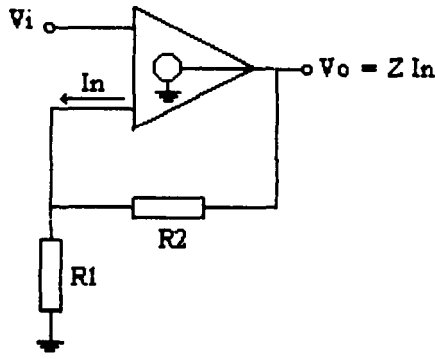
Fig 4.8.5

4.9 : GAIN REQUIREMENTS

Figure 4.9.1 shows how the gain of the system is distributed through the processing circuits.
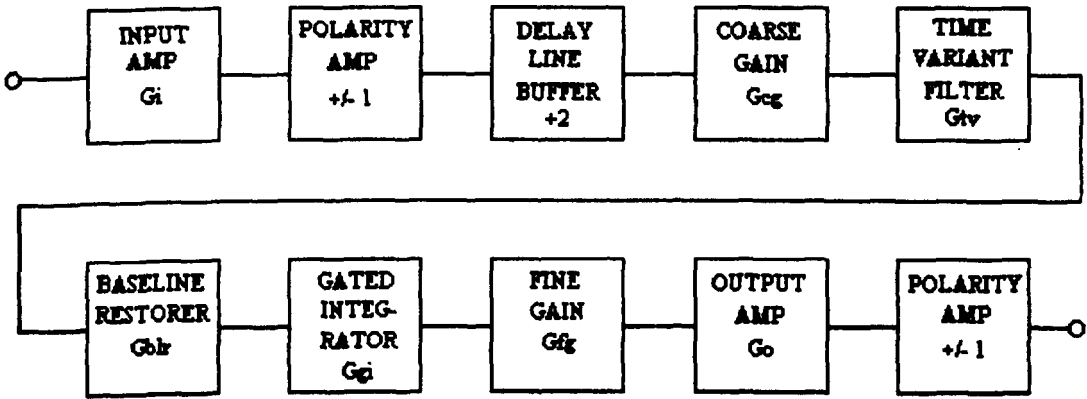
Fig 4.9.1

The normalised output of the time-variant filter will be $1 - \exp\left(\dfrac{-T}{\tau_1}\right)$ where T is the processing time and τ_1 is the circuit time-constant. If $T = 2\tau_1$ is assumed, then:

$$G_{tv} = 0.865 \qquad\qquad (4.9.1).$$

The normalised output of the gated integrator will be :

$$G_{tv}G_{gi} = \frac{-1}{\tau_2}\int_0^T \left(1 - \exp\left(\frac{-t}{\tau_1}\right)\right)dt \qquad\qquad (4.9.2)$$

where τ_2 is the product of the gated integrator's input resistance and feedback capacitance.

$$G_{tv}G_{gi} = \frac{-T}{\tau_2} \times 0.568 \qquad \text{if } T = 2\tau_1$$

$$\therefore G_{gi} = \frac{-T}{\tau_2} \times 0.657$$

$$G_{gi} = -0.263 \qquad \text{when } \frac{T}{\tau_2} = \frac{1}{2.5} \qquad\qquad (4.9.3)$$

If $\tau_2 = 2.5 \times T$ is used, larger valued input resistors can be used in the gated integrator, and the resistance of the input analogue switch is made less significant. It should be noted that if gain is not to change with a change in the processing time, the active integrator time constant should change in tandem. This is put into effect by switching in a different series resistance.

For gamma-ray detection in Ge detectors, the input signal amplitude will range from typically 4mV (100KeV into a 1.5pF integrating capacitor in the charge-amplifier) to 220mV (2MeV into a 0.5pF capacitor). To generate a typical NIM output pulse of 10V, system gains of 50 to 2500 are necessary. If smaller signals from Si X-ray detectors are to be accommodated, an upper gain of 5000 might be needed. The system gain in our implementation (see Figure 4.9.1) is given by:

$$G_{sys} = G_i \times G_{cg} \times G_{tv} \times G_{blr} \times G_{gi} \times G_{fg} \times G_o \qquad\qquad (4.9.4)$$

The gain of the delay line buffer only compensates for the losses incurred in terminating the delay line in its characteristics impedance. The system gain can be distributed as an input gain of 8, a coarse gain of 1, 2, 4, 8, 16, 32 or 64, a continuous fine gain of 0.5 to 1.5 and an output gain of 10. This latter figure is necessary as the fine gain stage is output amplitude limited to 2Volts in our implementation. The gain of the baseline restore circuit is therefore set to:

$$G_{blr} = \frac{1}{G_{gi}G_{tv}} \times \frac{50}{80} = 2.747 \qquad\qquad (4.9.5)$$

The overall system gain is therefore variable from 25 to 4800.

The coarse gain can be changed simply by switching various resistors to ground in an op-amp circuit, as shown in Figure 4.9.2.
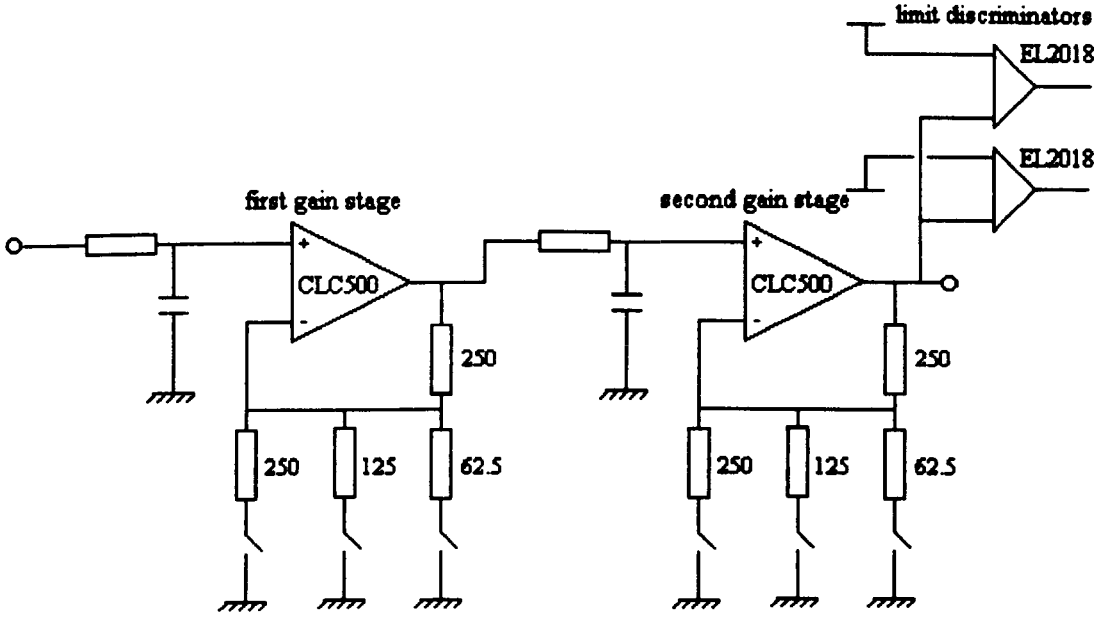
Fig 4.9.2

The use of relays eliminate the errors introduced by finite analogue switch resistance but the capacitance of the open contacts can cause deleterious effects.

It was shown in Section 4.8 that the loop-gain of a current feedback amplifier is given by :

$$T(jf) = \frac{Z(jf)}{R_2} \qquad (4.9.6)$$

The stricter definition[44] of loop-gain gives:

$$T(jf) = \frac{Z(jf)}{Z_t} \qquad (4.9.7)$$

where $Z(jf)$ is the internal forward transimpedance and Z_t is the feedback transimpedance given by:

$$Z_t = R_f + R_i\left(1 + \frac{R_f}{R_g}\right) \qquad (4.9.8)$$

where R_i is the finite output impedance at the inverting terminal of the amplifier. It is this definition of loop-gain that accounts for some variation in closed loop bandwidth

65

with closed loop gain for a fixed feedback resistor. The closed loop bandwidth and phase margin is determined by the intersection of the Z(s) and Z_t Bode plots (see Figure 4.9.3).
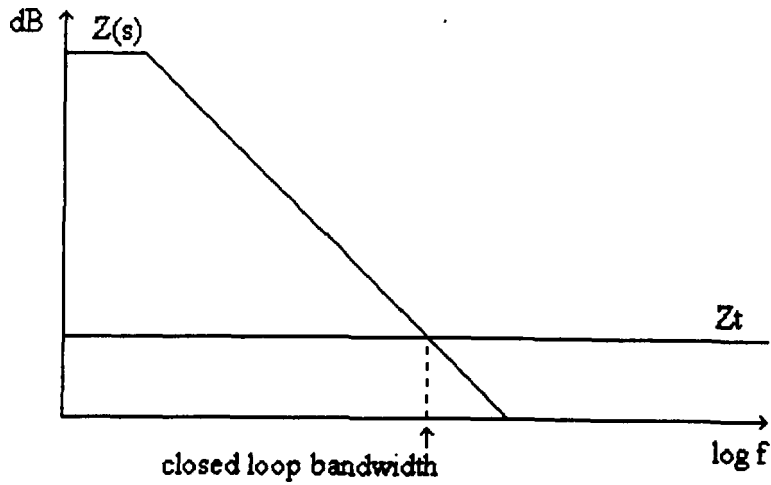
Fig 4.9.3

If there is significant capacitance C_g in parallel with the gain setting resistor R_g, then Z_t is modified to:

$$Z_t = R_f + R_i \left(1 + \frac{R_f}{Z_g} \right) \tag{4.9.9}$$

where Z_g is the impedance of R_g in parallel with C_g.

The zero at $f_c = \dfrac{1}{2\pi(R_i \| R_g \| R_f)C_g}$ can cause reduced phase margin as shown in Figure 4.9.4.
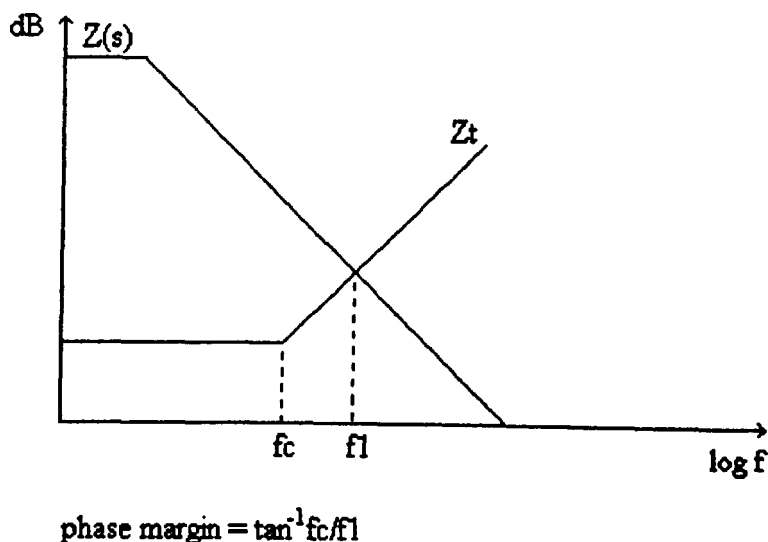
$$\text{phase margin} = \tan^{-1} fc/f1$$

Fig 4.9.4

The value of the parallel capacitance has to be relatively large for the phase margin to be affected. Of course, C_g also affects the demanded gain $D = 1 + \dfrac{R_f}{Z_g}$ and this can lead to closed loop gain peaking. In Appendix 2, a Bode plot is derived showing the open loop transimpedance gain together with the feedback transimpedances, demanded gains and closed loop gains of the circuit with none and all the relays closed. It can be seen that the closed loop bandwidth is set by the value of the feedback transimpedance, and that there is some gain peaking at the lowest demanded gain caused by the zero in the demanded gain equation. A second plot shows the effect of using a compensating time constant at the non-inverting input of the amplifier as shown in Figure 4.9.2.

In order to cover a continuous gain range, the fine gain control must be variable between 0.5 and 1.5. This control is implemented by using a wide bandwidth analogue multiplier that forms the product $\dfrac{V_x V_y}{2}$, where V_y is the signal and V_x is a DC control voltage generated by a DAC. In this implementation, the 5V DAC has 16bit resolution, generating 1V to 3V at its output from front panel control settings ranging from 0.5000 to 1.5000. This facilitates an incremental gain change of 0.01%, allowing a peak at the high end of an 8K channel MCA to be moved by just one channel.

The circuit must be prevented from overloading. If the amplifier saturates, the recovery time could impose an unacceptable dead-time on the system. The input amplifier used can be clamped so that its output does not exceed a set voltage and its recovery from

clamping is very fast. This facility is needed at the input because very large signals are often detected, generated by microphony in the detector or by the detection of high energy cosmic rays. The output of the coarse gain stage is also clamped and this clamping is detected by discriminators that inform the state machine controlling the unit. The state machine will initiate a head-amplifier reset. This action is needed as many head-amplifiers can saturate on power-on or on application of EHT to the detector.

4.10 : NOISE REQUIREMENTS

The noise generated by the processing amplifier should be negligible compared to the noise seen at the output of the charge amplifier. Taking the Canberra 2001 charge amplifier as an example of a low noise specification, the noise is quoted as 770eV FWHM(Ge) for a 10pF detector; it is input referred noise. The input referred noise in Coulombs RMS (see Section 2.1) is given by:

$$Q_i = \frac{FWHM \times e}{2.36 \times w} \tag{4.10.1}$$

$$Q_i = \frac{770 \times 1.6 \times 10^{-19}}{2.36 \times 2.98} = 1.76 \times 10^{-17}$$

The sensitivity of the charge amplifier is quoted as 2V/pC. The output referred noise is therefore given by:

$$V_o = \frac{1.76 \times 10^{-17} \times 2}{1 \times 10^{-12}} = 35 \mu V \text{ RMS} \tag{4.10.2}$$

The equation giving ENC at the output of a shaping amplifier was derived in Section 2.3 as:

$$ENC^2 = \frac{2kTR_n C_t^2}{q^2} \times \frac{N_d^2}{T_p} + \frac{I_n}{q} \times N_s^2 T_p \tag{4.10.3}$$

Multiplying by the factor $\dfrac{q^2 h_{peak}^2}{C_f^2}$ converts ENC^2 to mean squared noise:

$$\sigma_o^2 = \frac{4kTR_nC_t^2}{C_f^2} \times \frac{N_d^2 h_{peak}^2}{2T_p} + \frac{2I_n q}{C_f^2} \times \frac{N_s^2 T_p h_{peak}^2}{2} \qquad (4.10.4)$$

Taking h_{peak}^2 as the gain of the filter, it can be seen that the input referred impulse noise is given by:

$$\sigma_{ii}^2 = \frac{4kTR_nC_t^2}{C_f^2} \times \frac{N_d^2}{2T_p} \qquad (4.10.5)$$

We know that the input referred noise density is given by $\frac{4kTR_nC_t^2}{C_f^2}$. The impulse noise power bandwidth is therefore given by:

$$NPBW = \frac{N_d^2}{2T_p}. \qquad (4.10.6)$$

The (optimum) noise figures are given for a 4µs shaping semi-Gaussian filter, for which a delta noise index of $2.53/T_p$ can be assumed (see Section 3.1). At the optimum shaping the contributions of delta noise and step noise are equal. Therefore :-

$$\sigma_i = \sqrt{\sigma_{ii}^2 + \sigma_{is}^2} = 35\mu V$$
$$\sigma_{ii} = \sigma_{is} = 25\mu V \qquad (4.10.7)$$

This figure can be combined with the noise power bandwidth derived above to give the spectrometer noise density referred to its output.

$$v_{ii} = \sigma_{ii} \times \sqrt{\frac{2T_p}{N_d^2}} = 44\frac{nV}{\sqrt{Hz}} \qquad (4.10.8)$$

The noise generated by the filter will be impulse noise and should be negligible compared to this figure.

The input stage of the new processor is shown with all relevant noise sources in Figure 4.10.1.
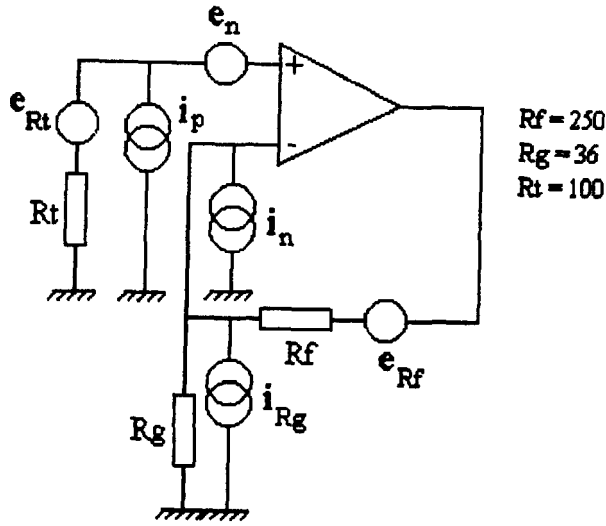
Fig 4.10.1

The non-inverting noise sources combine to give:

$$ei_1^2 = e_n^2 + i_p^2 R_t^2 + 4kTR_t \tag{4.10.9}$$

Assuming the voltage at the inverting input to be 0V, the inverting noise sources combine to give:

$$eo_2^2 = i_n^2 R_f^2 + i_{Rg}^2 R_f^2 + e_{Rf}^2$$

$$eo_2^2 = i_n^2 R_f^2 + \frac{4kTR_f^2}{R_g} + 4kTR_f$$

$$eo_2^2 = i_n^2 R_f^2 + 4kTR_f \left(1 + \frac{R_f}{R_g}\right) \tag{4.10.10}$$

If this noise is referred to the input :

$$ei_2^2 = \frac{i_n^2 R_f^2}{A_v^2} + \frac{4kTR_f}{A_v}$$

$$\text{where } A_v = 1 + \frac{R_f}{R_g} \tag{4.10.11}$$

The total noise at the input is developed below:

70

$$ei^2 = ei_1^2 + ei_2^2$$

$$ei^2 = e_n^2 + i_p^2 R_t^2 + 4kTR_f + \frac{i_n^2 R_f^2}{A_v^2} + \frac{4kTR_f}{A_v} \qquad (4.10.12)$$

For the CLC500 amplifier and the resistor values shown in Figure 4.10.1, $ei = 2.9 \dfrac{nV}{\sqrt{Hz}}$.

This figure added in quadrature to the output noise of the charge amplifier increases the total noise by less than 0.25%.

It has been assumed that the noise contributions of components further down the processing chain can be ignored when they are referred to the processor's input, since they are attenuated by, at least, the input stage gain.

A further assumption was made that the noise densities e_n, i_n and i_p were constant with frequency. In fact, the noise densities exhibit a $\dfrac{1}{f}$ characteristic below a certain break frequency ($\approx 10^4$ Hz for the CLC500). In practice, the noise power bandwidth is sufficiently large to make the increase in the total noise at the output negligible.

4.11 : STATE MACHINE

The pulse processing amplifier's operation is controlled by a synchronous state machine implemented in a programmable logic device (PLD). The state machine drives the processor through the time periods T_{ss}, T, T_h, T_d and T_{xo} described in Section 3.2, and generates the appropriate signals to control the main processing elements as shown in Figures 4.11.1 and 4.11.2.

SO22

SO3

SO1

SO4

SO5

SO2

Filter   Baseline Restorer   Gated Integrator

Fig 4.11.1

SO1

SO2   SO22

SO3

SO4

SO5

T_{ss} T T_h T_d T_{xo}
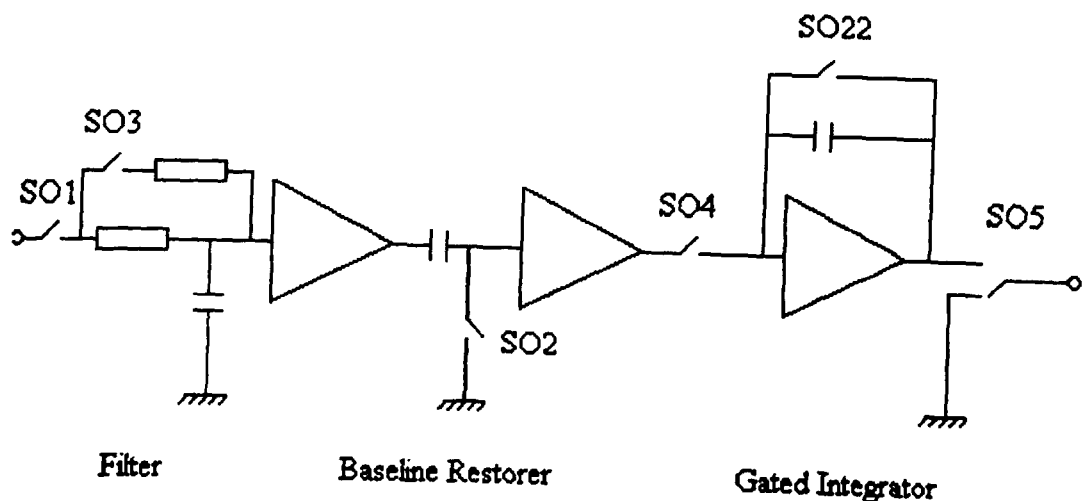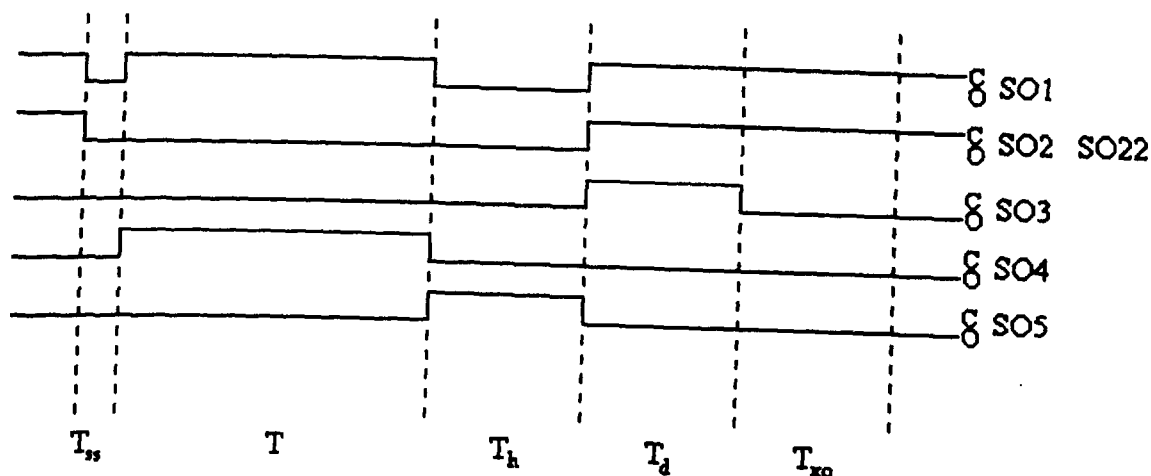
Fig 4.11.2

Switches SO1 and SO3 are not driven directly by the state machine. Another PLD combines the SO1, SO3 control lines from the state machine with data indicating the selected processing time to generate the appropriate signals for the time-variant filter (see Section 4.3).

The length of the time periods are held in five 16 bit registers. At the appropriate time, the state machine loads the contents of the relevant register into a 16 bit down-counter and enables the device to count down at the system clock frequency of 20MHz. When the count down is complete, the counter signals to the state machine and the next time period is loaded into the counter. These timings are synchronised to the initiating event because the signal causing the state machine to move from its idle state also starts the system clock. This eliminates the problem of timing jitter. Without this synchronisation, even the relatively small 50nS time variation between a valid event and the triggering of the state machine, achieved with a 20MHz clock, can cause a

resolution degradation due to timing errors in sampling the baseline. The system clock is stopped by the state machine as it returns to its idle state.

The state machine also generates a signal to reset the pole-zero compensating circuit, a signal to reset the charge-amplifier, a zero stabiliser strobe and a signal for implementing live-time correction in a MCA.

The full list of input and output signals is shown in Table 4.11.1. Figure 4.11.3 illustrates the state sequencing and the conditions for state transitions.

Table 4.11.1

SIGNAL	I/P OR O/P	DESCRIPTION
FT	I/P	trigger from fast recognition channel
ST	I/P	trigger from slow recognition channel
/COMP	I/P	countdown complete
/ULD	I/P	trigger from upper limit discriminator
/LLD	I/P	trigger from lower limit discriminator
/RES	I/P	system reset
INH	I/P	processor inhibit
ZST	I/P	request for zero stabilisation cycle
AA	O/P	state bit (LSB)
BB	O/P	state bit
CC	O/P	state bit
DD	O/P	state bit
EE	O/P	state bit (MSB)
SO1	O/P	series switch control
SO2	O/P	baseline restoration control
SO22	O/P	gated integrator reset (inverse of SO2)
SO3	O/P	decay time-constant control
SO4	O/P	gated integrator input gate control
SO5	O/P	output gate control and pole-zero cct reset
SO55	O/P	output to gnd control (inverse of SO5)
CS	O/P	stop system clock
/EN	O/P	enable 16 bit counter
/PEN	O/P	load 16 bit counter with protection time T_{xo}
/DEN	O/P	load 16 bit counter with decay time T_d
/CTREN	O/P	load 16 bit counter with processing time T
/RTDEN	O/P	load 16 bit counter with series switch time T_{ss}
/HEN	O/P	load 16 bit counter with hold time T_h
ZSTROBE	O/P	strobe zero stabiliser
ZZSTROBE	O/P	inverse of ZZSTROBE
BUSY	O/P	dead-time indication
BBUSY	O/P	inverse of BUSY
RESCA	O/P	reset charge amplifier
RRESCA	O/P	inverse of RESCA

Fig 4.11.3

A=AUTO
B=ST*/INH*/(LLD+ULD)
C=COMP*/(FT+ST)

D=ULD+LLD
E=COMP*/FT*/(ULD+LLD)
F=FT*/(ULD+LLD)

M=COMP
P=FT+ST
S=ST*/(ULD+LLD)
Z=ZST*/ST*/(ULD+LLD)
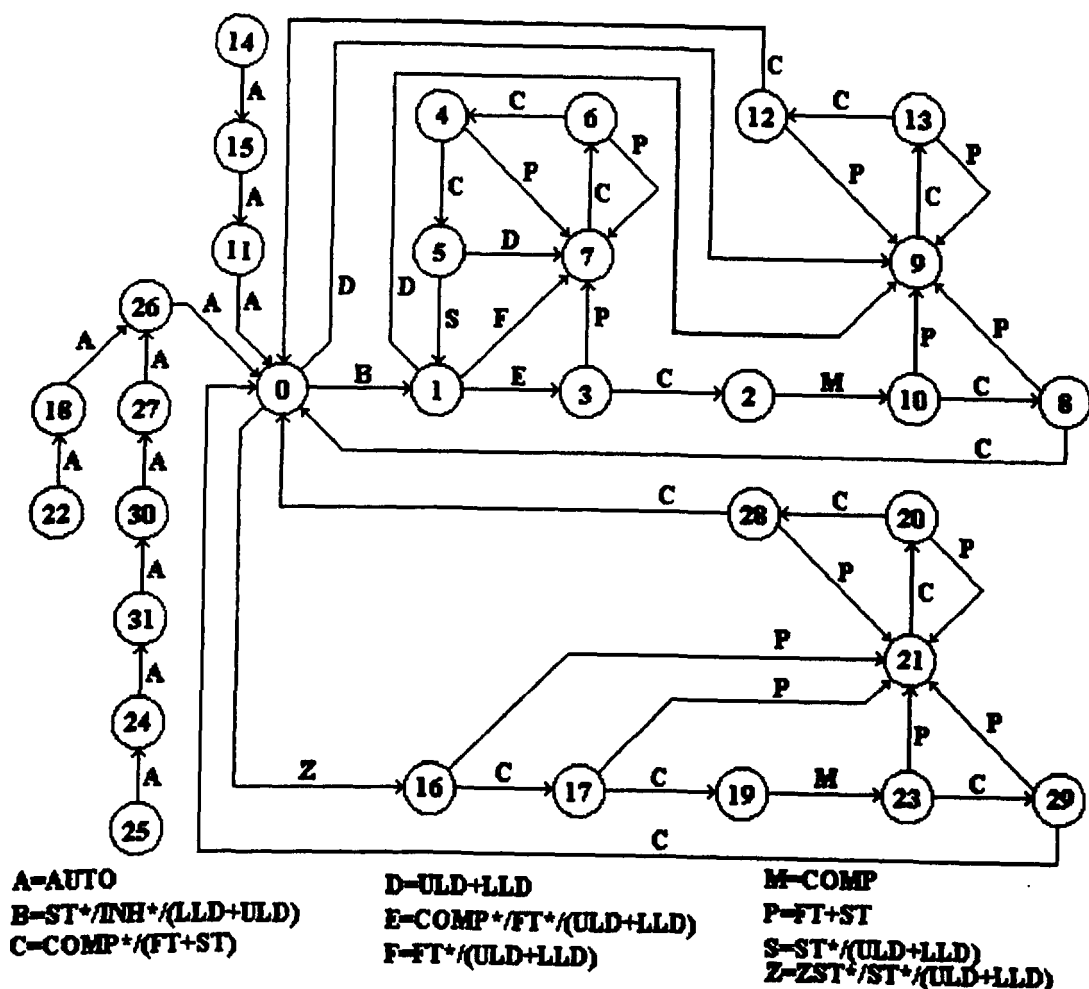
Transitions 25-24-31-30-27-26-0, 22-18-26-0 and 14-15-11-0 are automatic transitions used to populate each state and ensure that no lock-up states exist.

Transition 0-1-3-2-10-8-0 is the main processing sequence; states 1,3,2,10 and 8 generating the timings T_{as}, T, T_h, T_d and T_{xo} respectively. Transitions 9-13-12 and 7-6-4 mirror the 2-10-8 sequence and represent pulse pile-up conditions, with a charge amplifier reset in states 9 and 7, as in state 2.

Two different types of pile-up exists. Tail pile-up occurs when a secondary pulse arrives after the amplitude of the first pulse has been measured, but before the residual voltages in the processing circuit have decayed. In this case, the secondary event is rejected, the charge amplifier is reset and the decay sequence T_d and T_{xo} is re-started; this is the 9-13-12 sequence.

Rise-time pile-up occurs when the secondary pulse arrives before the amplitude of the first pulse has been captured. In this case, both events have to be rejected. If the pile-up sequence described above for tail pile-up is used, an inadequate amount of live-time is added to compensate for the loss of two pulses. Figure 4.11.4 illustrates the point.

Tail pile-up, four valid events seen

Rise-time pile-up, three valid events seen

Dead Time
Live Time
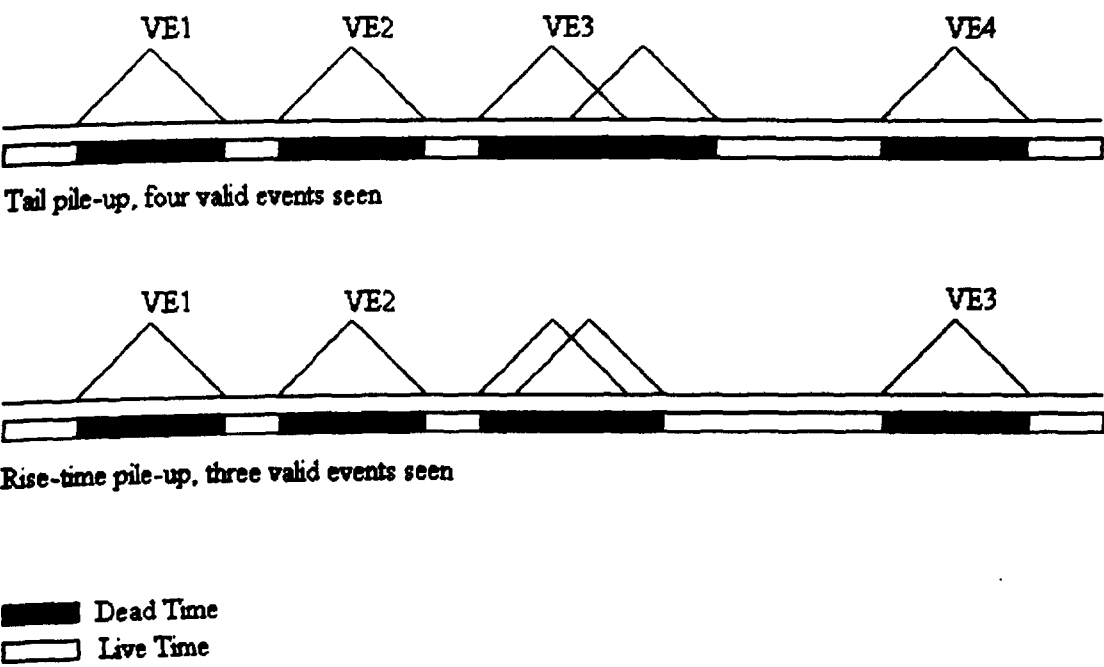
Fig 4.11.4

In the upper sequence, four events are seen in the given live-time, but in the lower sequence, only three events are seen in a longer live-time. It can be shown (see Appendix 3) that a statistical correction can be made by stopping the live-time clock until the next valid event occurs. The sequence 7-6-4-5 does this by using state 5 as an idle state but with 'busy' indicated.

It can be seen that signal processing is initiated by a signal from the slow trigger channel. A pile-up sequence, however, is initiated by either the slow or fast trigger channels. The fast channel can resolve pulses that are closer together, but the higher bandwidth means more noise and a higher discriminator threshold. The slow trigger channel is useful for detecting the pile-up of low amplitude secondary signals. Only the fast channel is used in state 1 due to the width of the sequence initiating slow channel trigger.

The processor can be inhibited from going into a processing cycle by the application of an external signal INH.

The idle states and state 1 have exits to the reset sequences that are initiated by the upper or lower limit discriminators. This resets the charge-amplifier and processor in the event of the charge-amplifier saturating (e.g. when the EHT is changed) or in the event of the processor circuits limiting.

The lower half of the state diagram implements a zero stabilisation sequence that mimics the normal processing sequence, but without the provision of a pile-up with live-time correction. If the processor is idling, it is prompted every 2mS to enter an artificial processing cycle with the resulting output voltage being a measure of the baseline of the system. The zero stabiliser is prompted to compensate for any fluctuation. An incoming event causes the cycle to be abandoned and the processor behaves as if there had been a tail pile-up.

Tables 4.11.2 and 4.11.3 show the status of the various outputs for a given state. The effect of the output signal on the associated switch is shown for SO1, SO2, SO22, SO3, SO4, SO5 and SO55. The other outputs are shown as either active ($\sqrt{}$) or inactive(X).

Table 4.11.2

STATE	SO1	SO2	SO22	SO3	SO4	SO5	SO55	BUSY BBUSY	RESCA RRESCA
0	CLOSE	CLOSE	CLOSE	OPEN	OPEN	OPEN	CLOSE	X	X
1	OPEN	OPEN	OPEN	OPEN	OPEN	OPEN	CLOSE	√	X
2	OPEN	OPEN	OPEN	OPEN	OPEN	CLOSE	OPEN	√	√
3	CLOSE	OPEN	OPEN	OPEN	CLOSE	OPEN	CLOSE	√	X
4	CLOSE	CLOSE	CLOSE	OPEN	OPEN	OPEN	CLOSE	√	X
5	CLOSE	CLOSE	CLOSE	OPEN	OPEN	OPEN	CLOSE	√	X
6	CLOSE	CLOSE	CLOSE	CLOSE	OPEN	OPEN	CLOSE	√	X
7	CLOSE	CLOSE	CLOSE	OPEN	OPEN	OPEN	CLOSE	√	√
8	CLOSE	CLOSE	CLOSE	OPEN	OPEN	OPEN	CLOSE	√	X
9	CLOSE	CLOSE	CLOSE	OPEN	OPEN	OPEN	CLOSE	√	√
10	CLOSE	CLOSE	CLOSE	CLOSE	OPEN	OPEN	CLOSE	√	X
11	CLOSE	CLOSE	CLOSE	OPEN	OPEN	OPEN	CLOSE	√	X
12	CLOSE	CLOSE	CLOSE	OPEN	OPEN	OPEN	CLOSE	√	X
13	CLOSE	CLOSE	CLOSE	CLOSE	OPEN	OPEN	CLOSE	√	X
14	CLOSE	CLOSE	CLOSE	OPEN	OPEN	OPEN	CLOSE	√	X
15	CLOSE	CLOSE	CLOSE	OPEN	OPEN	OPEN	CLOSE	√	X
16	OPEN	OPEN	OPEN	OPEN	OPEN	OPEN	CLOSE	√	X
17	CLOSE	OPEN	OPEN	OPEN	CLOSE	OPEN	CLOSE	√	X
18	CLOSE	CLOSE	CLOSE	OPEN	OPEN	OPEN	CLOSE	√	X
19	OPEN	OPEN	OPEN	OPEN	OPEN	CLOSE	OPEN	√	√
20	CLOSE	CLOSE	CLOSE	CLOSE	OPEN	OPEN	CLOSE	√	X
21	CLOSE	CLOSE	CLOSE	OPEN	OPEN	OPEN	CLOSE	√	√
22	CLOSE	CLOSE	CLOSE	OPEN	OPEN	OPEN	CLOSE	√	X
23	CLOSE	CLOSE	CLOSE	CLOSE	OPEN	OPEN	CLOSE	√	X
24	CLOSE	CLOSE	CLOSE	OPEN	OPEN	OPEN	CLOSE	√	X
25	CLOSE	CLOSE	CLOSE	OPEN	OPEN	OPEN	CLOSE	√	X
26	CLOSE	CLOSE	CLOSE	OPEN	OPEN	OPEN	CLOSE	√	X
27	CLOSE	CLOSE	CLOSE	OPEN	OPEN	OPEN	CLOSE	√	X
28	CLOSE	CLOSE	CLOSE	OPEN	OPEN	OPEN	CLOSE	√	X
29	CLOSE	CLOSE	CLOSE	OPEN	OPEN	OPEN	CLOSE	√	X
30	CLOSE	CLOSE	CLOSE	OPEN	OPEN	OPEN	CLOSE	√	X
31	CLOSE	CLOSE	CLOSE	OPEN	OPEN	OPEN	CLOSE	√	X

Table 4.11.3

STATE	/EN	/RTDEN	/CTREN	/HEN	/DEN	/PEN	CS	ZSTROBE ZZSTROBE
0	X	X	X	X	X	X	√	X
1	√	√	X	X	X	X	X	X
2	√	X	X	√	X	X	X	X
3	√	X	√	X	X	X	X	X
4	√	X	X	X	X	√	X	X
5	X	X	X	X	X	X	√	X
6	√	X	X	X	√	X	X	X
7	√	X	X	√	X	X	X	X
8	√	X	X	X	X	√	X	X
9	√	X	X	√	X	X	X	X
10	√	X	X	X	√	X	X	X
11	X	X	X	X	X	X	X	X
12	√	X	X	X	X	√	X	X
13	√	X	X	X	√	X	X	X
14	X	X	X	X	X	X	X	X
15	X	X	X	X	X	X	X	X
16	√	√	X	X	X	X	X	X
17	√	X	√	X	X	X	X	X
18	X	X	X	X	X	X	X	X
19	√	X	X	√	X	X	X	√
20	√	X	X	X	√	X	X	X
21	√	X	X	√	X	X	X	X
22	X	X	X	X	√	X	X	X
23	√	X	X	X	X	X	X	X
24	X	X	X	X	X	X	X	X
25	X	X	X	X	X	X	X	X
26	X	X	X	X	X	X	X	X
27	X	X	X	X	X	X	X	X
28	√	X	X	X	X	√	X	X
29	√	X	X	X	X	√	X	X
30	X	X	X	X	X	X	X	X
31	X	X	X	X	X	X	X	X

4.12 : FRONT PANEL CONTROL

The unit is controlled by the user via a small single board computer piggy-backed onto the digital board. The computer is a TDS9090 from Triangle Data Systems; it runs 'Forth' programmes. The interface is implemented with four Siemens intelligent displays (four digit LEDs), five push-buttons and a rotary encoder, as shown in Figure 4.12.1.
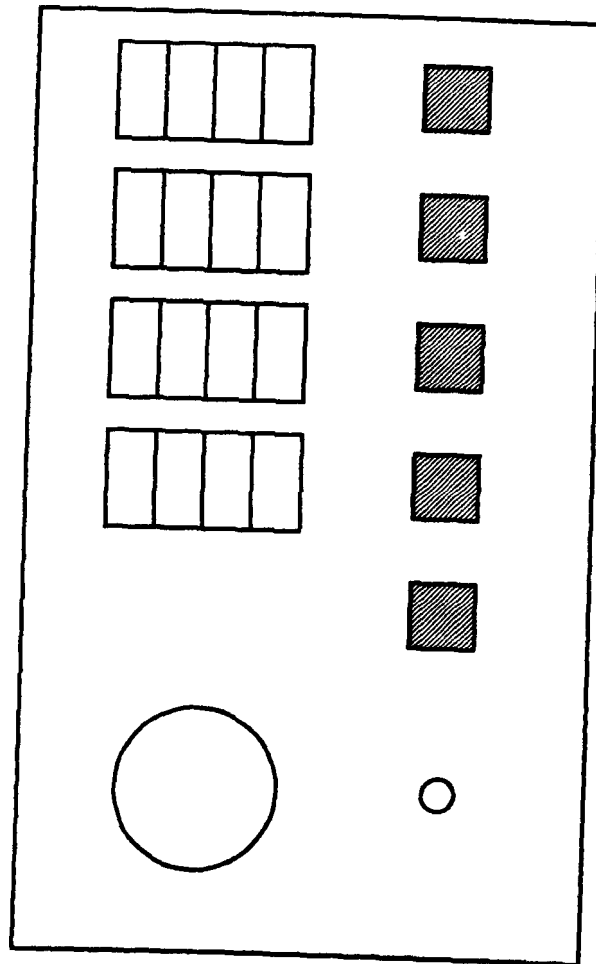

Fig 4.12.1

The basic operation involves pressing one of the four push-buttons associated with the four displays. The other displays are blanked out and a rotation of the rotary encoder clockwise or anti-clockwise will increase or decrease the displayed setting. When the desired value is selected, the lower push-button is pressed to de-select the display and all four displays will be illuminated.

This arrangement is very flexible and the display format, including the number of parameters that can be controlled, can be changed easily by re-programming the control computer. The current programme uses the lower display to select page number one, two or three. Page one, if selected, displays Coarse Gain (50 to 3200), Fine Gain (0.51 to 1.49) and Super Fine Gain (-100 to +100) in the other three windows. Page two displays Processing Time (0.50 to 64.0), Slow Trigger Threshold and Fast Trigger Threshold (0 to 128). Page three displays Pole-zero Compensation (0 to 128).

The use of super fine gain allows the user to set the overall gain with a resolution of 10^{-4}; this allows a peak near to the top of an 8K MCA to be moved by one channel.

The resolution of the trigger threshold control allows the discriminator thresholds of the fast and slow trigger channels to be changed by just 7mV.

It can be shown (see Appendix 4) that the resolution of the pole-zero compensation control is sufficient to limit the amplitude error at the end of a long processing time to less than 1% . This increase in unlikely to be seen by the user during the set-up.

The front panel includes a socket to enable the pole-zero circuit output waveform to be observed on an oscilloscope during set-up.

All front panel settings are stored in non-volatile memory so that instrument settings are not lost when power is switched off.

It would be possible to add a security facility to the instrument whereby a code would have to be input before a front panel setting could be changed. This would make the instrument tamper-proof for use in industrial applications.

The instrument is fitted with an RS232 serial interface that can be used to link the TDS9090 control computer with a remote PC. It would be possible to change the front panel parameters by issuing commands from the PC.

4.13 : RESULTS

The design of the analogue pulse processor was established after extensive trials with a prototype unit. The module was used with a Harwell 993005 ADC and a Canberra MCA.

Figures 4.13.1 and 4.13.2 show spectra produced by a relatively low energy gamma source Americium241. The main peak is generated by a 60keV gamma; the next peak in intensity is a 19keV X-ray. The spectrometer used for these spectra is a Link Systems' Germanium detector coupled to a NM8030 optical reset charge-amplifier having a cooled input stage.

Figure 4.13.1 is the spectrum produced by the prototype pulse processing amplifier. Figure 4.13.2 is shown for comparison; it is the spectrum produced by the NM8841 pulse processor and its associated ADC, the NM8871. These are commercial units employing similar time-variant techniques. The best resolution measurement for the prototype was 447eV for the 60keV peak. This compares with 440eV for the NM8841. The processing time used in both cases was 2µs. The input rate was a low 1 to 2 Kpps.

Figures 4.13.3 and 4.13.4 show the spectra produced by a Cobalt60 source. The gamma energies are much higher; the two main peaks having energies of 1.17MeV and 1.33MeV. Figure 4.13.3 is the spectrum from the prototype PPA, and 4.13.4 is a comparable spectrum from the NM8841. The best resolution measured for the PPA was 3.7keV for the 1.33MeV peak, compared to 3.0keV for the NM8841. Again, processing times of 2µs were used. The input rate was a moderate 8 to 9 Kpps. The spectrometer used for these measurements was a DSG NGC-14 n-type HPGe detector, used with a Harwell 930128 optical reset charge-amplifier. The input stage was not cooled, and the input FET was an 8553 (a short gate 4416).

A third detector used was the Canberra 7229P, a p-type HPGe crystal. The charge-amplifier had a cooled input stage and was restored by a feedback resistor. Figure 4.13.5 is the Co^{60} spectrum produced when this spectrometer was used with a semi-Gaussian time-invariant amplifier (EG&G 575) set to 3µs shaping time-constant. With its pole-zero compensation set, the resolution of the 1.33MeV peak was measured at 2.4keV.

Figure 4.13.6 shows the Co^{60} spectrum produced by the same spectrometer used with the NM8841 pulse processor. The problem of low energy tails, discussed in Section 4.5, can be seen clearly. Only optical or transistor reset charge-amplifiers could be used with this unit.

The same problem can be seen in Figure 4.13.7. This is the equivalent spectrum generated by the PPA used without the pole-zero circuit. When the compensation is included, the low energy tailing is reduced considerably, as seen in Figure 4.13.8. The two small shadow peaks seen on the low energy side of the 1.17Mev and 1.33Mev peaks are a demonstration of the processor's greater susceptibility to overloading when the pole-zero compensator is used (discussed in Section 4.5). The limit discriminator threshold would normally be set to ensure that overloading pulses were not processed.
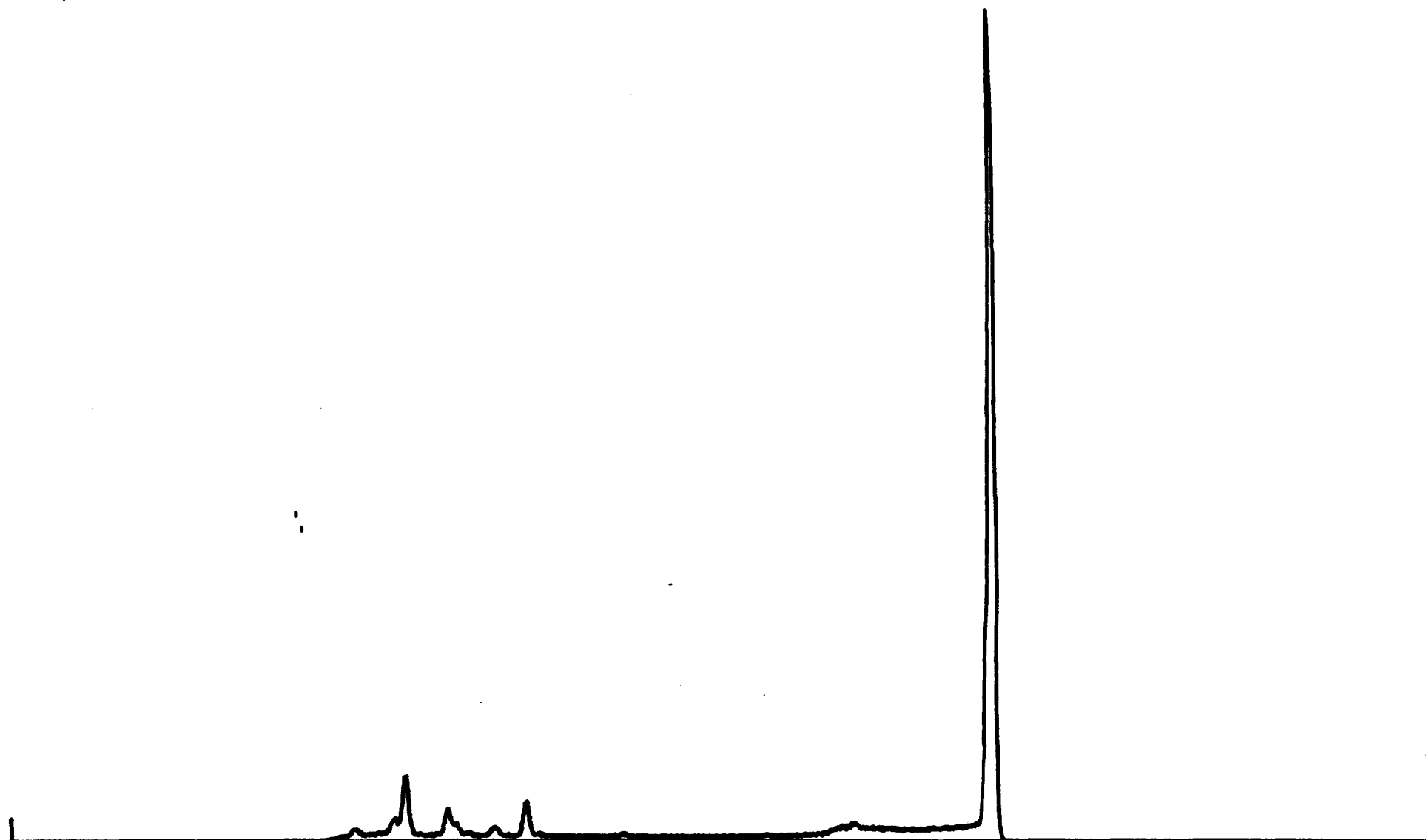
Fig 4.13.1 : Am241 spectrum generated by the new versatile Harwell processor.

TAG NO. = 0   SERIES 40   V- 2.2   11:40   20 SEP 1991
CH# 0   MEMORY = 1/2   VFS =   16K   CH# 4095
                                                                    CANBERRA

LL= CH# 0   FROM CH# 0   TO CH# 4095   PSET(L) 1000
COUNTS 423   INT 697692   ELAP(L) 423
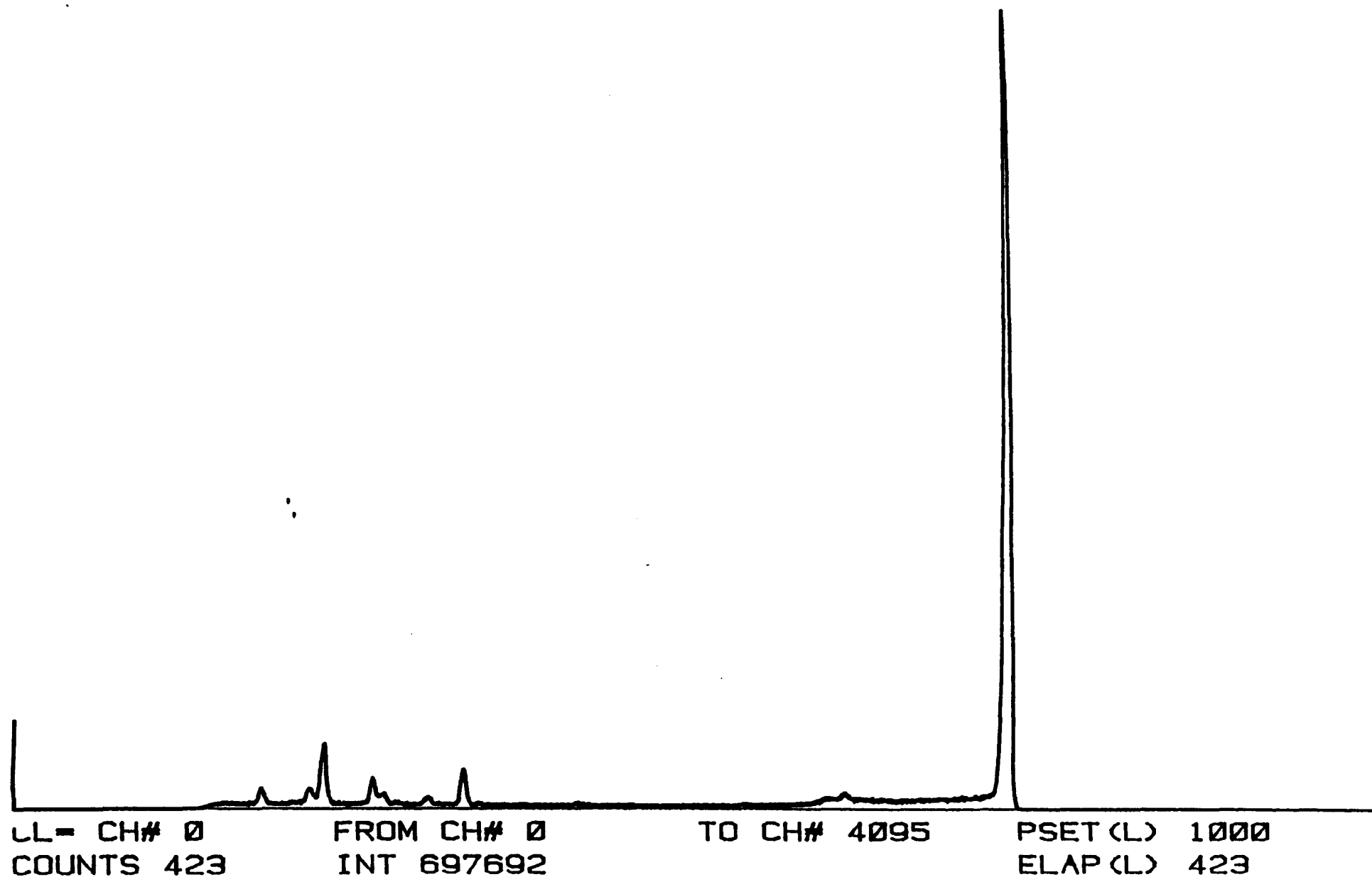
Fig 4.13.2 : Am241 spectrum generated by the 8841 Harwell processor.

TAG NO. = 4   SERIES 40   V- 2.2   20:08   16 JAN 1992
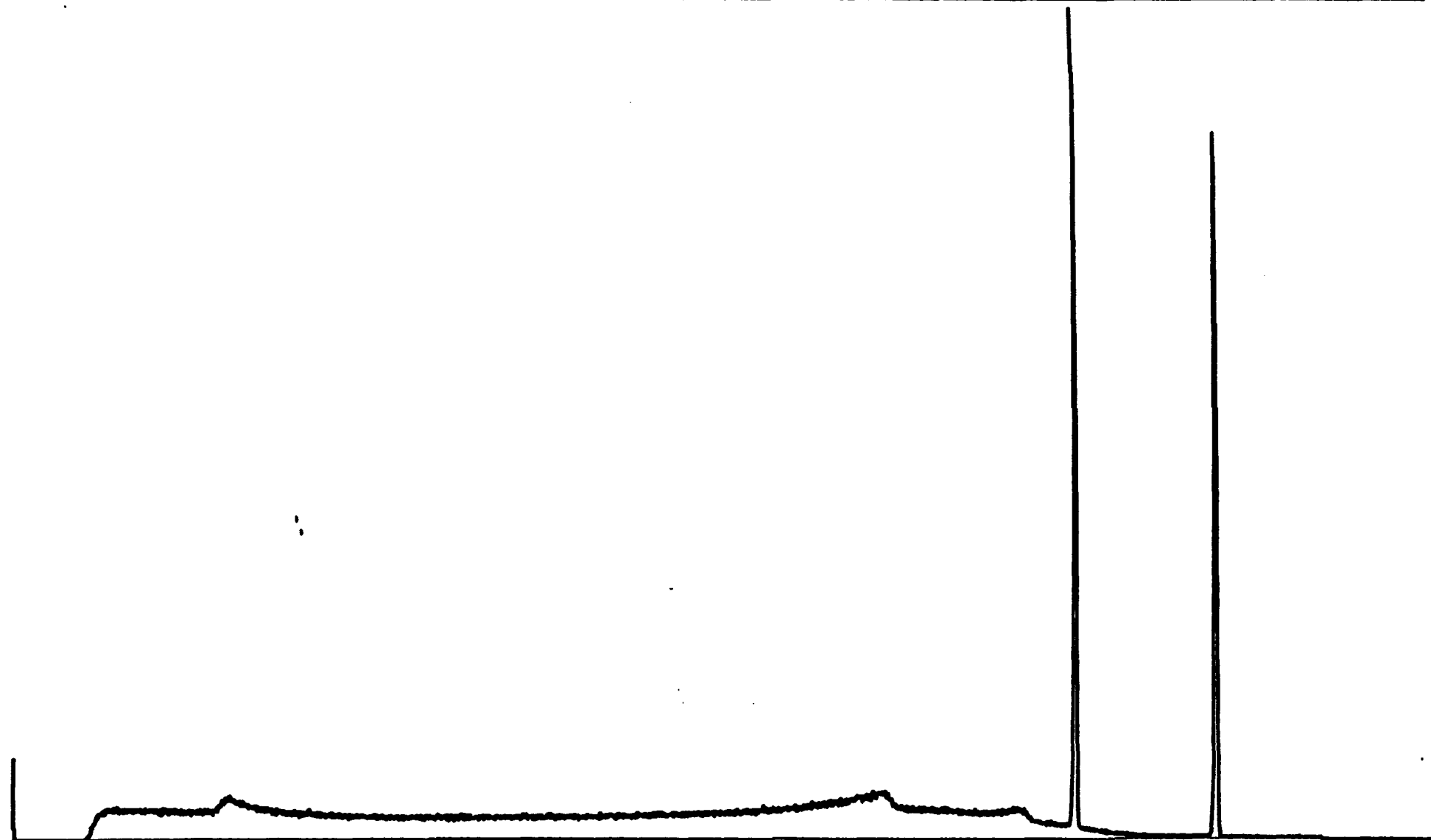CH# 0   MEMORY = 1/2   VFS =   16K   CH# 4095
    CANBERRA
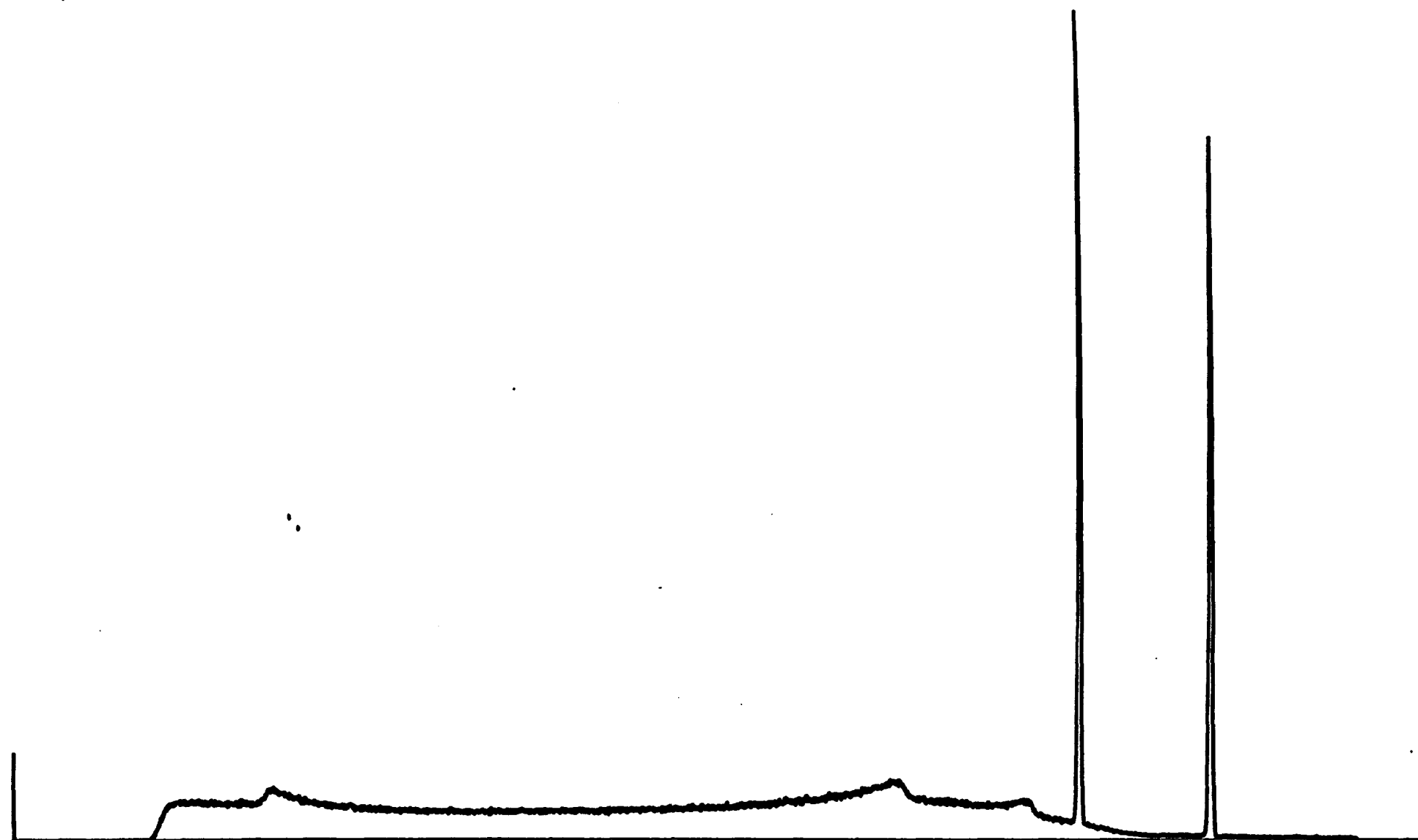
CL= CH# 0   FROM CH# 0   TO CH# 4095   PSET (L)   1000
COUNTS 274   ELAP (L)   274

Fig 4.13.3 : Co60 spectrum generated by the new versatile Harwell processor.

CL= CH# 0   FROM CH# 0   TO CH# 4095   PSET (L) 1000
COUNTS 237   ELAP (L) 237

Fig 4.13.4 : Co60 spectrum generated by the 8841 Harwell processor.

Fig 4.13.5 : Co60 spectrum generated by a resistor-restore charge-amplifier and a time-invariant semi-Gaussian shaper (Ortec 575).
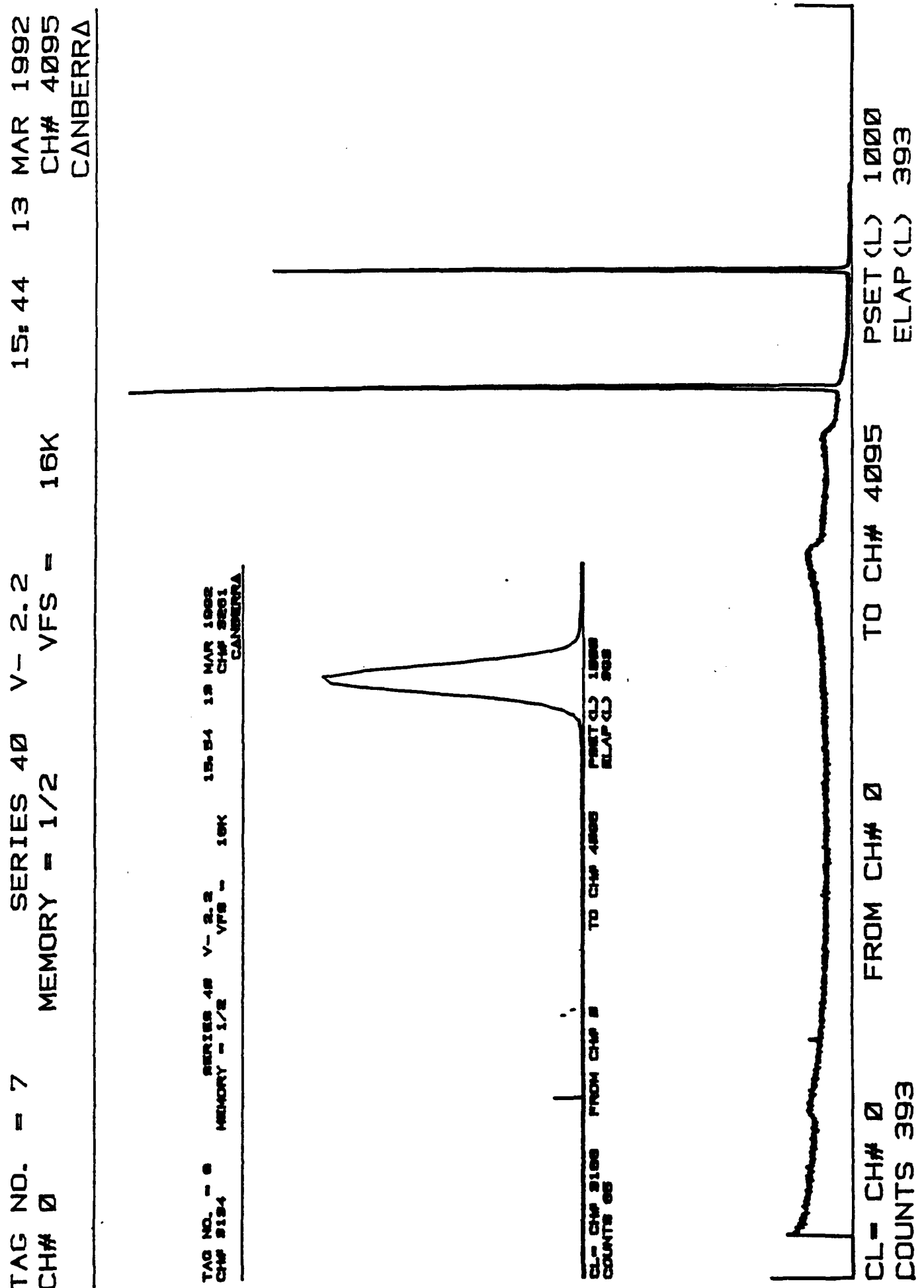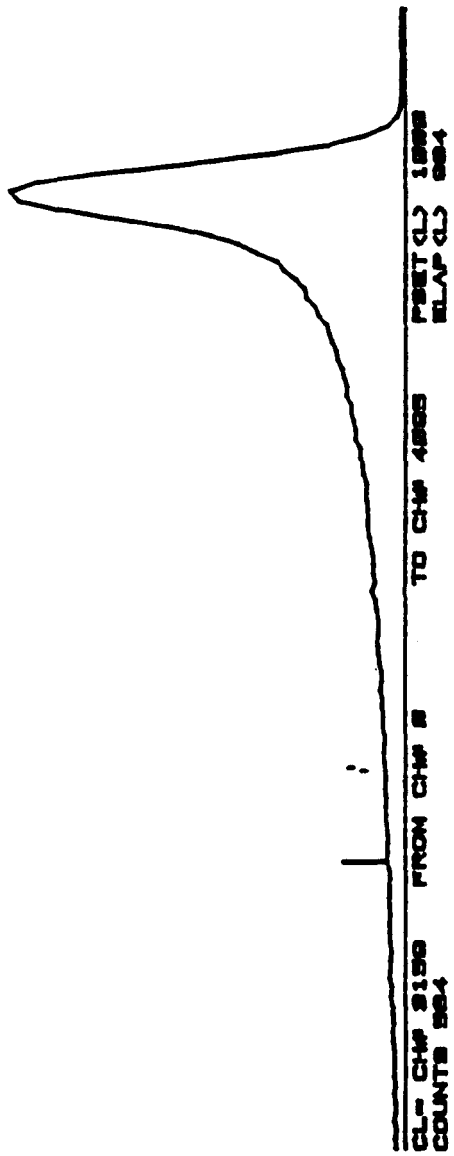
TAG NO. = 7   SERIES 40   V- 2.2   15:44   13 MAR 1992
CH# Ø   MEMORY = 1/2   VFS = 16K   CH# 4Ø95
CANBERRA

PSET (L) 1ØØØ
ELAP (L) 393

CL- CH# Ø   FROM CH# Ø   TO CH# 4Ø95
COUNTS 393

Fig 4.13.6 : Co60 spectrum generated by a resistor-restore charge-amplifier and the 8841 Harwell time-variant processor.

Fig 4.13.7 : Co60 spectrum generated by a resistor-restore charge-amplifier and the new versatile Harwell processor, used without pole-zero compensation.
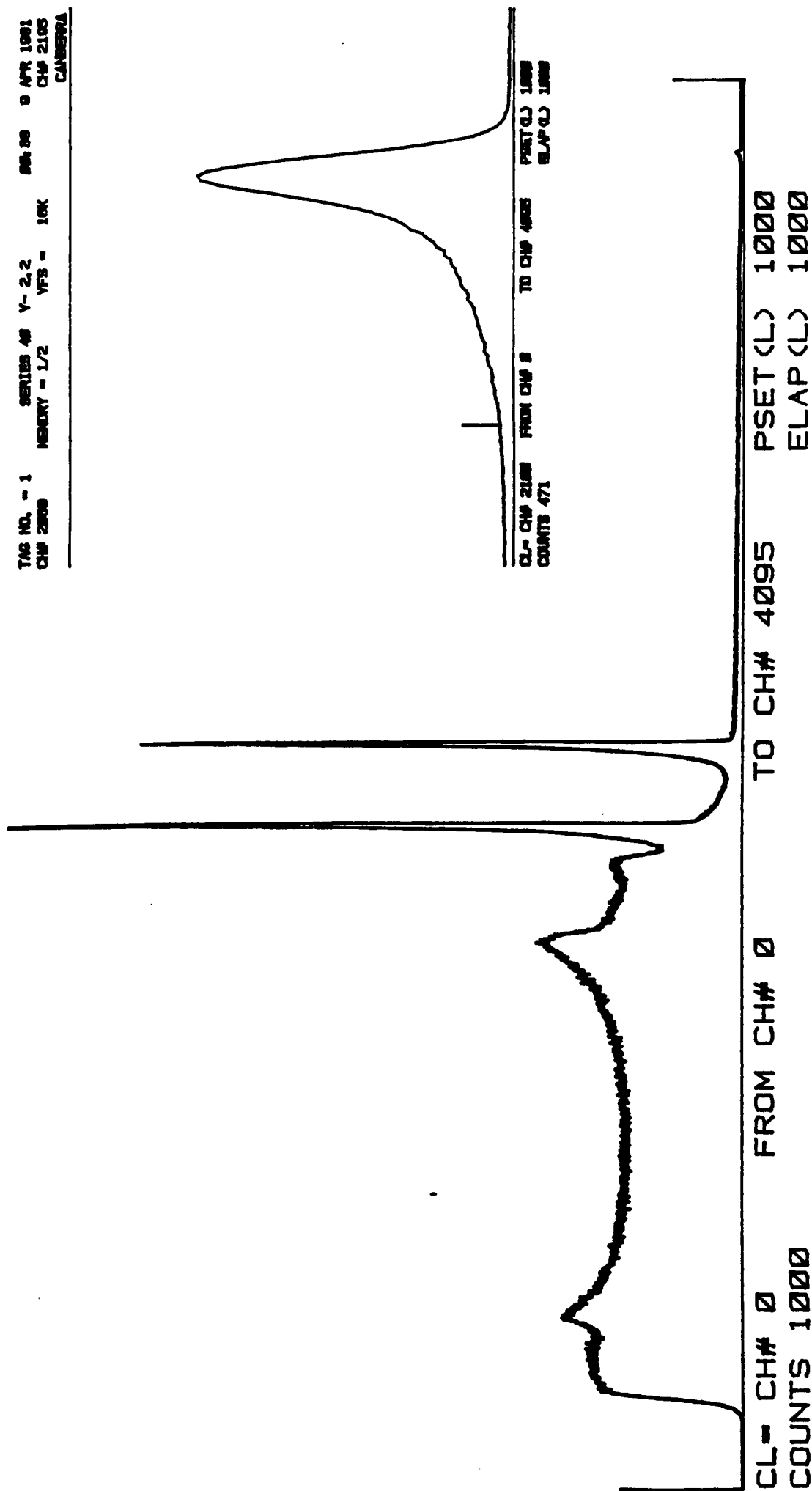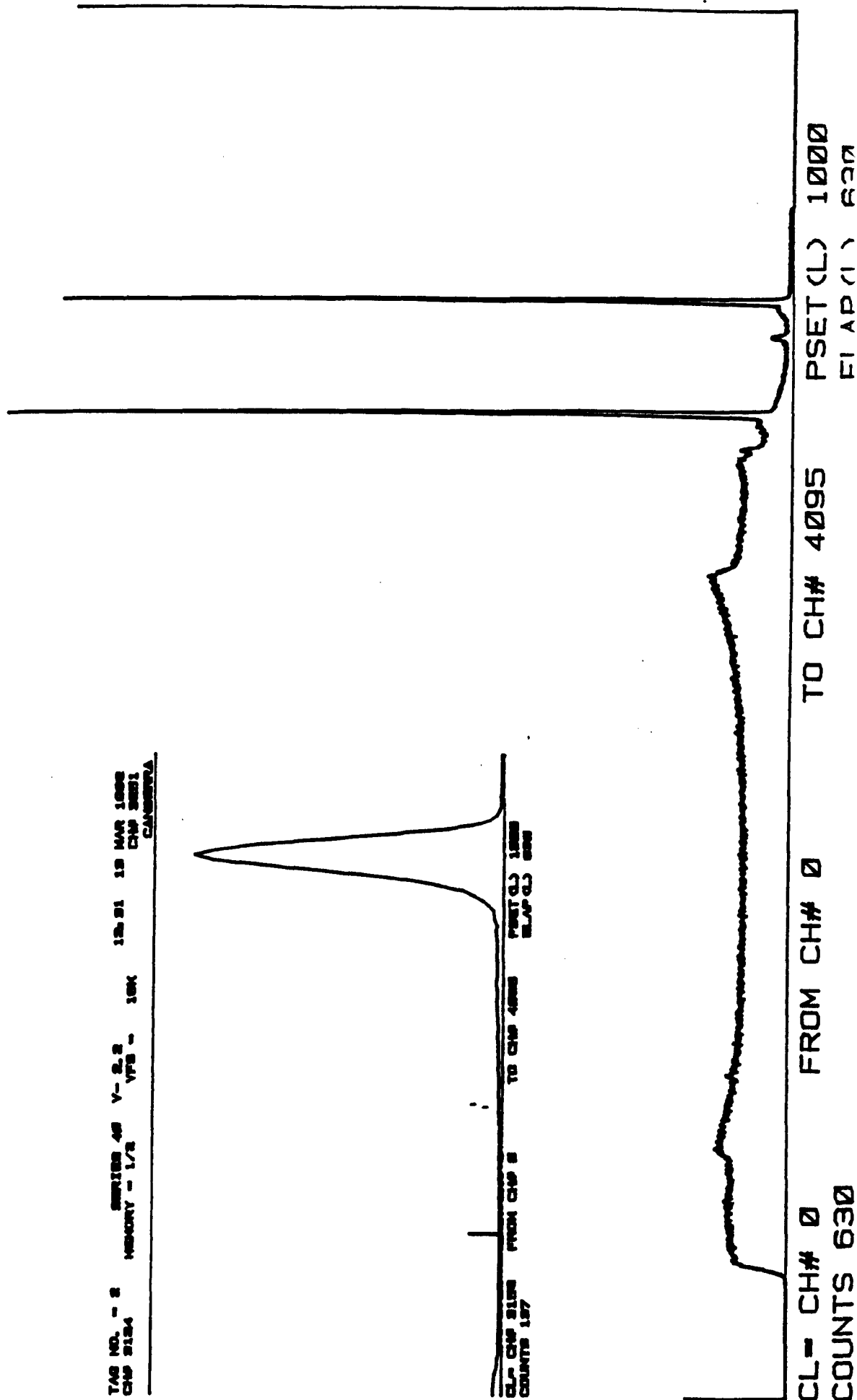
Fig 4.13.8 : Co60 spectrum generated by a resistor-restore charge-amplifier and the new versatile Harwell processor, used with pole-zero compensation.

CHAPTER 5 : A DIGITAL MATCHED FILTER

5.1 : INTRODUCTION

Digital signal processing (DSP) is spreading into many fields where signals were traditionally processed using analogue techniques. The rapid advancement of the technology, particularly in the development of faster, higher resolution ADCs and faster, more flexible digital signal processors, means that an increasing uptake of the technology is inevitable.

In a DSP process, the signal is sampled and digitised by the ADC; the numbers are then processed by an algorithm implemented in software or hardware or a combination of both. A DAC is often needed to reconstitute an analogue signal at the output.
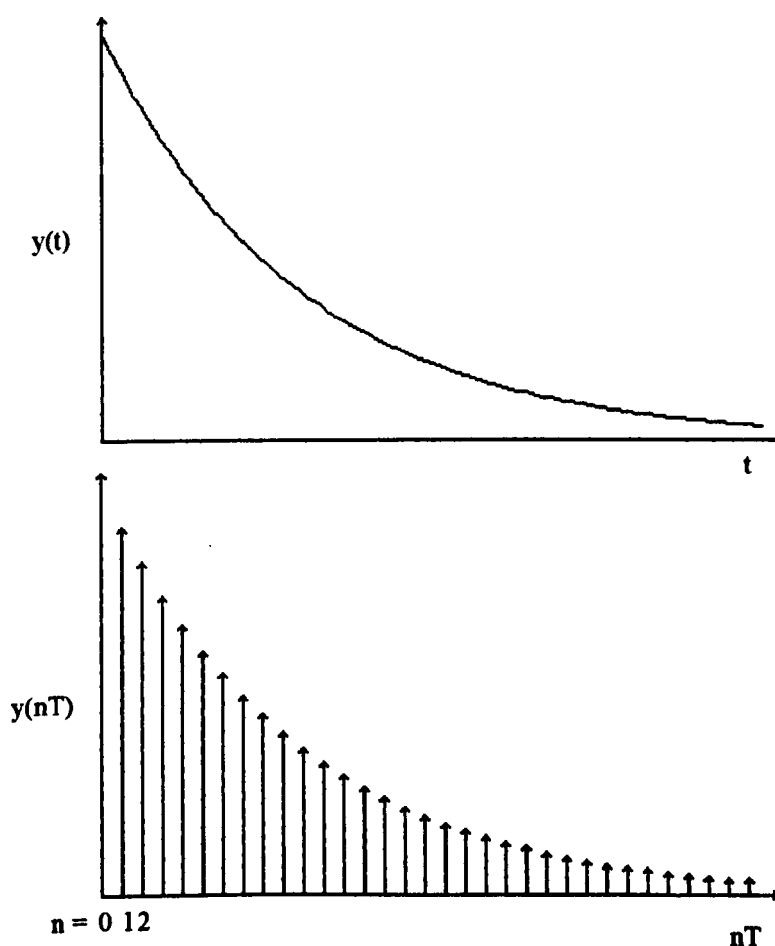

Fig 5.1.1

Figure 5.1.1 shows the continuous and sampled versions of the same signal; the sampled signal can be described by the expression $\sum_n y(nT)$, where T is the sampling period. When dealing with a discrete representation of a signal, it is often convenient

to think of the waveform mapped out by the envelope of the sampled data. Steiglitz[47] proved that there was no fundamental difference between the theory of processing continuous and discrete representations of a signal.

An indispensable tool in the digital domain is the Z-Transform. It is equivalent to the Laplace Transform in the analogue domain. The Laplace Transform of a sampled signal $\sum_n y(nT)$ is given by:

$$Y(s) = y(0) + y(T)e^{-sT} + y(2T)e^{-2sT} + ...$$

$$Y(s) = \sum_n y(nT)e^{-snT} \qquad (5.1.1)$$

where e^{-sT} represents an unit delay. The Z-Transform is derived by substituting $Z = e^{sT}$

$$Y(Z) = \sum_n y(n)Z^{-n} \qquad (5.1.2)$$

In the Z-Transform, Z^{-1} represent the unit delay.

In Section 2.2, it was seen that the output $s_o(t)$ of a filter with an impulse response $h(t)$ could be calculated for any input $s_i(t)$ by evaluating the convolution $h(t)*s_i(t)$. The same property is true for the discrete case:

$$y(n) = \sum_k x(n-k)h(k) \qquad (5.1.3)$$

where $y(n)$ is the output, $x(n)$ is the input and $h(n)$ is the impulse response. It can be shown that the Z-Transform is given by:

$$Y(Z) = X(Z)H(Z)$$

$$H(Z) = \frac{Y(Z)}{X(Z)} = \sum_n h(n)Z^{-n} \qquad (5.1.4)$$

where $H(Z)$ is the system function.

A large sub-set of linear time-invariant discrete systems can be described by the difference equation, relating output sequence $y(n)$ to input sequence $x(n)$ in the following way:

$$y(n) = \sum_{m=0}^{M} b_m x(n-m) - \sum_{k=1}^{N} a_k y(n-k) \qquad (5.1.5)$$

$$y(n) = b_0 x(n) + b_1 x(n-1) + b_2 x(n-2) + \ldots + b_M x(n-M)$$
$$-a_1 y(n-1) - a_2 y(n-2) - \ldots - a_N y(n-N) \qquad (5.1.6)$$

The present output sample is computed from the present input sample, M past input samples and N past output samples. In terms of the z transform it can be written:

$$Y(z) = b_0 X(z) + b_1 X(z)z^{-1} + b_2 X(z)z^{-2} + \ldots + b_M X(z)z^{-M}$$
$$-a_1 Y(z)z^{-1} - a_2 Y(z)z^{-2} - \ldots - a_N Y(z)z^{-N} \qquad (5.1.7)$$

$$\frac{Y(z)}{X(z)} = H(z) = \frac{\sum\limits_{m=0}^{M} b_m z^{-m}}{1 + \sum\limits_{k=1}^{N} a_k z^{-k}} \qquad (5.1.8)$$

This filter can be implemented directly by the structure shown in Figure 5.1.2. Because there is feedback, the implementation is said to be recursive. Such structures are usually associated with infinite impulse response filters (IIR).
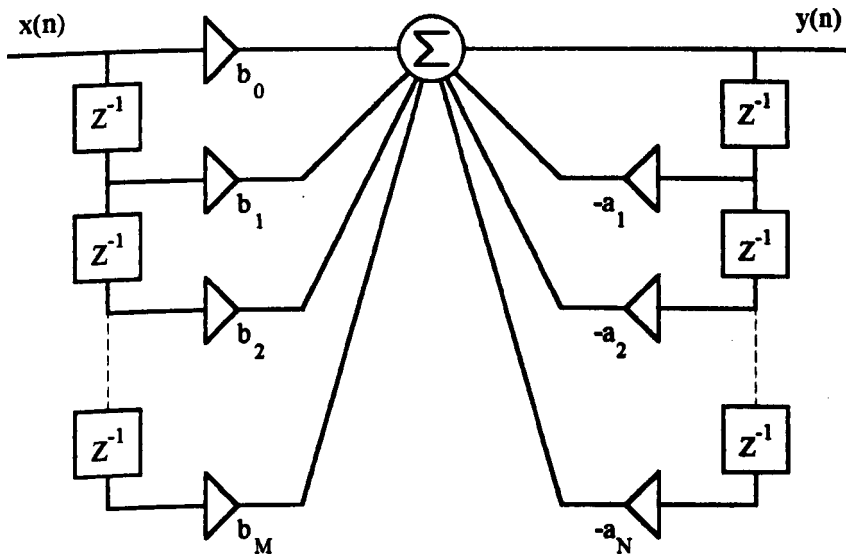

Fig 5.1.2

If all the coefficients a_k were zero, the system function has the form:

$$H(z) = \sum_{m=0}^{M} b_m z^{-m} \qquad\qquad (5.1.9)$$

The direct implementation of this system function is shown in Figure 5.1.3. There is no feedback and the structure is said to be non-recursive. This arrangement implements finite impulse response filters (FIR). Such filters are easier to design; the lack of poles in the system function makes them unconditionally stable.
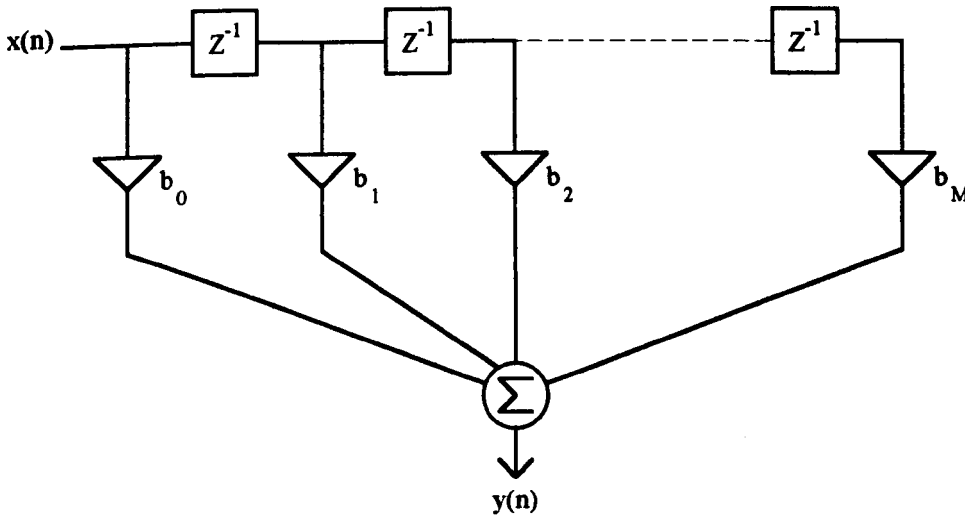

Fig 5.1.3

5.2 : DIGITAL FILTERING IN NUCLEAR SPECTROSCOPY

Nuclear spectroscopy is one field that has been relatively slow in adopting DSP techniques. The filtering of nuclear pulses represents a challenging problem in that the pulse amplitudes, pulse arrival times and pulse shapes are all variable; analogue solutions were evolved over many years. The short shaping times used in high-throughput, high resolution gamma spectroscopy are particularly problematic, requiring fast digitisers and fast processing algorithms. In fact, with the notable exception of the work of Koeman in 1974[48,49,50], DSP techniques were not seen in nuclear spectroscopy until the mid-1980s. Koeman's work, years ahead of its time, depended on a custom-built 12bit ADC, sampling at 200nS.

In the ten years after Koeman's work, various authors reported on sampled data processors, but the implementation was analogue. Miller and Robinson[51], Baertsch[52] and Melbert[53] all reported on transversal filters for nuclear spectroscopy implemented with charge coupled devices (CCDs). The basic structure of these filters is shown in Figure 5.2.1.
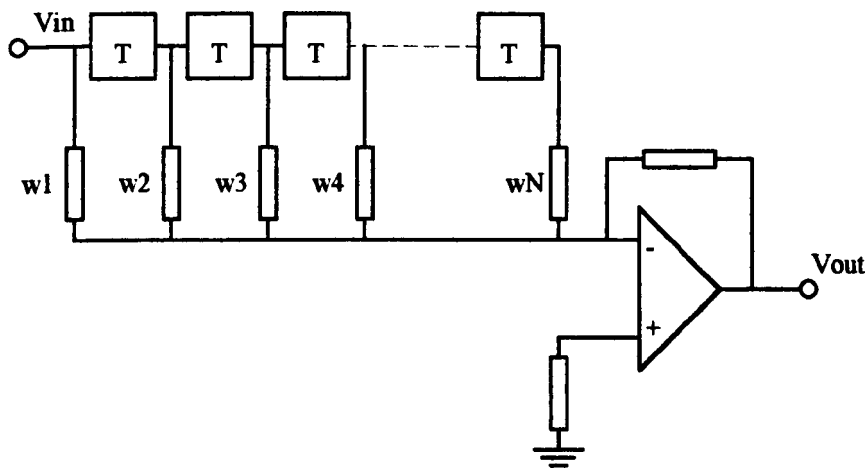
Fig 5.2.1

It can be seen that the output of the filter comprises the weighted sum of successively delayed samples of the input signal. The similarity of this structure with that shown in Figure 5.1.3 is obvious; the weights given to the samples therefore define the impulse response of the filter. Matched filter considerations require the impulse response to have the form $e^{\frac{t}{\tau}}$ if the input signal is the output of the pre-whitening filter $e^{\frac{-t}{\tau}}$; the values given to the weights follow the pattern shown in Figure 5.2.2a. The output waveform approximates the optimum cusp shape. These filters, though, were easily modified to accept the step waveform of the charge amplifier by modifying the weights as shown in Figure 5.2.2b. Again the output resembles a cusp waveform, but now the pre-whitening and matched filters are incorporated into the same structure.
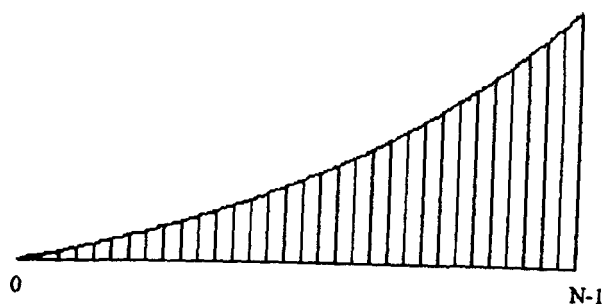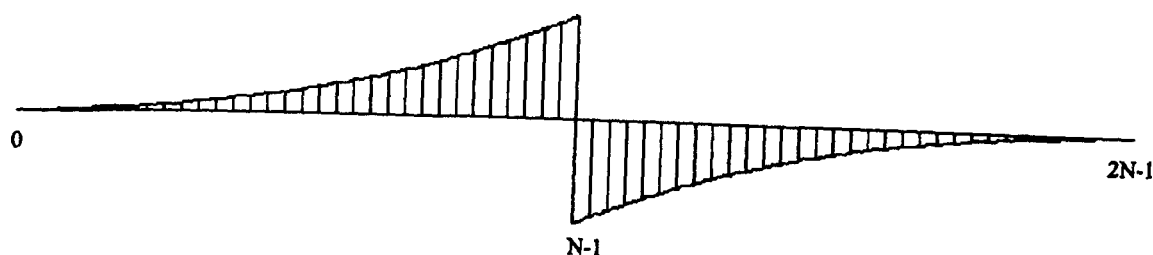
Fig 5.2.2a

Fig 5.2.2b

Since 1985 several authors have reported on 'digital signal processing in nuclear spectroscopy'; very few propose a fully digital, real-time processor. In many cases, conventional analogue shaping is used before digitisation, DSP techniques are then used to enhance the spectrum in some way:

Hilserath et al[54] digitised a semi-Gaussian pulse and used a single chip processor to detect the peak height, to calculate the peak area and to identify pile-up. Karp et al[55] digitised a shaped pulse from a NaI detector and used a mainframe to provide an integration time adapted to the time-intervals between pulses.

Chrien and Sutter[56] fed a semi-Gaussian pulse with short shaping into a transient recorder linked into a PC for off-line spectrum analysis. The algorithm corrected pulses corrupted by pile-up without rejecting the piled-up events, calculated a baseline restoration and reduced the delta and step noise. The overall effect was similar to the use of a gated integrator in analogue systems. In the same vein, Ortlepp and Romaguera[57] digitised a short shaped Gaussian pulse, using dedicated hardware to generate peak area integration in real time. The effect of a gated integrator can be approximated by running a moving average filter over a short shaped pulse, but the slow return to baseline of the output pulse causes problems when threshold based ADCs are used; Jordanov and Knoll[58] used a digital moving average filter, implemented in hardware, to surmount these problems.

97

Bingefors et al[59] and Ripamonti et al[60] use sampled data methods to reduce the duration of conventionally shaped pulses. Bingefors uses deconvolution to extract the original detector pulse shape. Interestingly the system was tested by digital methods but implemented using analogue sampling techniques. Ripamonti's approach was tail cancellation by digital filtering.

Other authors have chosen to digitise the spectrometer signal up-front using transient recorders or high speed sampling oscilloscopes feeding into a PC. The algorithms described are used off-line or on-line for very low input count rates (less than 1000cps):

Drndarevic et al[61] calculated the peak area of a NaI pulse after removing noise spikes and correcting piled-up events. Gast and Georgiev[62] used deconvolution to recover the original charge distribution produced by the detector, avoiding ballistic deficit errors and generating a true trapezoidal noise shaping function in the process.

Cosulich and Gatti[63] used convolution with a reference pulse shape to emulate analogue optimum filtering with the matched filter. A pulse shape factor was also used to reject corrupted pulses, improving pile-up detection. A shape factor was also used by Takahashi et al[64] to improve the peak to Compton ratio; peak height was calculated by a simple summation of a number of samples taken before and after the arrival of a pulse.

Los Arcos and Garcia-Torano[65,66] described an algorithm for calculating pulse height by fitting pulses to an analytical expression by a least squares minimisation method. A similar technique was used by Bertuccio et al[67,68] but this system used an analogue pre-filter in front of the time-sampler.

Koeman developed the first digital filter for nuclear spectroscopy in 1973. The basic structure is shown in Figure 5.2.3.
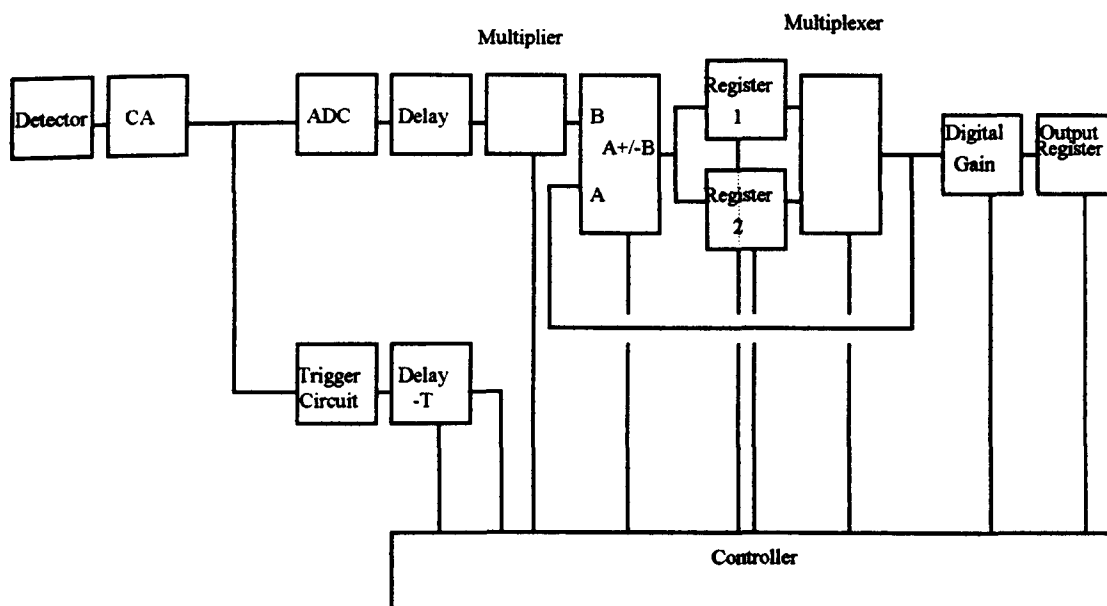
Fig 5.2.3

The signal from a pulsed reset charge amplifier is digitised to 12 bits every 200nS and the samples are fed into a delay pipeline. In parallel, an analogue trigger channel recognises valid events and instructs the controller to start processing. N samples before the event are multiplied by appropriate weighting factors and subtracted from the accumulator. The first quarter of the samples are multiplied by W1, the second quarter by W2, the third quarter by W3 and the last quarter by W4. N samples after the event are multiplied by the weighting factors in reverse W4, W3, W2 and W1; these samples are added to the accumulator. The final accumulator content is a signal amplitude estimation with baseline subtraction.

In order to exploit the full throughput of the system, it is necessary to be able to measure the signal amplitude of one pulse and the baseline of a next pulse that may be overlapping. Two multiplexed accumulators are effectively used. Two multiply and accumulate operations are therefore needed in one clock period. The multiply operation is simplified by choosing easily implemented weight factors e.g. 1,1,1,1 or 1,2,4,8. The impulse and step responses of the system are shown in Figure 5.2.4.
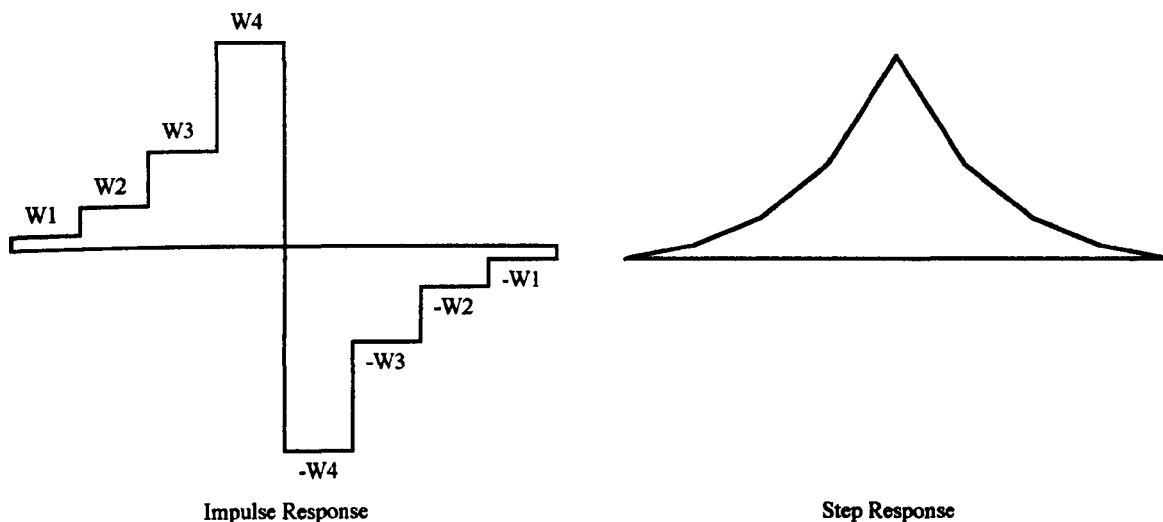
Impulse Response   Step Response

Fig 5.2.4

The output is seen to approximate the cusp response. Uniform weights generated a triangular step response.

The resolution at low input rates was found to be a little inferior to the best analogue systems such as the time-variant Harwell processor, but high count rate performance was better. Throughput, or maximum analysis rate, was also found to be superior for the digital system. The system was designed for X-ray spectrometry and processing times between 3 and 100µs could be selected.

Lakatos[69,70] described a very similar system; again, a custom designed 12bit fast ADC was used. Lakatos could claim the first fully digital system as the recognition channel was also implemented digitally. The main difference in this system was the use of adaptive filtering. In the event of a secondary pulse arriving before the end of the processing time of a first pulse, the processing of that first pulse was ended, the result stored and the processing of the second pulse initiated. Throughput rate was greatly enhanced by this innovation. The application was X-ray spectroscopy at a processing time of 64µs.

The systems described by Koeman and Lakatos are time variant; the impulse response is related to the time of occurrence of a valid event that has to be detected by a secondary channel. Recently, a time-invariant approach has been adopted by Jordanov and Knoll[71]. One of the structures proposed by these authors is shown in Figure 5.2.5.
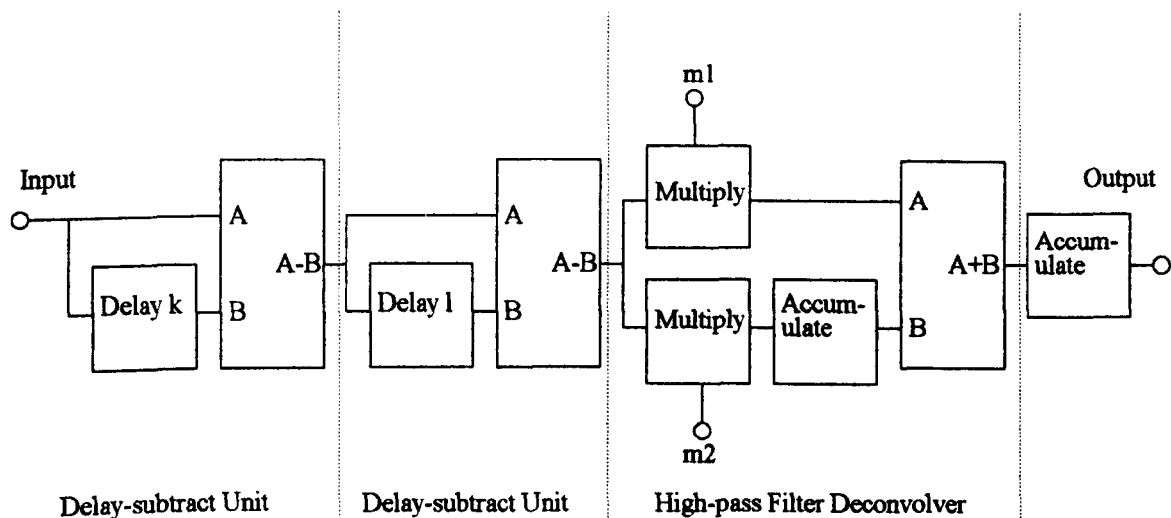
100

Fig 5.2.5

The high-pass filter deconvolver is seen to be the digital equivalent of the analogue pole-zero compensator described in Section 4.5. It removes the effect of the decay time constant introduced into the input signal by resistor restored charge amplifiers or by having the pre-whitening filter implemented with analogue components placed in front of the digitiser. The ratio of m1 to m2 is set to the decay time constant. The deconvolver is effectively bypassed when step-like signals are digitised.

The step response of the two delay-subtract units in series and the output waveform of the whole processor are shown in Figure 5.2.6. It can be seen that time-invariant trapezoidal or triangular shaping is generated by this algorithm. Peaks are detected by monitoring sign changes in the result of the addition that preceded the final accumulation.
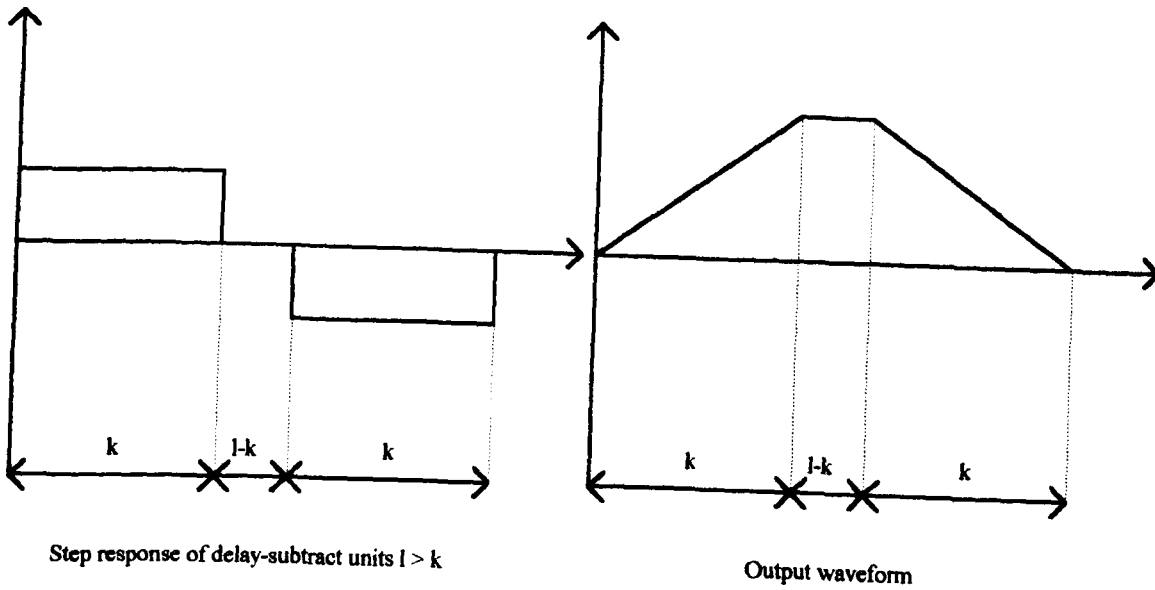
Step response of delay-subtract units l > k

Output waveform

Fig 5.2.6

Only preliminary results have been reported for the hardware implementation of this processor, used with a commercial 12bit 20MHz ADC.

Jordanov and Knoll have also proposed and simulated similar structures to generate cusp-like output waveforms[72].

5.3) A DIGITAL MATCHED FILTER FOR PULSE SPECTROSCOPY

Owens[73] had also proposed an all digital matched filter pulse processor in 1987, pre-dating Lakatos and Jordanov/Knoll. The theory is described below:

The whitening filter is shown in Section 2.2 to need the frequency response:

$$H_w(jW) = \frac{jW}{(a + jW)}$$

(5.3.1)

where a is the noise corner of the input noise. The step-invariant method can be used to derive the system function of the equivalent digital filter:

$$H_w(z) = \frac{1 - z^{-1}}{1 - e^{-aT} z^{-1}}$$

(5.3.2)

This is the closed form with N = ∞ of the following equation:

$$H_W(z) = (1 - z^{-1}) \times (1 + A^{-1}z^{-1} + A^{-2}z^{-2} + \ldots + A^{-(N-1)}z^{-(N-1)})$$

where $A = e^{aT}$

$$(5.3.4)$$

The matched filter will have the response:

$$h(n) = e^{anT} \quad \text{where } 0 \le n \le N-1$$

$$(5.3.5)$$

Scaling by the largest coefficient gives the expression:

$$h(n) = e^{anT} \times e^{-a(N-1)T}$$

$$h(n) = e^{a(n-N+1)T}$$

$$(5.3.6)$$

The matched filter system function can therefore be written as:

$$H_M(z) = \sum_{n=0}^{N-1} e^{a(n-N+1)T} z^{-n}$$

$$H_M(z) = A^{1-N}(1 + Az^{-1} + A^2z^{-2} + \ldots A^{N-1}z^{-(N-1)})$$

$$(5.3.7)$$

In closed form:

$$H_M(z) = \frac{1 - e^{aNT} z^{-N}}{1 - e^{aT} z^{-1}} \times e^{a(1-N)T}$$

$$(5.3.8)$$

Figure 5.3.1 show how the expressions derived above could be implemented directly in DSP hardware:
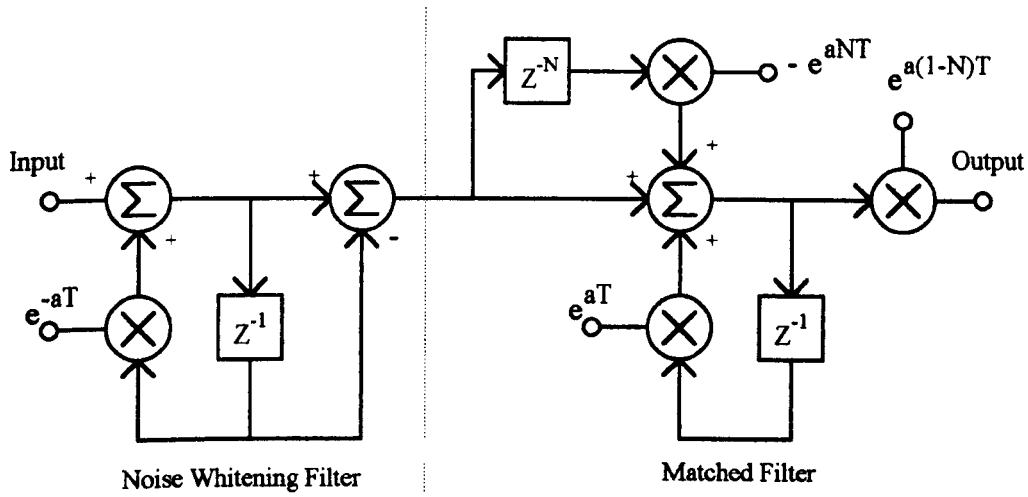
Fig 5.3.1

By combining both functions into one filter the system function becomes:

$$H(z) = H_W(z) \times H_M(z)$$

$$H(z) = \frac{(1 - z^{-1}) \times (1 - e^{aNT} z^{-N})}{(1 - e^{aT} z^{-1}) \times (1 - e^{-aT} z^{-1})} \times e^{a(1-N)T}$$

$$H(z) = \frac{(1 - z^{-1}) \times (1 - e^{aNT} z^{-N})}{(1 - 2\cosh(aT) z^{-1} + z^{-2})} \times e^{a(1-N)T} \tag{5.3.9}$$

The direct implementation of this function is shown in Figure 5.3.2.
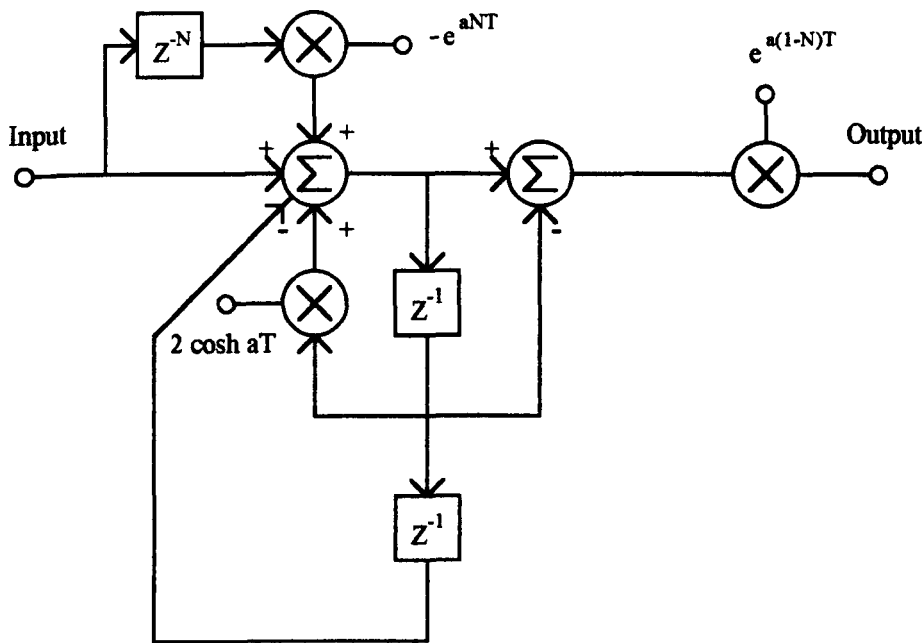
Fig 5.3.2

These structures could be built with multipliers, arithmetic units and delay units. However the required data rate of 20MHz (see below) could not be achieved with hardware available at the time. To overcome this hurdle, Owens proposed the scheme shown in Figure 5.3.3.

Fig 5.3.3

A trigger signal informs the state machine that a valid event is entering the system. After a short delay to ensure that the step signal has reached its full height, the state-machine enables a counter, the outputs of which address a coefficient memory. As the

counter counts down, N coefficients are generated that are used to multiply N samples of the step signal as they enter the system. T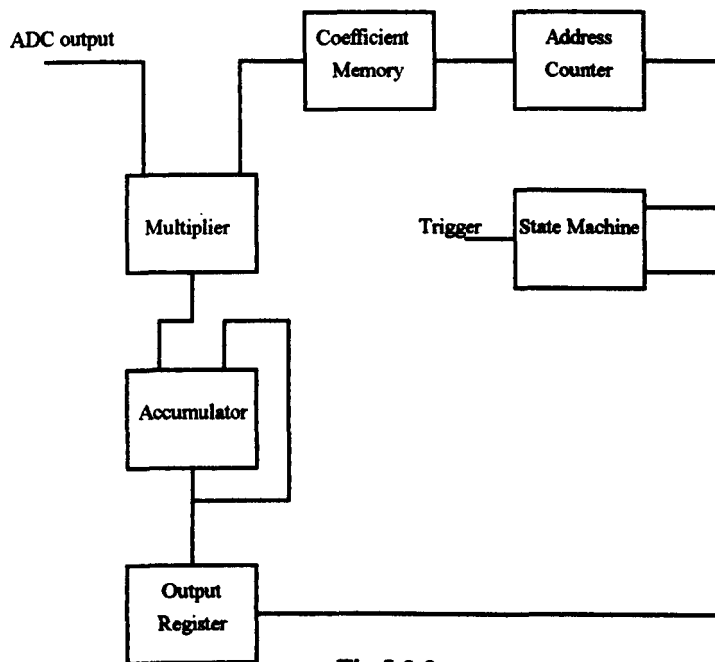he result of each multiplication is added to the contents of an accumulator. At the end of the process, the output of the accumulator is loaded into an output register. Figure 5.3.4 shows how this process relates to the concept of the FIR filter described above.
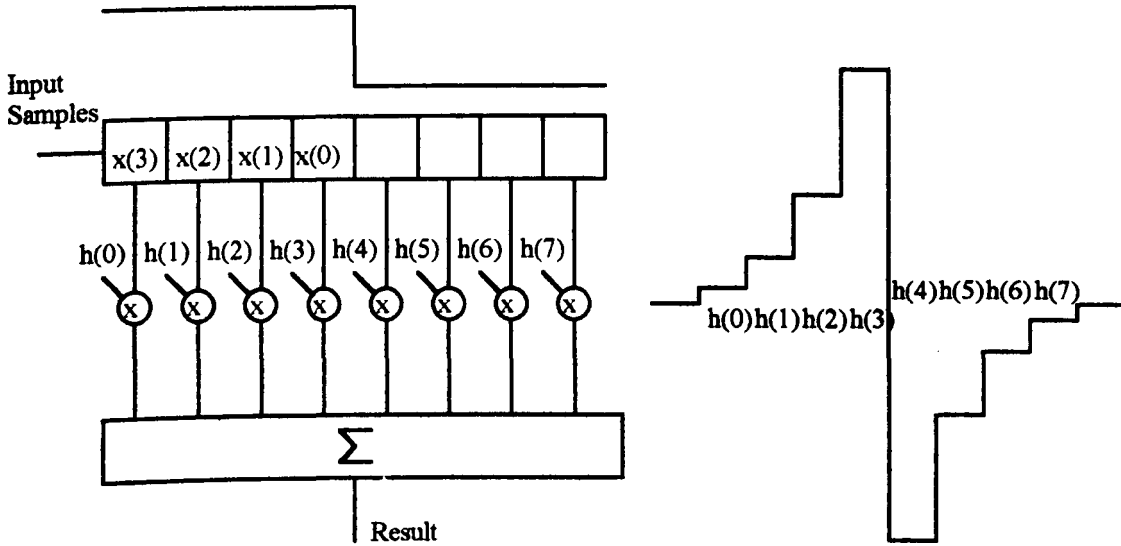
Fig 5.3.4

The result is a computation of the peak height of the cusp, given by:

$$y(N-1) = \sum_{n=0}^{N-1} h(n)y(N-1-n) \qquad (5.3.10)$$

The assumption is made that the step is imposed on a stable baseline and that the charge amplifier is reset immediately after the computation of the peak height on a pulse by pulse basis.

5.4 : COEFFICIENTS USED BY MULTIPLIER/ACCUMULATOR

The coefficients used to define the impulse response of the combined whitening and matched filters are calculated as follows:

$$H_W = (1-z^{-1})(1+A^{-1}z^{-1} + A^{-2}z^{-2}+...+A^{-(N-1)}z^{-(N-1)}) \qquad (5.4.1)$$

$$H_M = (1+Az^{-1} + A^2z^{-2}+...+A^{N-1}z^{-(N-1)}) \qquad (5.4.2)$$

106

where the scaling factor has not been used in the expression for the matched filter coefficients. The z-transform of the complete filter is given by:

$$H(z) = (1 - z^{-1}) \times \sum_{k=0}^{N-1} A^k z^{-k} \times \sum_{j=0}^{N-1} A^{-j} z^{-j} \qquad (5.4.3)$$

This expression can be manipulated to give:

$$H(z) = (1 - z^{-1}) \times \sum_{r=0}^{2N-2} C_1(r) z^{-r}$$

$$\text{where } C_1(r) = \sum_{q=0}^{Q1} A^{Q1} A^{-2q} \qquad (5.4.4)$$

and $\quad Q1 = r \qquad\qquad$ if $\quad 0 \le r \le N-1$

$\qquad Q1 = 2N - 2 - r \quad$ if $\quad N \le r \le 2N - 2$

The expression can be developed further to give:

$$H(z) = \sum_{r=0}^{2N-1} C_2(r) z^{-r} = \sum_{r=0}^{2N-2} C_1(r) z^{-r} - \sum_{r=1}^{2N-1} C_0(r) z^{-r}$$

$$\text{where } C_0(r) = \sum_{q=0}^{Q0} A^{Q0} A^{-2q} \qquad (5.4.5)$$

and $\quad Q0 = r - 1 \qquad$ if $\quad 1 \le r \le N-1$

$\qquad Q0 = 2N - 1 - r \quad$ if $\quad N \le r \le 2N - 1$

These equations are developed in Appendix 5 to give the following expressions for the coefficients:

$$C_2(r) = \frac{\cosh\left(\left(r + \frac{1}{2}\right) aT\right)}{\cosh\left(\frac{aT}{2}\right)} \quad \text{if } 0 \le r \le N-1 \qquad (5.4.6)$$

$$C_2(r) = -1 \times \frac{\cosh\left(\left(2N - r - \frac{1}{2}\right) aT\right)}{\cosh\left(\frac{aT}{2}\right)} \quad \text{if } N \le r \le 2N-1 \qquad (5.4.7)$$

The negative coefficients are not used in the scheme described above.

5.5 : FRONT-END CONVERTER

A data rate of 20MHz allows the construction of a weighting function with a peaking time of 1μs - 3μs with 20 - 60 samples. Peaking times of this order can be used for HPGe detectors. At the time of Owens' report, 20MHz ADCs were limited to 10bit resolution. Fortunately, it can be shown that the filtering action can reduce the effective quantisation noise to below that of a 12bit ADC, generally considered acceptable for high resolution work.

An input signal E produces an output amplitude given by:

$$S_0 = G_s E$$

(5.5.1)

where G_S the filter signal gain is given by:

$$G_s = \sum_{m=0}^{N-1} C_2(m)$$

(5.5.2)

For the coefficients derived in Section 5.4:

$$G_s = \sum_{m=0}^{N-1} \frac{A^{(m+0.5)} + A^{-(m+0.5)}}{A^{0.5} + A^{-0.5}} = \frac{A^N - A^{-N}}{A - A^{-1}}$$

(5.5.3)

Using standard theory, the quantisation noise power in one sample is given by $\frac{q^2}{12}$, where q is the quantising interval. This noise has uniform distribution. At the output of the filter, the quantisation noise power is the weighted sum of the noise powers associated with each sample, and the weighting factors are the squares of the coefficient values multiplying each sample, i.e.:

$$N_0^2 = \sum_{m=0}^{N-1} C_2^2(m) \frac{q^2}{12}$$

$$N_0^2 = G_N^2 \frac{q^2}{12}$$

(5.5.4)

For the coefficients derived in Section 5.4:

$$G_N^2 = \sum_{m=0}^{N-1} \left(\frac{A^{(m+0.5)} + A^{-(m+0.5)}}{A^{0.5} + A^{-0.5}} \right)^2 = \frac{A^{2N} - A^{-2N} + 2N(A - A^{-1})}{(A - A^{-1})(A + A^{-2} + 2)}$$

$$(5.5.5)$$

The signal to quantisation noise at the output is given by:

$$\frac{S_0^2}{N_0^2} = \frac{G_S^2 E^2 \times 12}{G_N^2 \times q^2}$$

$$\frac{S_0^2}{N_0^2} = \frac{E^2 \times 12}{q'^2}$$

$$(5.5.6)$$

where q' is the quantising level of an equivalent ADC producing the same signal to quantisation noise.

$$q' = q \times \frac{G_N}{G_S}$$

$$(5.5.7)$$

If $\frac{G_N}{G_S} < 0.25$ then the equivalent quantising interval is that of an ADC with more than 2bits of improved resolution.

Table 5.5.1 shows the value of $\frac{G_N}{G_S}$ for filter lengths of 16, 32 and 64 and for typical noise-corners of 0.25, 0.5, 1, 2, 4 and 8μs (i.e. a = 4, 2, 1, 0.5, 0.25 and 0.125).

	N=16	N=32	N=64
a=4	0.320	0.316	0.316
a=2	0.262	0.226	0.224
a=1	0.251	0.185	0.160
a=0.5	0.250	0.177	0.131
a=0.25	0.250	0.177	0.126
a=0.125	0.250	0.177	0.125

Table 5.5.1

For N > 16 and a < 4 there is more than 2 bit improvement in resolution, and a 10 bit ADC can be used. (If the negative coefficients were used, signal gain would be unchanged but quantisation noise would be doubled, leading to a further restriction in the selection of a above.)

5.6 : SIGNAL RECOGNITION CHANNEL

Owens' proposed system also had a digital implementation for the trigger channel. The circuit is shown in Figure 5.6.1.
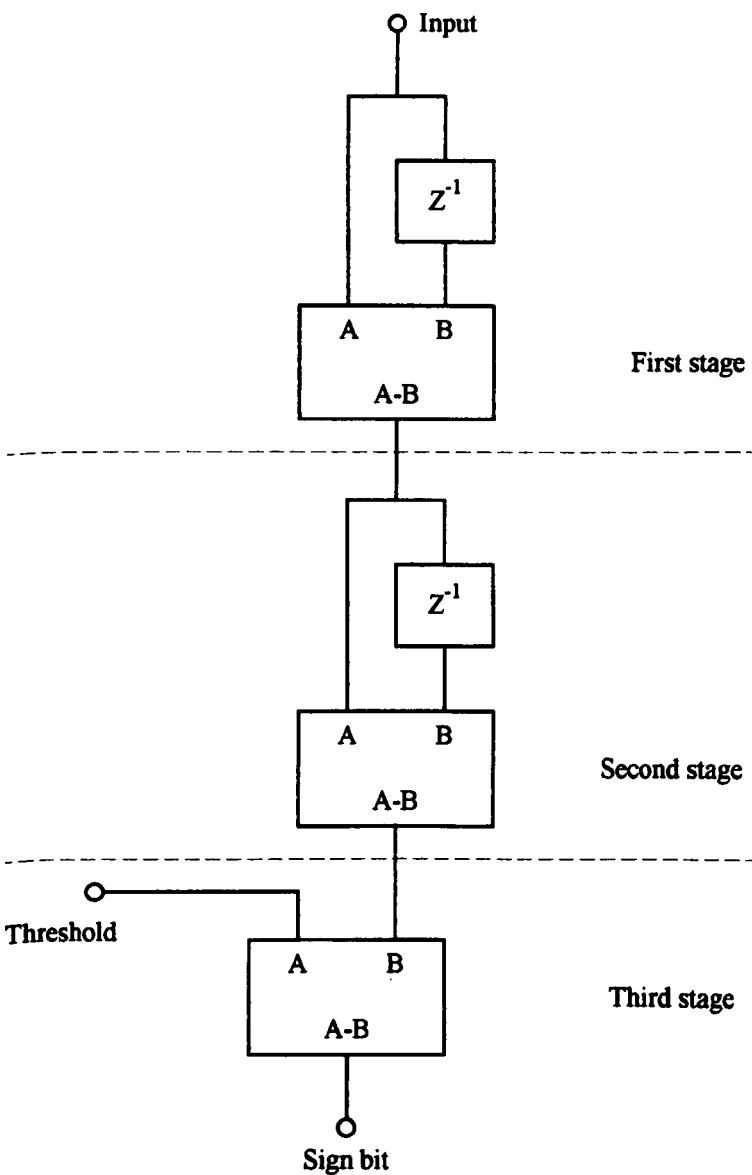

Fig 5.6.1

The system function of the first two stages is seen to be:

$$H(z) = 1 - z^{-1}$$

This implements a digital differentiator (compare the system function of the whitening filter with $a \rightarrow \infty$). The circuit output is shown in Figure 5.6.2.

Input signal.

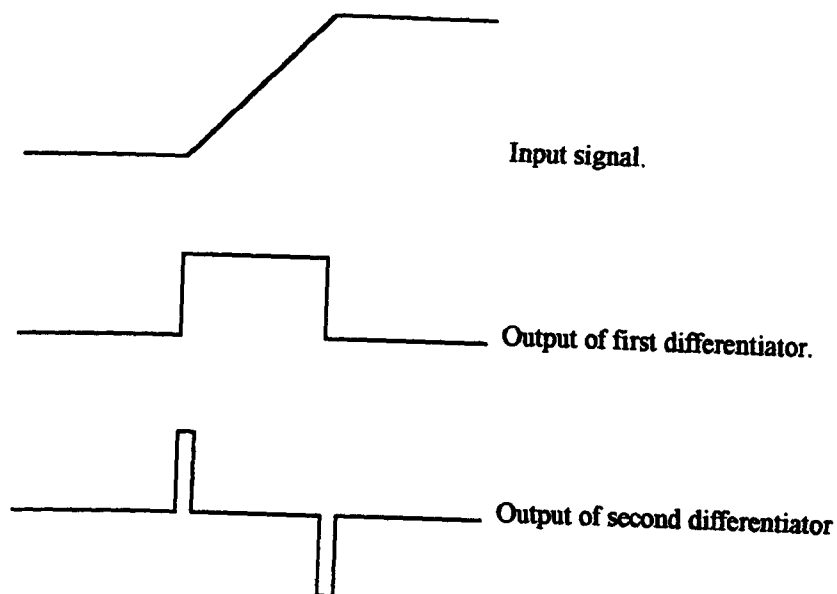Output of first differentiator.

Output of second differentiator

Fig 5.6.2

The third stage is a digital comparator, giving a one clock wide trigger pulse if the output of the second stage exceeds the threshold. The narrow width of the trigger pulse (50ns in a 20MHz system) allows the pile-up of closely spaced events to be detected and rejected.

CHAPTER 6 : PRACTICAL IMPLEMENTATION OF DMF

6.1 : REALISATION IN HARDWARE

A digital matched filter was built and tested at Harwell, employing the principles outlined in Chapter 5.

A TDC1020E1C ADC evaluation board from TRW was used as the front-end of the system. This board comprised a 10bit 20MSPS ADC, supplied with an input buffer amplifier, voltage references, tri-state output buffer and a fast DAC for reconstructing the output waveform. The input buffer circuit was modified to enable the input to range between 0Volts and +2Volts. Another modification was the addition of a pair of fast comparators and some logic to the input point, to generate an 'out of range' signal. Initially , these limits were set to the input range of the ADC.

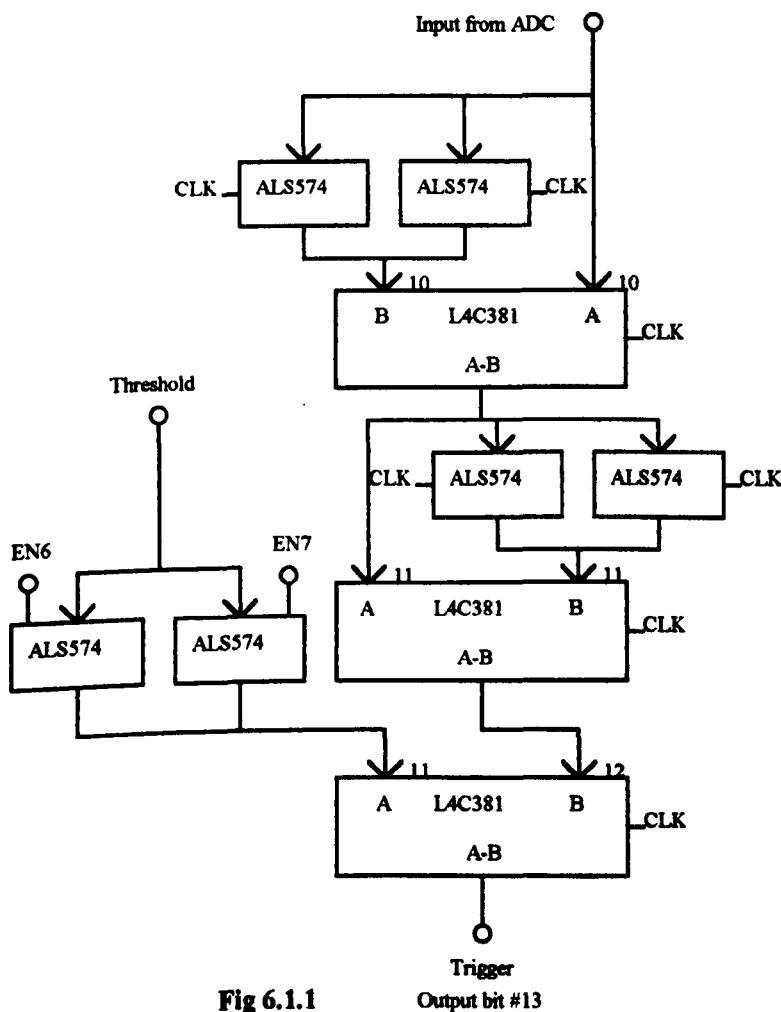Figure 6.1.1 shows the block diagram of the signal recognition circuit.

Fig 6.1.1   Output bit #13

112

The circuit is a straight-forward implementation of the scheme proposed in Section 5.6. The L4C381 is a 16bit ALU, configured here to give the output A-B. The output of the first differentiator needs to be 11bits wide, i.e.10bits magnitude and a sign bit. Similarly, the output of the second differentiator needs to be 12bits wide, i.e.11bits magnitude and a sign bit. The final result can have 12bits magnitude and bit13 is taken as the sign bit. In order to facilitate the two's complement arithmetic, the A and B inputs of the second differentiator, and the B input of the digital comparator are sign extended, i.e. bit#11 is connected to bit#12 in the former and bit#12 is connected to bit#13 in the latter. All other inputs are grounded.

A delay of one clock period is generated by clocking the data through ALS574 octal latches.

ALS574s are also used to store the 11bit value of the threshold setting. Each latch is loaded from the data bus by pulsing EN6 and EN7 (see below).

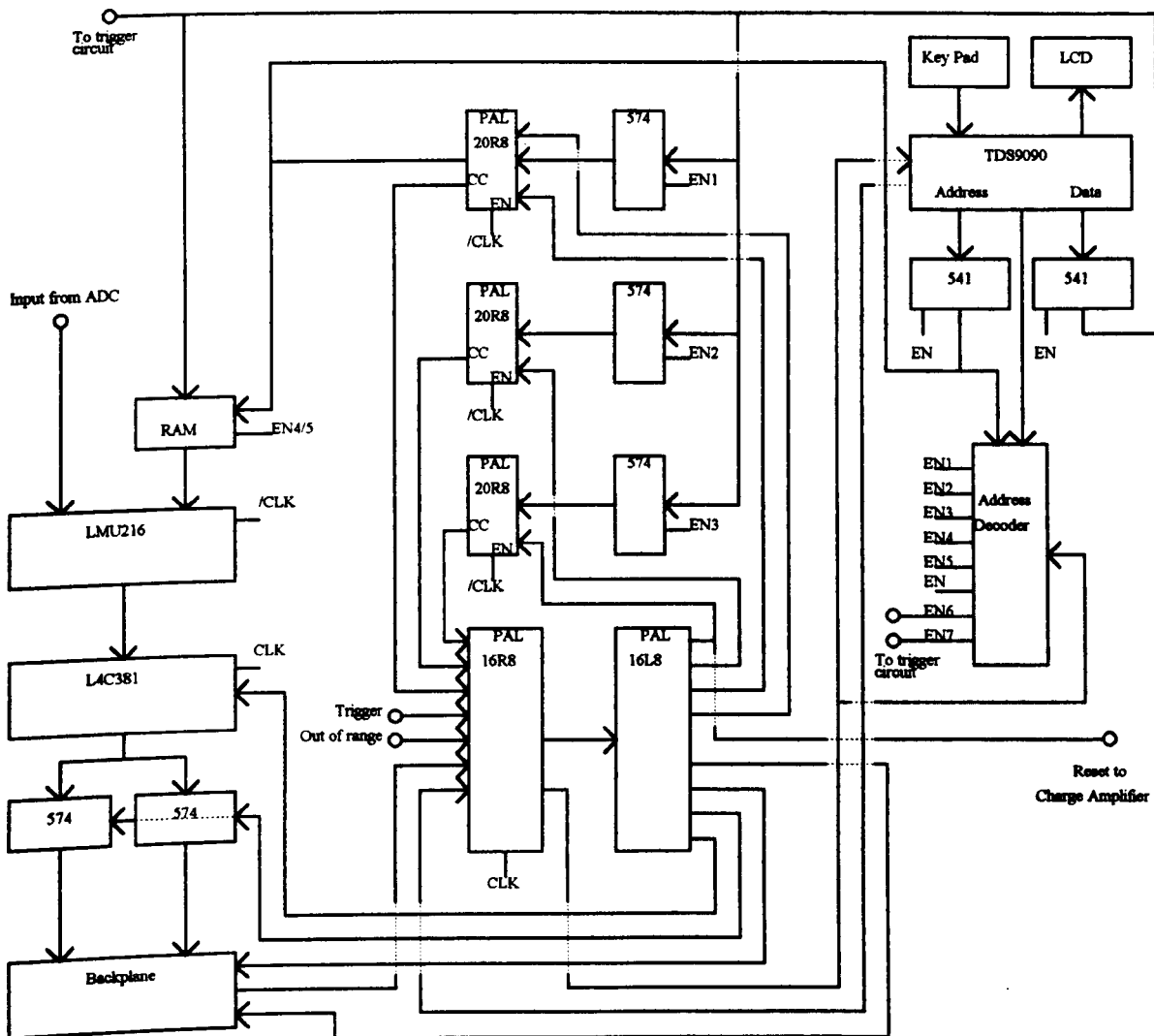Figure 6.1.2 is a block diagram of the matched filter and control circuit.

Fig 6.1.2

The LMU216 16x16 bit multiplier, and the L4C381 16bit ALU, configured as an accumulator, implement the filtering action. A 16bit RAM holds the coefficients needed by the multiplier. The output of the multiplier is the 16 most significant and rounded-off bits of a 32 bit product. To reduce the round-off errors introduced, the output must be as large as possible consistent with not overloading the accumulator in its accumulation of N products.

The output of the accumulator is 16bits (but only the 12 most significant are stored in the ALS574 output registers and linked to the MCA via the backplane). The signal gain, therefore, needs to be approximately 64 (65535/1023), where signal gain was defined in Section 5.5 as $G_s = \sum_{m=0}^{N-1} C_2(m)$. In Appendix 6 it is shown that such gains cannot be set by the coefficient profile constrained by a 16bit definition; the problem is especially bad at short shaping times. Part of the gain is therefore set by a left shift of the ADC bits into the multiplier; a shift of 3 bits is a compromise that allows relatively

114

short shaping to be used without causing the coefficients of longer shaping to be too small to maintain the accuracy of the computation.

The operation of the filter and the sequencing of the system is controlled by a state-machine implemented in programmable logic. Timings used in the processing cycle are generated by enabling pre-loaded counters (PAL20R8s) and allowing them to count down under the control of the system clock. A 'counter complete' signal instructs the state machine to move to the next state. A similar sequencing system was used in the analogue processor described in Section 4.11. The counter defining the processing time has its outputs connected to the address bus of the coefficient RAM. Thus, N coefficients are presented to the multiplier during the processing time.

A registered PAL16R8 defines the current state of the state-machine and a combinatorial PAL16L8, fed by the state bits, generates most of the state outputs. The state diagram is shown in figure 6.1.3, and the state outputs are shown in Table 6.1.1.
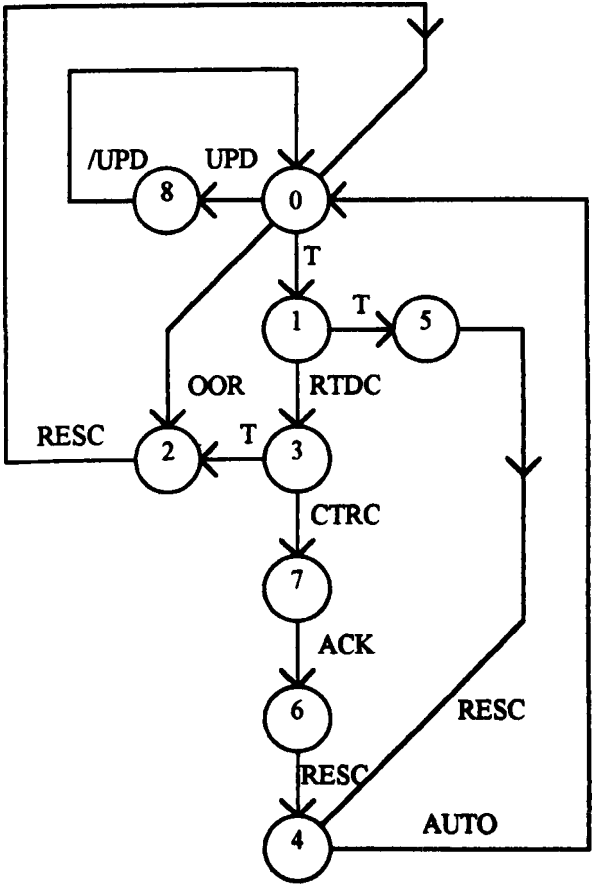

Fig 6.1.3

115

STATE	ACTIVE OUTPUTS			
0	CLEAR	OECTR		NACT
1	CLEAR	OECTR	ENRTD	
2	CLEAR	OECTR	ENRES	
3		OECTR	ENCTR	
4	CLEAR	OECTR		
5	CLEAR	OECTR	ENRES	
6	CLEAR	OECTR	ENRES	
7		OECTR		DRDY
8	CLEAR			UPDEN

Table 6.1.1

The main processing sequence is S0 → S1 → S3 → S7 → S6 → S4 → S0. A trigger pulse (T) initiates the cycle. In state S1, the rise-time delay counter is enabled; this function mimics the action of the series switch in the analogue processor in that it allows the input signal to reach its full amplitude before processing is initiated. The counter complete signal (RTDC) moves the sequence to state S3, where the main signal processing takes place. The coefficient counter is enabled, and the counter complete signal causes a state change to S7. The state-machine now signals to the remote MCA that data is ready (DRDY) and the MCA has to acknowledge receipt of the data (ACK) before state S6 is entered. (Some glue logic returns an internal acknowledge signal after a time-out in the event that the MCA is not on-line.) In state S6, the reset time counter is enabled. This defines the width of the reset pulse applied to the charge-amplifier. The counter-complete signal (RESC) moves the sequence back to state S0 through the automatic state S4, used to maintain minimum state locus.

A second trigger during the rise-time delay or processing time causes an immediate reset to eliminate pile-up effects. An 'out of range' signal (OOR) also causes an immediate reset of the charge amplifier; the signal is derived from comparators monitoring the ADC's input.

An 'update request' signal (UPD) from the user interface computer causes an idle state-machine to enter state S8, where it signals an acknowledge to the computer (UPDEN). The computer can now update parameters before allowing the state machine to return to its idle state.

The remaining state-machine outputs are OECTR which tri-states the coefficient counter's outputs during updates so that the interface computer has control of the RAM address bus, CLEAR which holds the accumulator in its reset state until processing is initiated, NACT which indicates live-time to the MCA and a modified coefficient counter complete signal to clock the output buffer.

The user-interface is similar to that used in the analogue processor in that a TDS9090 Forth single-board computer is used to set system parameters. The interface in this case is implemented with a keypad and LCD display. The user has control of the rise-time delay, the reset time, the threshold used in the trigger circuit, the length of the filter (16, 32 or 64), and the noise-corner. In addition to the matched coefficients, there is also a facility for selecting uniform coefficients or for passing ADC samples to the MCA without any filtering. The Forth computer passes the parameters to on-board registers and the RAM by using the data bus and an address decoder.

6.2 : EXPERIMENTAL RESULTS

The system was initially tested with simulated detector pulses mixed with white noise. The arrangement is shown in Figure 6.2.1.
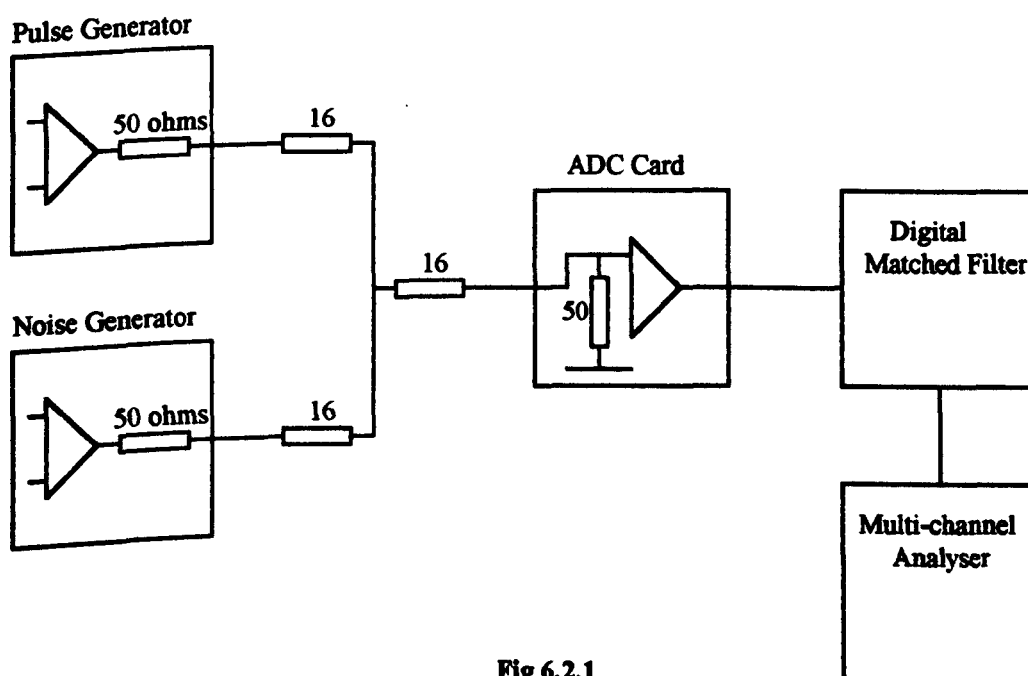

Fig 6.2.1

The Pulse Generator used was a Berkeley Nucleonics PB-4. A typical test signal used in the measurements was a rectangular pulse with 0.05µs rise-time, 1µs fall-time and 6 µs width.

The white noise generator is shown in Figure 6.2.2. The voltage developed by the saturation current of a reversed biased P-N junction is amplified by a wideband op-amp; the noise spectrum is flat between the roll-offs caused by the coupling time-constant and the amplifier's high-frequency response.
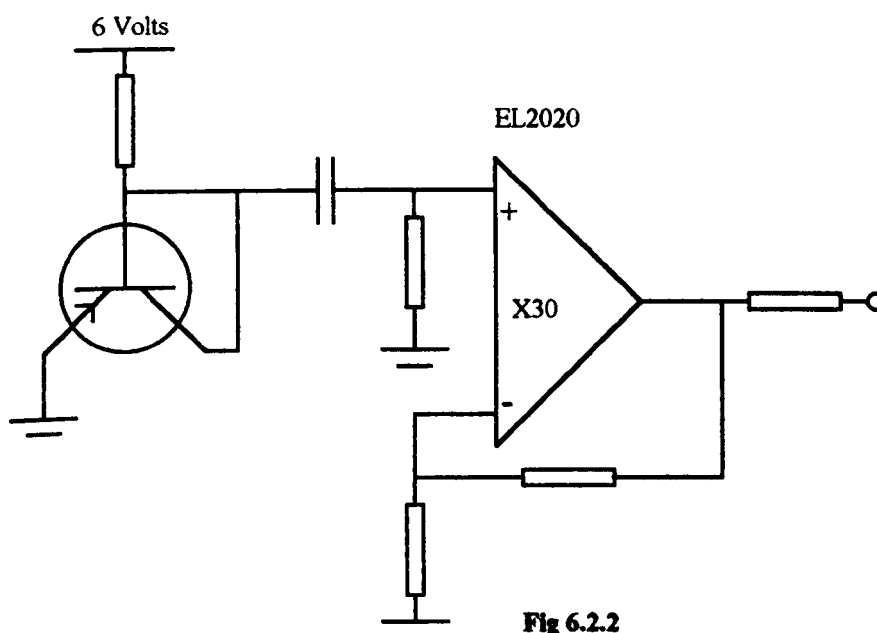

Fig 6.2.2

Figure 6.2.3a is the MCA output produced by sweeping the amplitude of a 'clean' pulse into the ADC card. The effect of the differential linearity of the ADC can be seen as unequal channel widths, leading to low counts in some channels and high counts in others. The greatest linearity errors occur at the major code changes. Even though the ADC's DNL is quoted as +/- 1%, this is clearly unacceptable for nuclear spectroscopy.

Figure 6.2.3b shows the MCA output when 50mV peak-to-peak noise is added to the input pulse. At the ADC's input, this noise translates to +/- 6LSBs. It can be seen that the differential linearity is improved but that system performance is still poor, and this level of noise is greater than that expected in a typical spectroscopy system (1/3 to 1/2 LSB RMS noise[74]). The linearity of the system could be improved considerably by using limit-reset charge-amplifiers. A given pulse amplitude is then converted into a wide range of ADC channels and the differential non-linearity is improved by averaging. The principle of converting a given pulse amplitude in different bins was

118

proposed by Gatti[10] as a method of improving the DNL of conventional ADCs; the DNL is reduced by M+1 where M is the number of channels exercised by the pulse. Unfortunately, limit reset compromises the resolution of the system as the maximum pulse amplitude has to be limited to, maybe, a quarter of the ADC's input range. This would mean that a 12bit 20MHz ADC would be required in commercial equipment. A limit reset scheme would also require a baseline estimation by the digital filter.

Figures 6.2.4a and 6.2.4b illustrate the noise reduction property of the digital filter. A set-up similar to that shown in Figures 6.2.1 and 6.2.2 is used to generate a fixed pulse amplitude corrupted by white noise. In Figure 6.2.4a, the resulting MCA output is shown when the pulse is passed through the system without any filtering. Figure 6.2.4b shows the output when a filter length of 32 and uniform coefficients are used.

The circuit shown in Figure 6.2.5 was built to shape the test noise spectrum to look like that of a typical spectrometer. The noise spectrum measured with a 40MHz spectrum analyser had break points set by the R_1C_1 and R_2C_1 time constants, as shown in Figure 6.2.6.
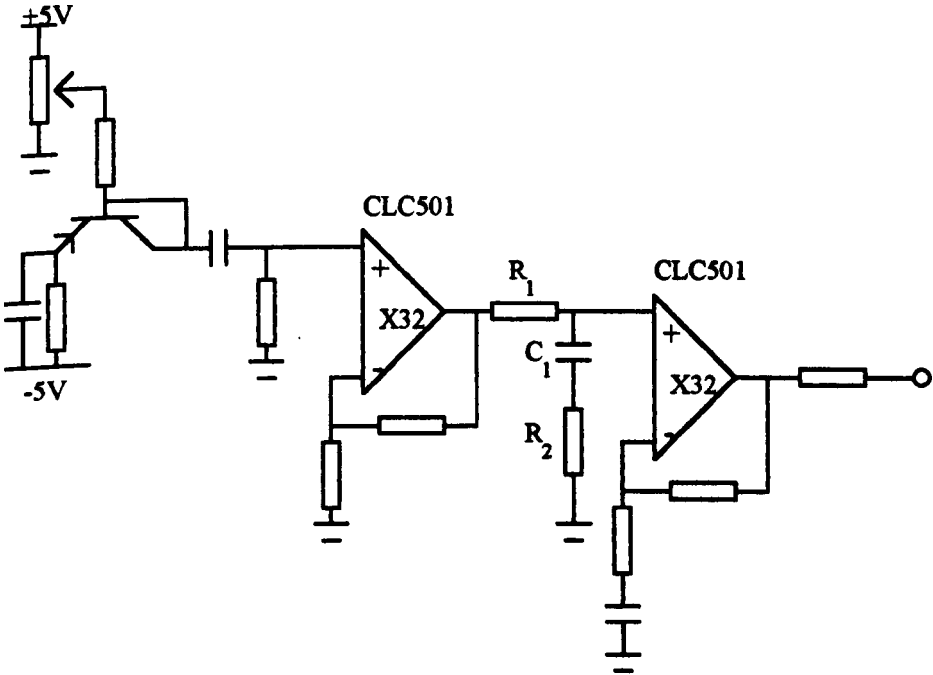

Fig 6.2.5
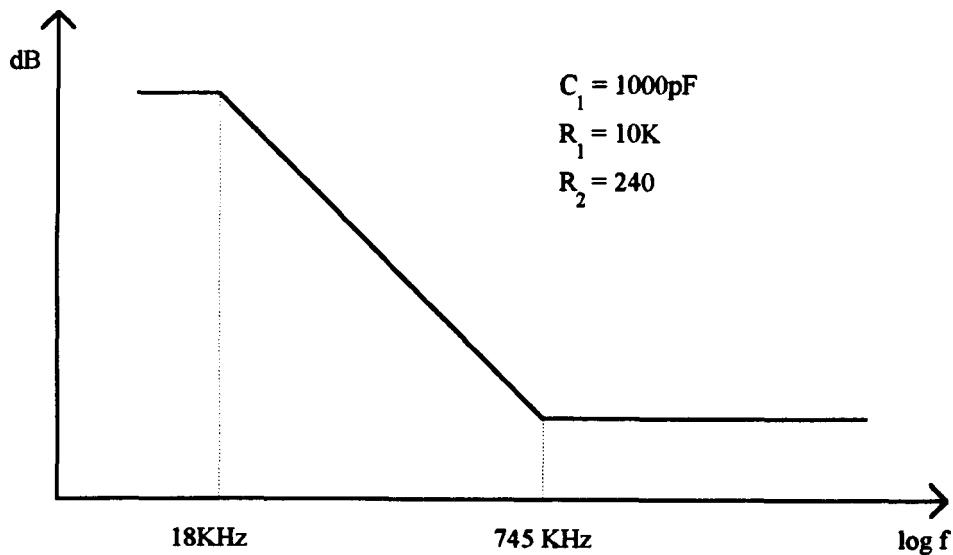
119

$C_1 = 1000pF$
$R_1 = 10K$
$R_2 = 240$

Fig 6.2.6

The shaped noise was added to the test pulse in a summing amplifier with variable noise gain, and fed into the ADC card. Table 6.2.1 summarises the results for a filter length of 32.

NOISE CORNER	COEFFICIENTS	SIGNAL-TO-NOISE
250nS	Uniform	74
	Matched to 250nS	59
620nS	Uniform	78
	Matched to 250nS	52
	Matched to 620nS	71
	Matched to 1240nS	86
	Matched to 1860nS	86
	Matched to 3100nS	78
2000nS	Uniform	81
	Matched to 250nS	50
	Matched to 500nS	67
	Matched to 1000nS	77
	Matched to 1500nS	81
	Matched to 2000nS	81

Table 6.2.1

The signal to noise ratio η is estimated from the formula : $\eta = \dfrac{2.36V}{V_{FWHM}}$ where V and

V_{FWHM} were measured from a Canberra Series85 MCA display. The accuracy of the

FWHM measurement was not good, especially for the figures given for the 620nS noise corner (+/- 10%). It is thought that measurement error explains the relatively good performance exhibited by coefficients matched to 1240nS and 1860nS used with 620nS noise. Ignoring these measurements, a pattern is clear; regardless of the actual noise corner used, the resolution of a matched coefficient system improves as the matched time-constant is increased, becoming as good as the resolution of an uniform coefficient system when the matched time-constant is long compared to the filter length (and the coefficients used become more uniform).

Table 6.2.2 shows the effect of using different filter lengths. The same pattern is seen; when the matched time-constant is short compared to the filter length the resolution is degraded, otherwise resolutions are comparable.

Noise Corner	Coefficients	SNR @ N=16	SNR @ N=32	SNR @ N=64
510nS	Uniform	84.1	112.2	146.1
	Matched to 510nS	85.1	96.8	98.0
2000nS	Uniform	65.6	93.3	129.0
	Matched to 2000nS	66.2	92.7	122.9

Table 6.2.2

These results were not expected from the theory of matched filters developed earlier. Because the system implemented does not have a direct analogue equivalent, it is necessary to develop expressions for the step and delta noise indices from digital signal processing theory. This is developed in Chapter 7.

Finally, a spectrometer was interfaced into the system to test the performance with real signals. The detector used was a DSG NSG-14 (n-type, HPGe); it was coupled to a Harwell 930128 charge-amplifier fitted with a room-temperature FET and pulse-by-pulse optical reset.

It was quickly realised that the digital recognition circuit described in Secction 5.6 was not sophisticated enough to be effective with real signals. The problem is caused by slow rise-time signals. In Appendix 7, the circuit output is calculated for an input pulse amplitude corresponding to one quarter of the ADC's dynamic range (perhaps the largest signal available in a limit restore system) and having a rise-time of 0.5μs. It can

be seen that the circuit output is low (but that the pile-up resolving time is good). It would be difficult to set a threshold that accepted smaller valid pulses without noise triggering. The circuit output could be boosted by increasing the delays in the first and second differentiators, and forming the system function $H(z) = 1 - Z^{-N}$. The penalty is worse pile-up resolving time; this is also shown in Appendix 7. Practically, increasing the delays means increasing the number of chips and board area of an already large circuit.

It was also realised that the use of a baseline estimator was unavoidable even in a pulse-by-pulse restore system. The integration of detector leakage current, especially at low input count rates, and the pile-up of undetected events cause a large variation in the baseline. Consequently, the largest signals of interest in a pulse-by-pulse reset system also need to be limited to some fraction of the ADC's dynamic range. On the plus side, pulse-by-pulse system might be expected to have better differential linearity than suggested previously.

Figure 6.2.3a Front-end converter binning in the absence of input noise.
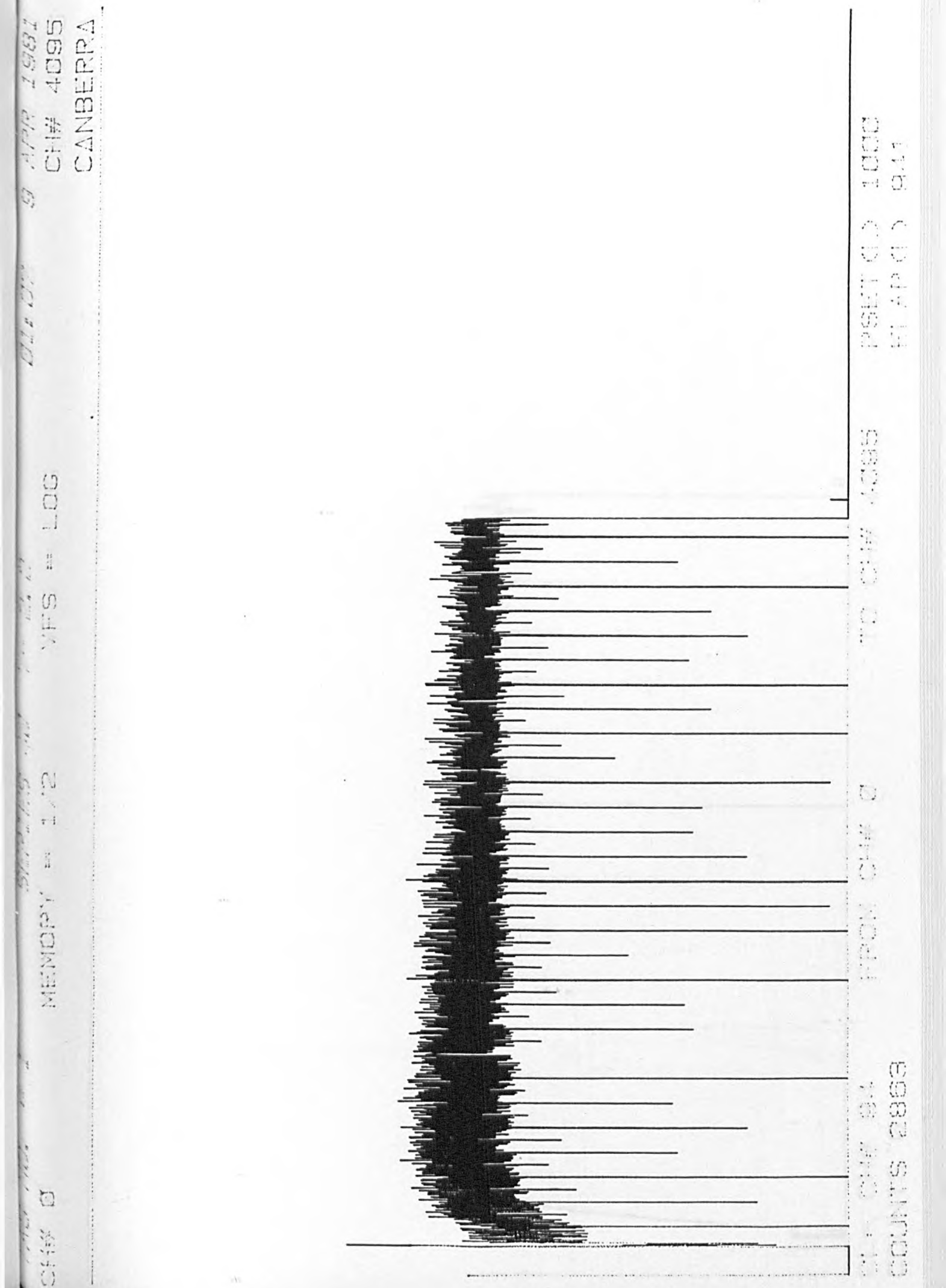
Figure 6.2.3b Front-end converter binning in the presence of 50mV peak-to-peak noise, showing improvement in differential non-linearity.
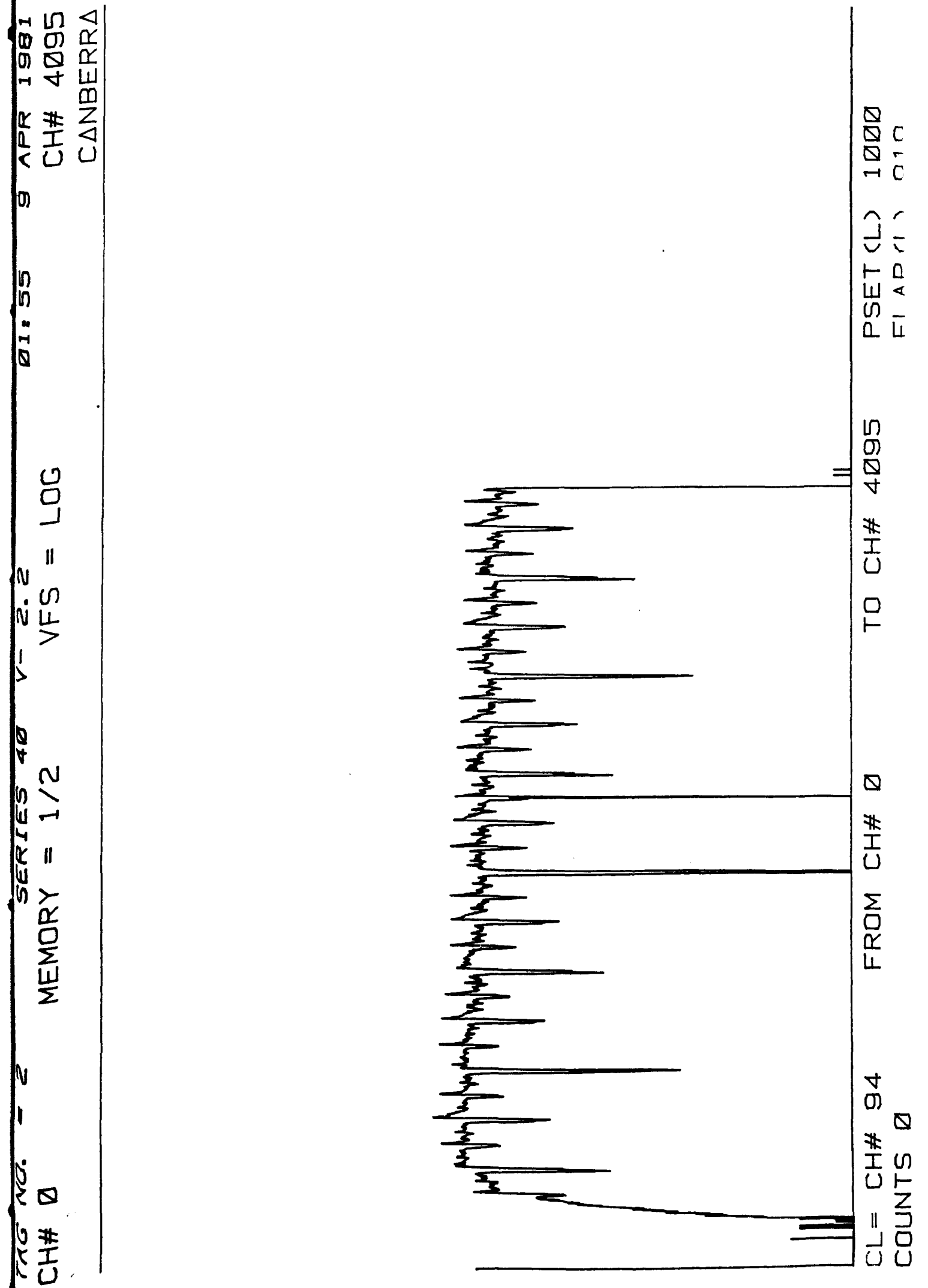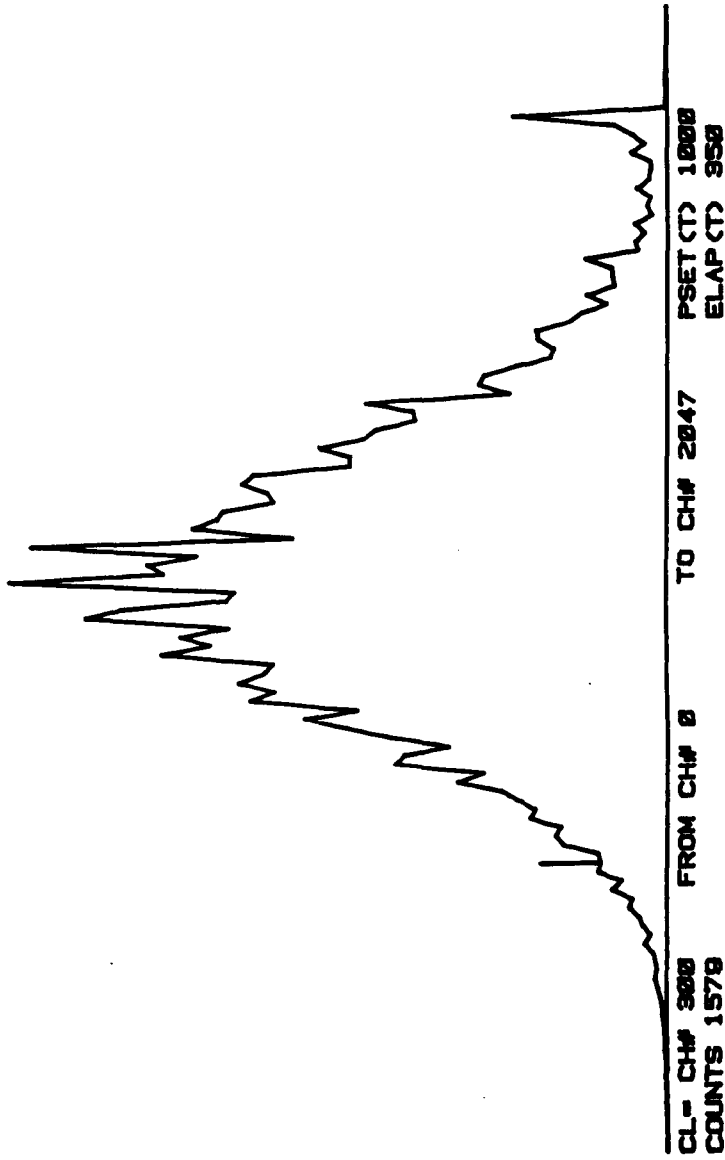
Figure 6.2.4a Fixed amplitude pulse, corrupted by white noise, passing through the digital pulse processor without filtering.

Figure 6.2.4b Fixed amplitude pulse, corrupted by white noise, filtered by an uniform coefficient filter of length 32.
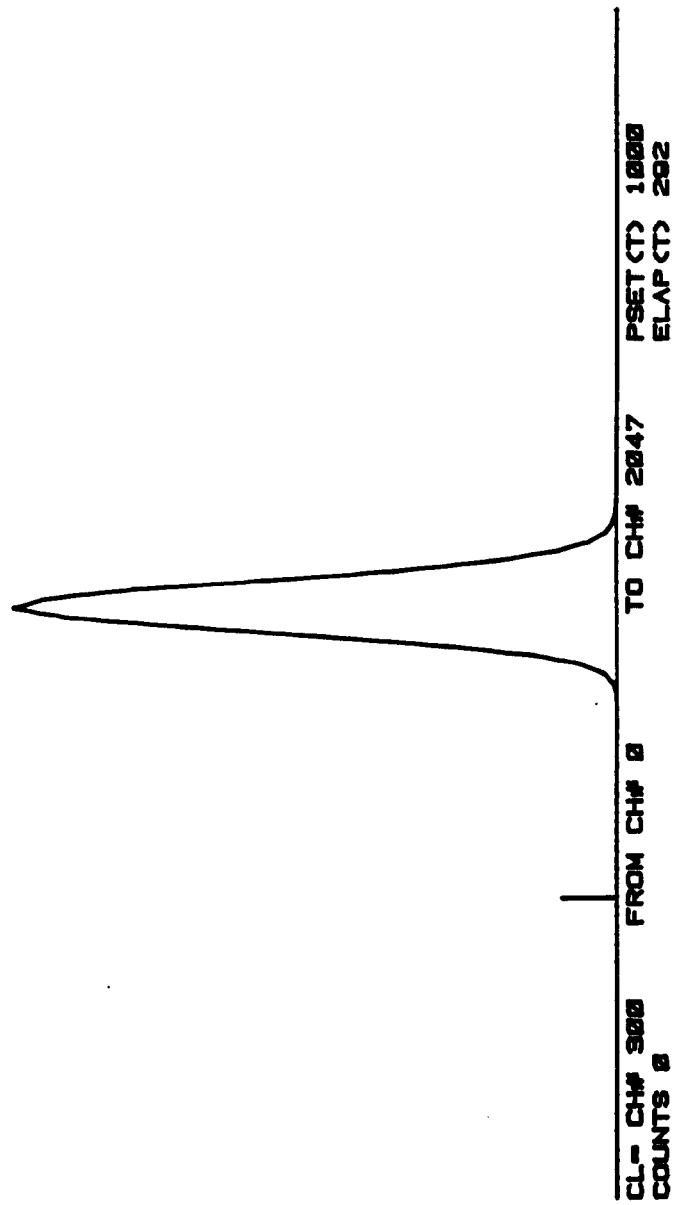
CHAPTER 7 : THE NOISE PERFORMANCE OF A DIGITAL PROCESSOR

7.1 : DELTA AND STEP NOISE INDICES FOR FIR DIGITAL FILTERS

If a digital filter of length N has coefficients $\sum_{n=0}^{N-1} C_n$ and only positive coefficients are used, then the peak output for a signal step V_s is given by:

$$V_{out} = V_s \sum_{n=0}^{N-1} C_n \qquad (7.1.1)$$

If the coefficients implement an impulse response of the type shown in Figure 5.2.2b, where $\dfrac{N}{2}$ positive coefficient are followed by $\dfrac{N}{2}$ negative coefficients, the peak output is given by:

$$V_{out} = V_s \sum_{n=0}^{\frac{N}{2}-1} C_n \qquad (7.1.2)$$

The signal gain of these filters is therefore given by:

$$G_s = \sum_{n=0}^{N-1} C_n \quad \text{or} \quad G_s = \sum_{n=0}^{\frac{N}{2}-1} C_n \qquad (7.1.3)$$

Owens[75] derived an expression for the variance of the noise at the output of a digital filter; it is given by:

$$\sigma^2 = \sum_{j=0}^{N-1} \sum_{k=0}^{N-1} C_j C_k R[jT, kT] \qquad (7.1.4)$$

where R[jT, kT] is the autocorrelation of two noise samples separated by time (j-k)T, T being the sampling period. The expression is an expansion of the formula:

$$\sigma^2 = E\left\{ \left(\sum_{n=0}^{N-1} C_n e_n \right)^2 \right\} \qquad (7.1.5)$$

where E{ } denotes mathematical expectation and $E\{e_j e_k\} = R[jT, kT]$[76].

Given that delta noise is stationary white noise with single-sided spectral density $2I = 4kTR_n \dfrac{C_i^2}{C_f^2}$ the autocorrelation function is known to be $R(\tau) = I\delta(\tau)$ [77] . It is an impulse of strength I located at $\tau = 0$.

autocorrelation of bandlimited white noise

spectral density of bandlimited wwhite noise

autocorrelation of sampled noise

spectral density of sampled noise
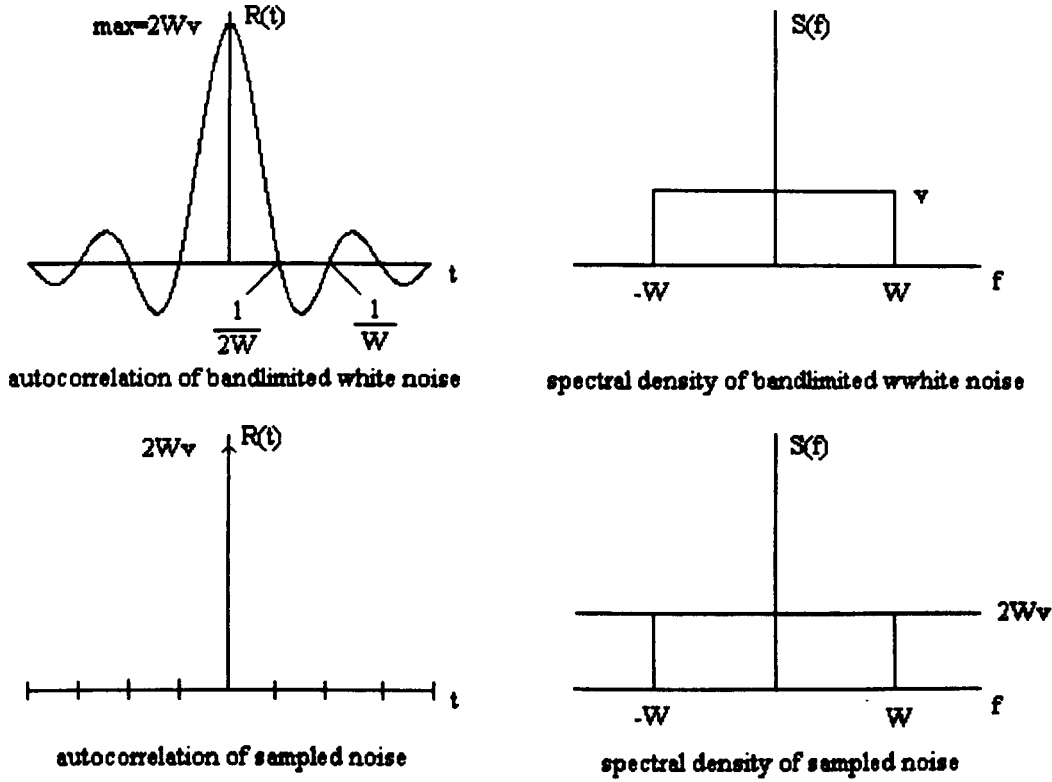
Fig 7.1.1

Figure 7.1.1 illustrates the case where bandlimited white noise is sampled[78] .If the sampling frequency is twice the bandwidth of the noise, the discrete noise is white and the discrete autocorrelation function is again an impulse at the origin. The impulse strength is modified to $\dfrac{I}{T}$ where T is the sampling period.

From the considerations above, $E\{e_j e_k\} = 0$ if $j \neq k$ and the variance of the noise at the output of the filter is given by:

$$\sigma^2 = \sum_{n=0}^{N-1} C_n^2 E\{e_n^2\} \qquad (7.1.6)$$

$$\sigma^2 = \frac{I}{T} \times \sum_{n=0}^{N-1} C_n^2 \qquad (7.1.7)$$

128

Comparing this expression with that developed in Section 2.3, it is clear that the summation is the discrete equivalent of the integration of the squared impulse response. For analogue systems, the delta noise index was defined to be:

$$N_d^2 = \frac{\int_{-\infty}^{\infty} h_i^2(t)\,dt}{h_{peak}^2} \qquad (7.1.8)$$

where h_{peak} is the peak response to an unit amplitude input signal. The corresponding index in a discrete system can now be defined:

$$N_d^2 = \frac{\sum_{n=0}^{N-1} C_n^2}{\left(\sum_{n=0}^{N-1} C_n\right)^2} \quad \text{positive coefficients only} \qquad (7.1.9)$$

$$N_d^2 = \frac{\sum_{n=0}^{N-1} C_n^2}{\left(\sum_{n=0}^{\frac{N}{2}-1} C_n\right)^2} \quad \text{positive/negative coefficients} \qquad (7.1.10)$$

Step noise is integrated by the charge-amplifier's feedback capacitor; it is therefore non-stationary and its variance increases from the time the charge-amplifier was reset. According to Papoulis[79], the integration of white noise is a Wiener process:

$$w(t) = \int_0^t v(\beta)\,d\beta \qquad (7.1.11)$$

In such a process, if the autocorrelation of the input stationary white noise is given by:

$$R_v(\tau) = \alpha\delta(\tau) \qquad (7.1.12)$$

then the autocorrelation of the output noise is given by:

$$R_w(t_1, t_2) = \alpha \min(t_1, t_2) \qquad (7.1.13)$$

Owens[80] showed that when the input noise source is a current generator of single-sided spectral density $2\alpha = 2qI_n$ then the equations for the Wiener process become:

$$w(t) = \frac{1}{C_f} \int_0^t i(\beta) d\beta \qquad (7.1.14)$$

$$R_i(\tau) = \alpha \delta(\tau) \qquad (7.1.15)$$

$$R_v(t_1, t_2) = \frac{\alpha}{C_f^2} \min(t_1, t_2) \qquad (7.1.16)$$

The following definitions are now made:

$$t_1 = ((N-k)+m)T$$
$$t_2 = ((N-j)+m)T \qquad (7.1.17)$$

where mT represents the delay between the last reset of the charge-amplifier and the start of the processing time.

If $j > k$ then $t_2 < t_1$ and $R[(j-k)T] = \frac{\alpha}{C_f^2}((N-j)+m)T \qquad (7.1.18)$

If $k > j$ then $t_1 < t_2$ and $R[(j-k)T] = \frac{\alpha}{C_f^2}((N-k)+m)T \qquad (7.1.19)$

The equation for the output variance can be now be expanded to give:

$$\begin{aligned}
\sigma^2 = \{ &C_0^2(N+m) + C_0C_1(N-1+m) + C_0C_2(N-2+m)+...+C_0C_{N-1}(1+m) \\
&+ C_1C_0(N-1+m) + C_1^2(N-1+m) + C_1C_2(N-2+m)+...+C_1C_{N-1}(1+m) \\
&+ C_2C_0(N-2+m) + C_2C_1(N-2+m) + C_2^2(N-2+m)+...+C_2C_{N-1}(1+m) \\
&+ \\
&+ C_{N-1}C_0(1+m) + C_{N-1}C_1(1+m) + C_{N-1}C_2(1+m)+...+C_{N-1}^2(1+m) \} \times T\frac{\alpha}{C_f^2}
\end{aligned}$$
$$(7.1.20)$$

The closed form of this expression can easily be shown to be:

$$\sigma^2 = T\frac{\alpha}{C_f^2} \left\{ \sum_{n=0}^{N-1} \left(\sum_{r=0}^{n} C_r \right)^2 + m \left(\sum_{r=0}^{N-1} C_r \right)^2 \right\} \qquad (7.1.21)$$

The expression within the brace is the discrete equivalent of the analogue integration of the filter's squared step response. The contribution of noise steps occurring after the last charge-amplifier reset, but before the start of the processing time, is defined by the second term. From the theory of Wiener processes, the variance time t after the start of the integration is known to be αt, in this case $mT\dfrac{\alpha}{C_f^2}$. This 'offset' is effectively multiplied by the gain of the filter.

For the analogue case, a step noise index was defined as:

$$N_s^2 = \frac{\displaystyle\int_{-\infty}^{\infty} h_s^2(t)\,dt}{h_{peak}^2} \tag{7.1.22}$$

From this, the step noise index for the discrete case can be defined as:

$$N_s^2 = \frac{\displaystyle\sum_{n=0}^{N-1}\left(\sum_{r=0}^{n} C_r\right)^2 + m\left(\sum_{r=0}^{N-1} C_r\right)^2}{\left(\displaystyle\sum_{r=0}^{N-1} C_r\right)^2} \quad \text{positive coefficients only} \tag{7.1.23}$$

$$N_s^2 = \frac{\displaystyle\sum_{n=0}^{N-1}\left(\sum_{r=0}^{n} C_r\right)^2 + m\left(\sum_{r=0}^{N-1} C_r\right)^2}{\left(\displaystyle\sum_{r=0}^{\frac{N}{2}-1} C_r\right)^2} \quad \text{positive/negative coefficients} \tag{7.1.24}$$

7.2 : MATCHED FILTER COEFFICIENTS

The matched coefficients derived in Section 5.4 can now be used in the equations derived above. Figures 7.2.1, 7.2.2 and 7.2.3 show how the delta noise index, the step noise index and the Goulding product vary as the noise corner matched by the coefficients is changed from 16µs to 0.5µs. The ordinate shows the ratio of the sampling time to the noise-corner aT. The filter length is 128. For comparison, the values for an uniform coefficient filter of the same length are also shown.
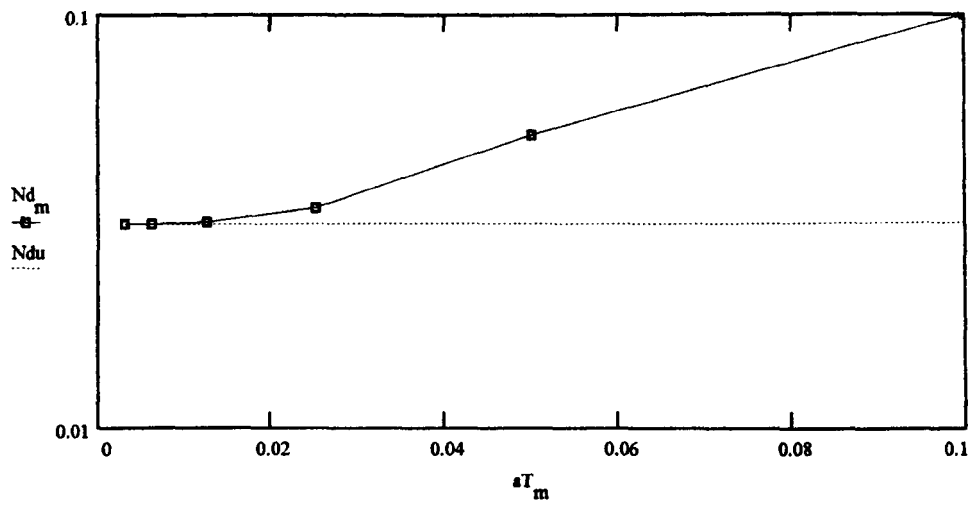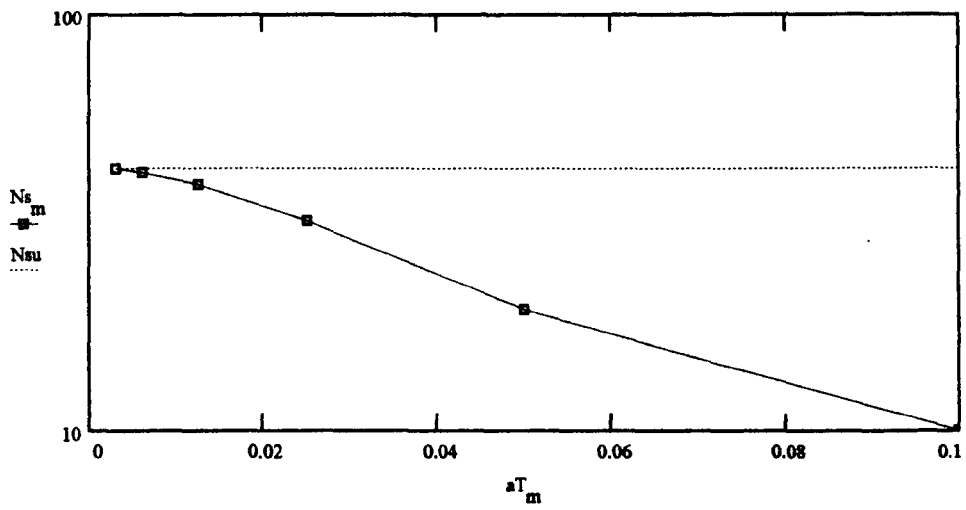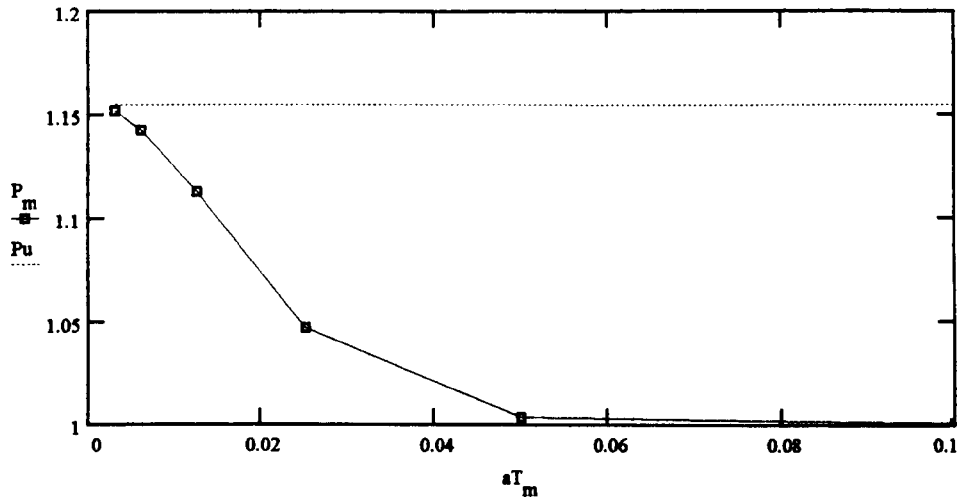
Fig 7.2.1

Fig7.2.2

Fig7.2.3

It can be seen that the Goulding product tends towards the ideal value of 1.00 as the noise corner time constant becomes shorter and the full range of the coefficient values can be accommodated by the filter length. As the noise corner time constant becomes longer the coefficients become more uniform, as only a part of the time constant is covered by the filter's N.T product. As a result, delta and step noise indices become those of an uniform coefficient filter. In this case, the Goulding product is seen to tend towards that of a triangular shaper (1.15), the triangle being the step response of uniform coefficients as discussed in Section 5.2.

It is worth noting that with these balanced positive and negative coefficients,

$$\left(\sum_{r=0}^{N-1} C_r \right)^2 = 0 \qquad (7.2.1)$$

and the noise steps accumulated before the processing time do not contribute to the output variance. The negative coefficients that cause the output pulse shape to decay also provide the filter with baseline estimation.

It is interesting to consider the case of a positive coefficient only filter, as described in Chapter 6. Figures 7.2.4, 7.2.5 and 7.2.6 show the delta noise index, step noise index and Goulding product assuming that there is no time between successive pulses, i.e. the next pulse occurs immediately after the reset of the charge-amplifier.
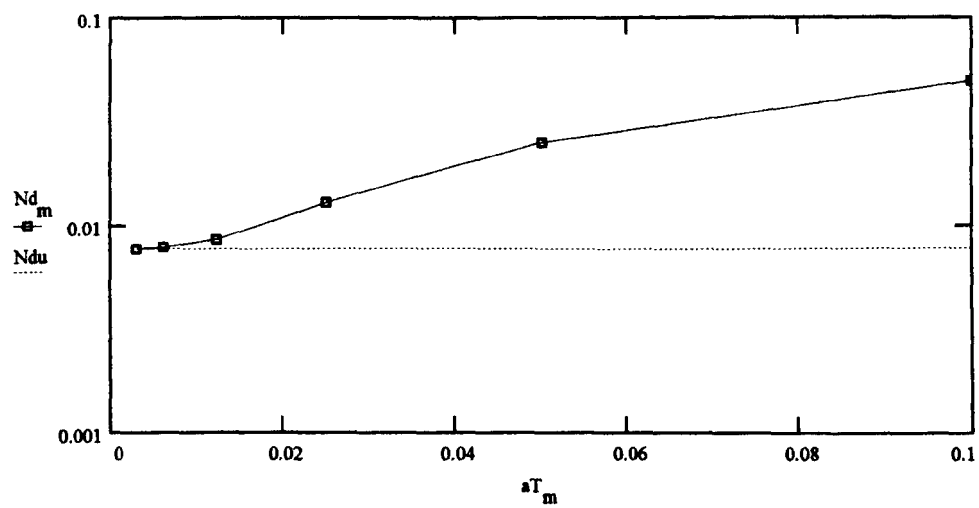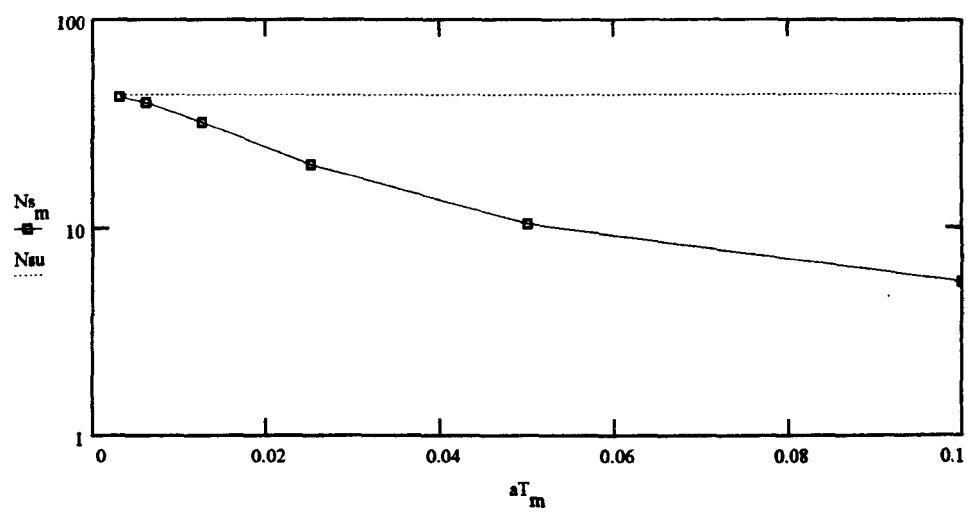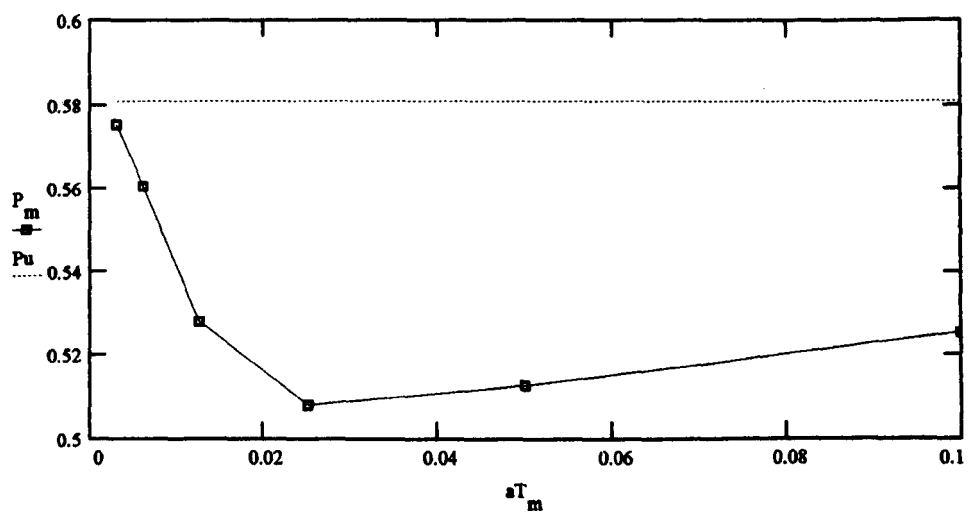
133

Fig7.2.4

Fig 7.2.5

Fig 7.2.6

Again, it can be seen that with longer noise corners, the filter behaves very much like one with uniform coefficients. Under the assumed conditions, that, unfortunately, would not happen in a practical system, such a filter is seen to have a Goulding product of less than 1.00. The improvement is a consequence of using the same number of coefficients in estimating signal and noise gains.

If the extra step noise accumulated between pulses is taken into consideration, the Goulding product is very much worse, as shown in Figure 7.2.7 where an input count rate of 10Kpps is assumed. In fact, the Goulding product has little value in this case; it is an indicator of filter 'goodness' only when delta and step noise contributions are equalised. Filters using positive coefficients only will be swamped by the step noise variance and, from this consideration alone, it is necessary to incorporate a baseline estimator.
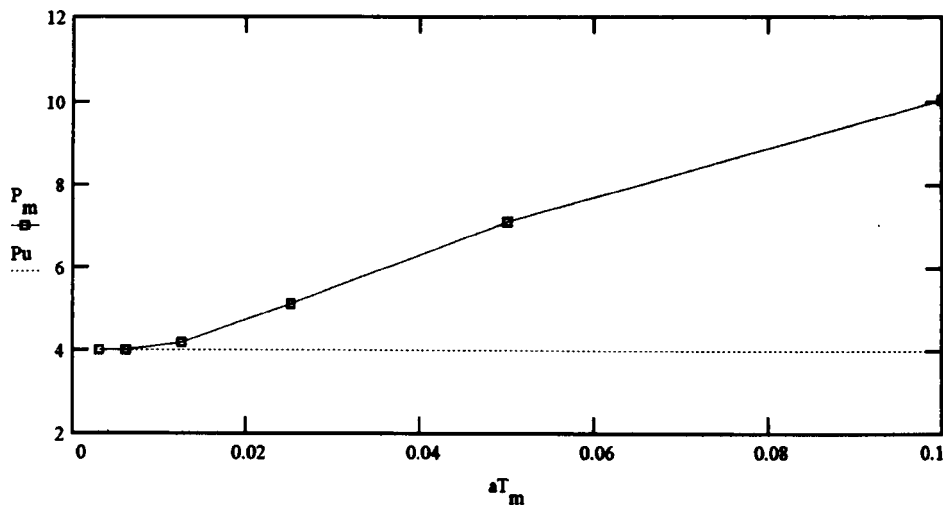

Fig 7.2.7

7.3 : UNIFORM COEFFICIENTS

An uniform coefficient profile is shown in Figure 7.3.1. Zero valued coefficients are used to eliminate ballistic deficit effects; they serve to introduce a flat top into the weighting function.
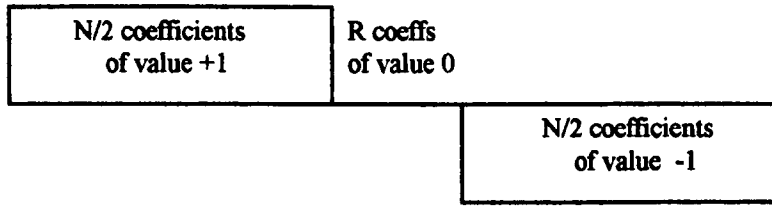
```
┌─────────────────────────┬─────────────────┐
│   N/2 coefficients      │  R coeffs       │
│     of value +1         │  of value 0     │
└─────────────────────────┴─────────────────┘
                    ┌─────────────────────────┐
                    │   N/2 coefficients      │
                    │     of value  -1        │
                    └─────────────────────────┘
```

Fig 7.3.1

Using Equation 7.1.10 it can be easily shown that:

$$N_d^2 = \frac{4}{N} \tag{7.3.1}$$

Using Equation 7.1.24 it can be shown that:

$$\sum_{n=0}^{N-1}\left(\sum_{r=0}^{n}C_r\right)^2 = \sum_{n=0}^{\frac{N}{2}-1}(n+1)^2 + R\left(\frac{N}{2}\right)^2 + \sum_{n=\frac{N}{2}}^{N-1}(N-1-n)^2 \tag{7.3.2}$$

$$\sum_{n=0}^{N-1}\left(\sum_{r=0}^{n}C_r\right)^2 = \sum_{r=1}^{\frac{N}{2}}r^2 + R\left(\frac{N}{2}\right)^2 + \sum_{r=0}^{\frac{N}{2}-1}r^2 \tag{7.3.3}$$

$$\sum_{n=0}^{N-1}\left(\sum_{r=0}^{n}C_r\right)^2 = \frac{\frac{N}{2}\left(\frac{N}{2}+1\right)(N+1)}{6} + R\left(\frac{N}{2}\right)^2 + \frac{\left(\frac{N}{2}-1\right)\left(\frac{N}{2}\right)(N-1)}{6} \tag{7.3.4}$$

The step noise index can now be written as:

$$N_s^2 = \frac{N^3+2N+3RN^2}{12}\times\frac{4}{N^2} = \frac{N^2+2+3RN}{3N} \tag{7.3.5}$$

Figures 7.3.2 and 7.3.3 shows how the delta noise index and the step noise index varies with the filter length. As expected, the delta noise index is inversely proportional and the step noise index is proportional to the time-scale of the filtering process.
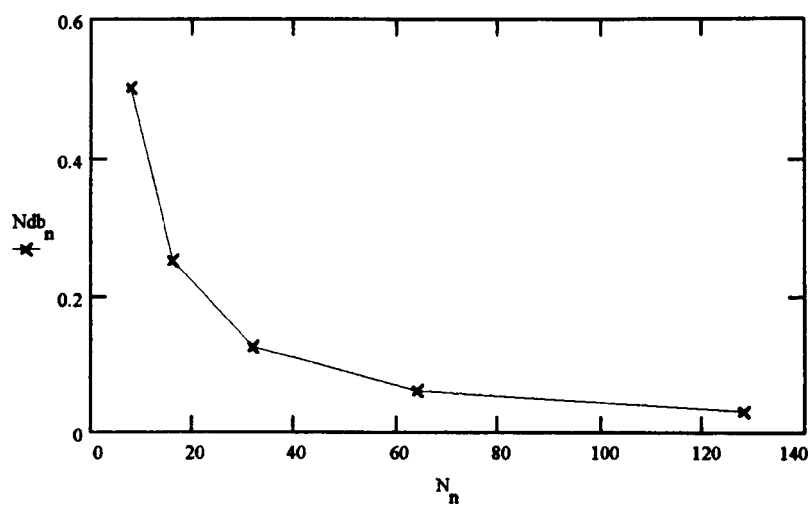
Fig 7.3.2
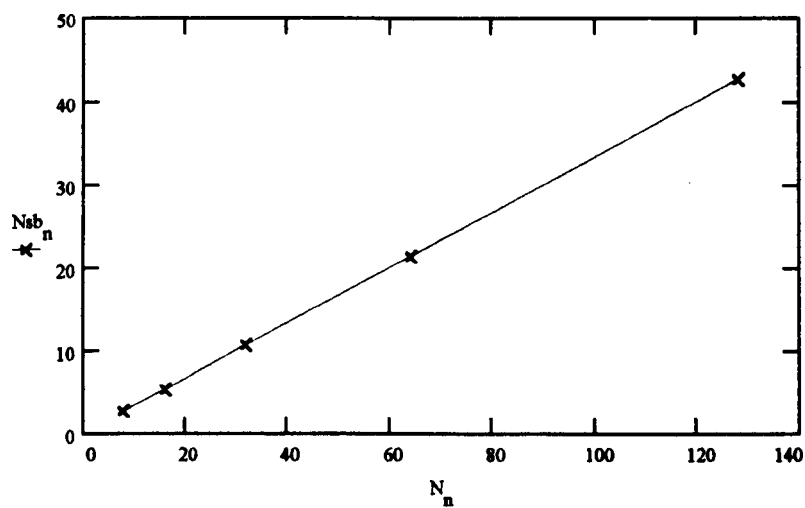
Fig 7.3.3

As the filter length is changed, the relative contributions of step noise and delta noise also changes. There is an optimum filter length for a given spectrometer and its particular noise-corner.

Filter length is 8x2^n
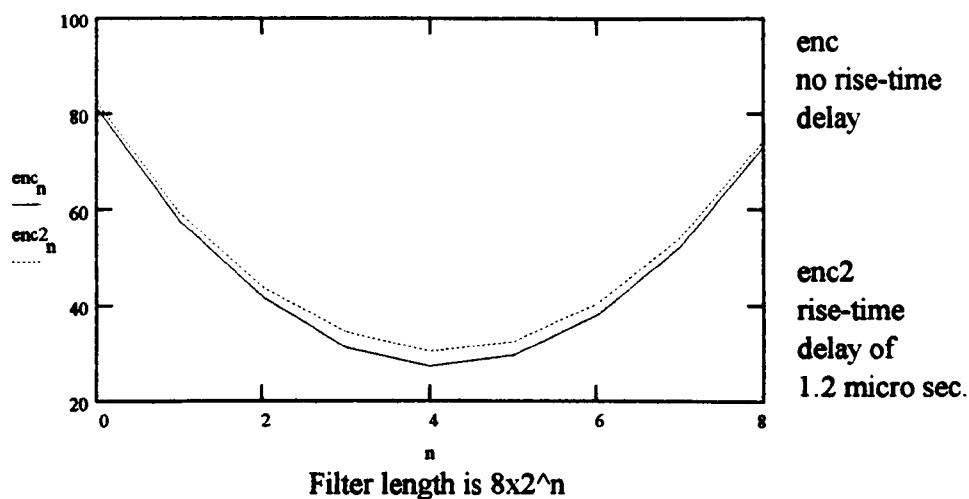
Fig 7.3.4

Figure 7.3.4 shows the equivalent noise charge generated by a spectrometer having a noise-corner of $2\mu s$ and a filter sampling at $50nS$. The optimum filter length seems to be 128. This represents a time scale of $6.4\mu s$. The theory of analogue time-invariant filters[81] defines the optimum duration of a triangular pulse shape as :

$$\tau_{opt} = 2\sqrt{3} \times \tau_c \qquad\qquad (7.3.6)$$

This equation predicts an optimum duration of $6.9\mu s$ for a $2\mu s$ noise-corner; the value suggested by the plot of Figure 7.3.4 is in good agreement.

CHAPTER 8 : A DIGITAL PULSE PROCESSOR

8.1 : SYSTEM LAYOUT

A digital filter incorporating a baseline estimator was built and the basic structure is shown in Figure 8.1.1. The ADC card described in Chapter 6 was used again, the only modification being the addition of a variable gain input amplifier. A modified version of the control circuitry was also used. The trigger circuit in this processor was analogue, using the $(CR)^2$-RC shaper developed for the analogue pulse processor.

Fig 8.1.1

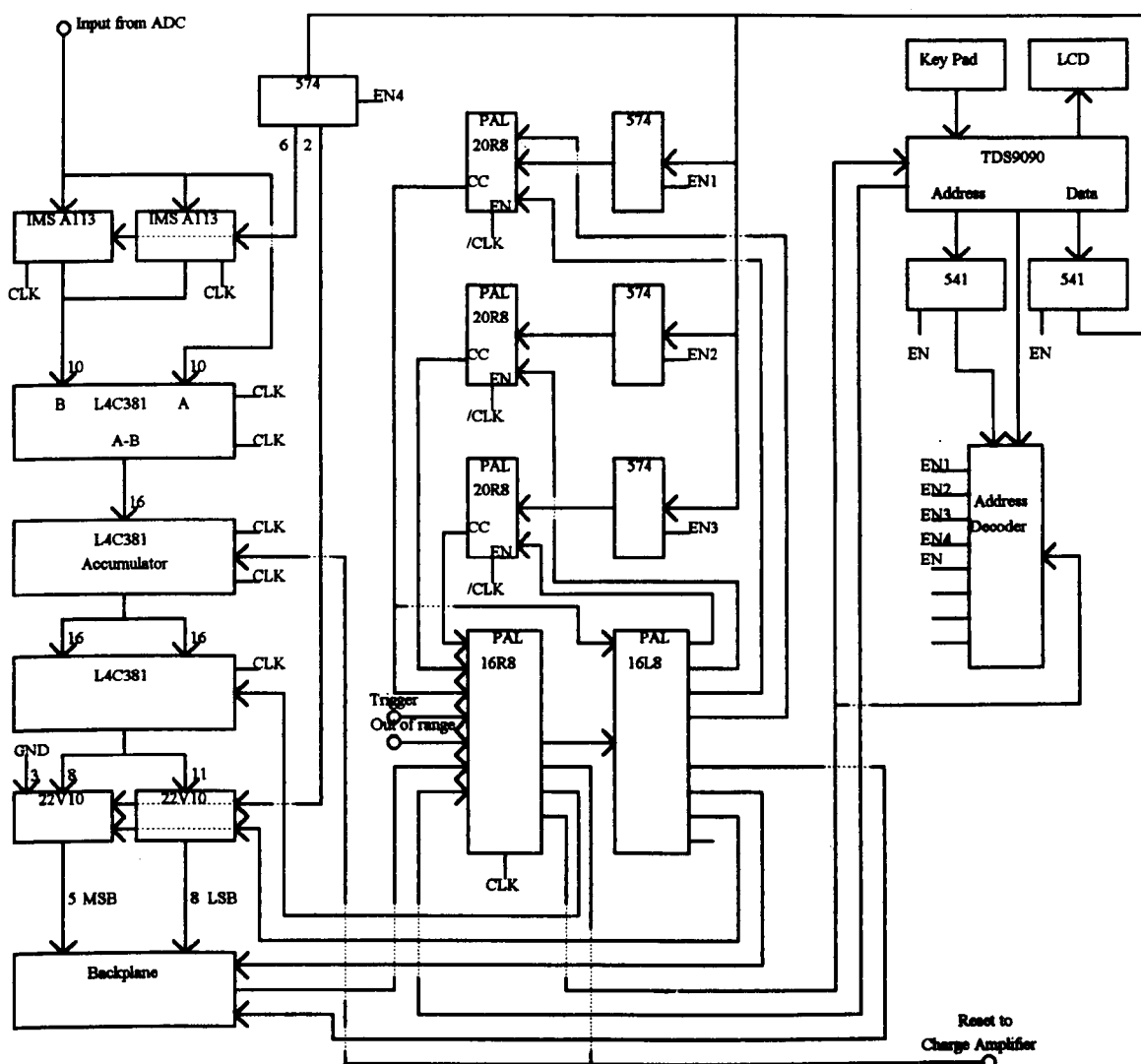The 10bit output of the ADC card passes through a variable length delay pipeline, implemented with a pair of Inmos A113 programmable length digital delay lines. The delay of these 9bit devices can be set to any value between 5 and 1317 clock periods.

In this implementation, a 6bit word held in a ALS574 register selects a delay of 8, 16, 32 or 64 clock periods.

The first ALU can be seen to implement the function $F_i = A_i - A_{i-N}$ where N is the delay set by the digital delay line. The second ALU is set-up as an accumulator and its output is therefore the sum of the last N samples from the ADC; it is a measure of the running average of the ADC's output. The accumulator is cleared at the end of the processing time, when the charge-amplifier is reset.

On receiving a pulse from the trigger circuit, the state-machine generates a short, one clock wide enable signal that allows the current value of the running average to be stored in the B input register of the third ALU. Preceding delays are arranged such that the running average at this time is an estimation of the charge-amplifier's baseline just prior to the arrival of a signal to be measured. This ALU generates an output A-B.

State-machine sequencing proceeds as described in Chapter 6, except that the pile-up exit from the rise-time delay state has been removed to allow wider trigger pulses from slower shaping networks to be used. At the end of the processing time, the third ALU's output is clocked into two 22V10 programmable logic devices. This output is an estimation of the charge-amplifier's new output level minus the stored estimation of the previous baseline. The output value is proportional to the filter length and the PLDs right-shift the 16bit result by 0, 1, 2 or 3 bits for lengths of 8, 16, 32 or 64 to generate a 13bit output.

The effective impulse and step responses of the filter are shown in Figure 8.1.2. The filter can generate a rise-time delay (RTD) to eliminate charge collection effects, as explained in Chapter 6. The performance expected is that of a trapezoidal shaper.
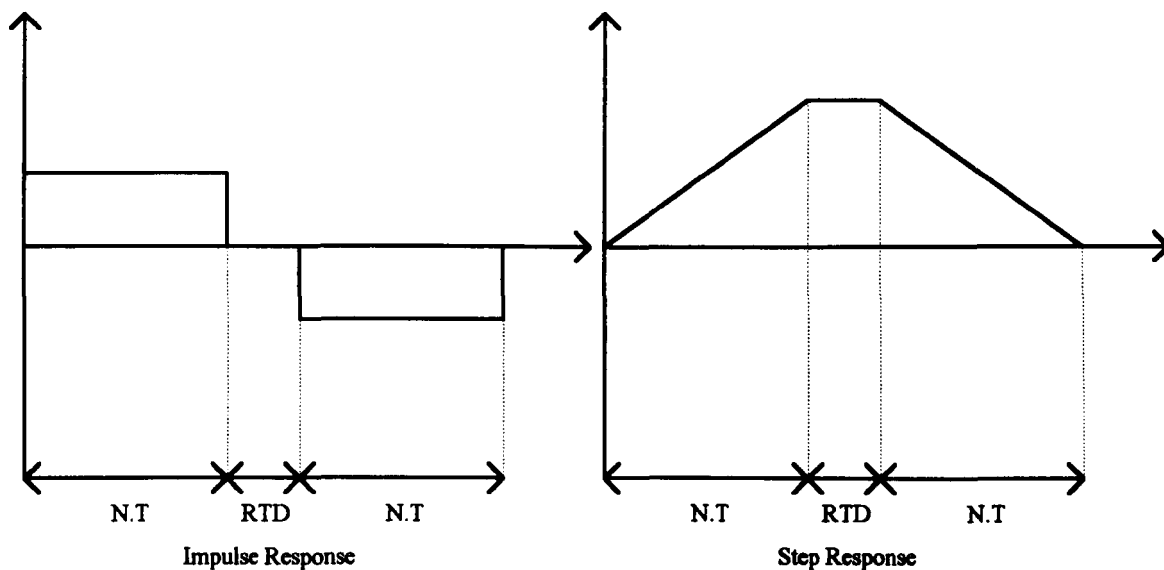
N.T   RTD   N.T   N.T   RTD   N.T

Impulse Response   Step Response

Fig 8.1.2

In this arrangement, the sloping baseline of the charge-amplifier is used to improve the differential linearity of the system and precautions have to be taken to eliminate energy dependent losses from the spectrum, where high energy events are more likely to be rejected for being out-of-range. The solution used here involves setting the limit discriminator threshold at the mid-point of the ADC's input range as shown in Figure 8.1.3. By connecting the least significant 12bits to the MCA, the system's maximum pulse amplitude is one that spans half the ADC's input range, and is never lost in the pulse-by-pulse reset method. Pulses are delayed into the limit discriminator, enabling the trigger to initiate the processing of pulses that exceed the threshold.

+2V

ADC
Input Range

Limit Discriminator
Upper Threshold

-2V

Maximum amplitude pulses superimposed
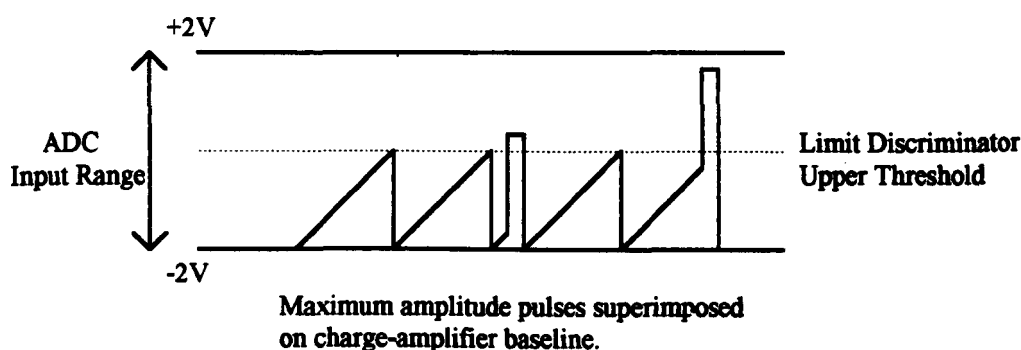on charge-amplifier baseline.

Fig 8.1.3

The charge-amplifier is held in the reset condition during an 'update parameters' routine. This prevents it saturating when the state-machine is busy sequencing the routine.

8.2 : EXPERIMENTAL RESULTS

A spectrometer was interfaced into the digital pulse processor described above. The detector was a coaxial-planar, n-type, intrinsic germanium crystal with a volume of 10-15cc and an efficiency of 8-10%. (Such a detector combines the good high energy response of a coaxial detector with the good charge collection properties of a planar detector.) The pre-amplifier was a Harwell 930128 optical-reset charge-amplifier used with a room temperature BF815 FET.

Originally, a short shaping time-constant of 22nS was used in the trigger channel. The narrow trigger pulse could be used to latch the baseline estimation directly and rise-time pile-up could be detected. Figure 8.2.1 shows the Cobalt60 spectrum; it is obvious that noise triggering is causing most events to be rejected and the effect is worse as the event amplitude is increased. In Figure 8.2.2, the trigger channel threshold has been increased. The energy dependent rejection of events is seen to be improved but low energy peaks would not be recorded.

Figure 8.2.3 shows the Cobalt60 spectrum taken with 220nS trigger channel shaping. The filter length is 64 and the rise-time delay is set to 1μS. The input count rate is approximately 1.5Kpps. The state-machine had to be modified to accept wider triggers and the pile-up at higher count rates would be compromised. Ideally, the system needs fast and slow recognition channels.

Figures 8.2.4, 8.2.5 and 8.2.6 show the Cobalt60 spectra taken with filter lengths of 64, 32 and 8 respectively. The measured resolutions are summarised in Table 8.2.1. The resolution of the Cobalt60 1.17Mev peak measured with the same spectrometer and a Harwell time-variant analogue pulse processor was 2.8KeV.

Filter Length	Resolution of 1.17MeV peak
8	6.9KeV
16	4.6KeV
32	4.1KeV
64	4.0KeV

Table 8.2.1

A high-energy tail can be seen on the peaks, especially with longer filter lengths. This is thought to be due to pulses that arrive before the baseline estimation filter has filled with samples after a previous reset. At high input rates, this would be a serious problem and an additional dead-time needs to be introduced after the charge-amplifier reset, during which input pulses would be rejected and the charge-amplifier reset again.

The apparent shift in gain with filter length seen in Figures 8.2.4, 8.2.5 and 8.2.6 is partly caused by the digital delay line chips implementing a delay one clock period greater than expected, causing the gain to increase as the filter length decreases. This implementation error masks an inherent zero shift in the other direction caused by charge-amplifier slew. The positive slope of the charge amplifier's baseline causes an offset in the measured pulse amplitude that increses with filter length.

Figure 8.2.1 Cobalt60 spectrum produced by the digital pulse processor (used with an analogue trigger channel shaping of 22nS and a trigger threshold of 170mV).
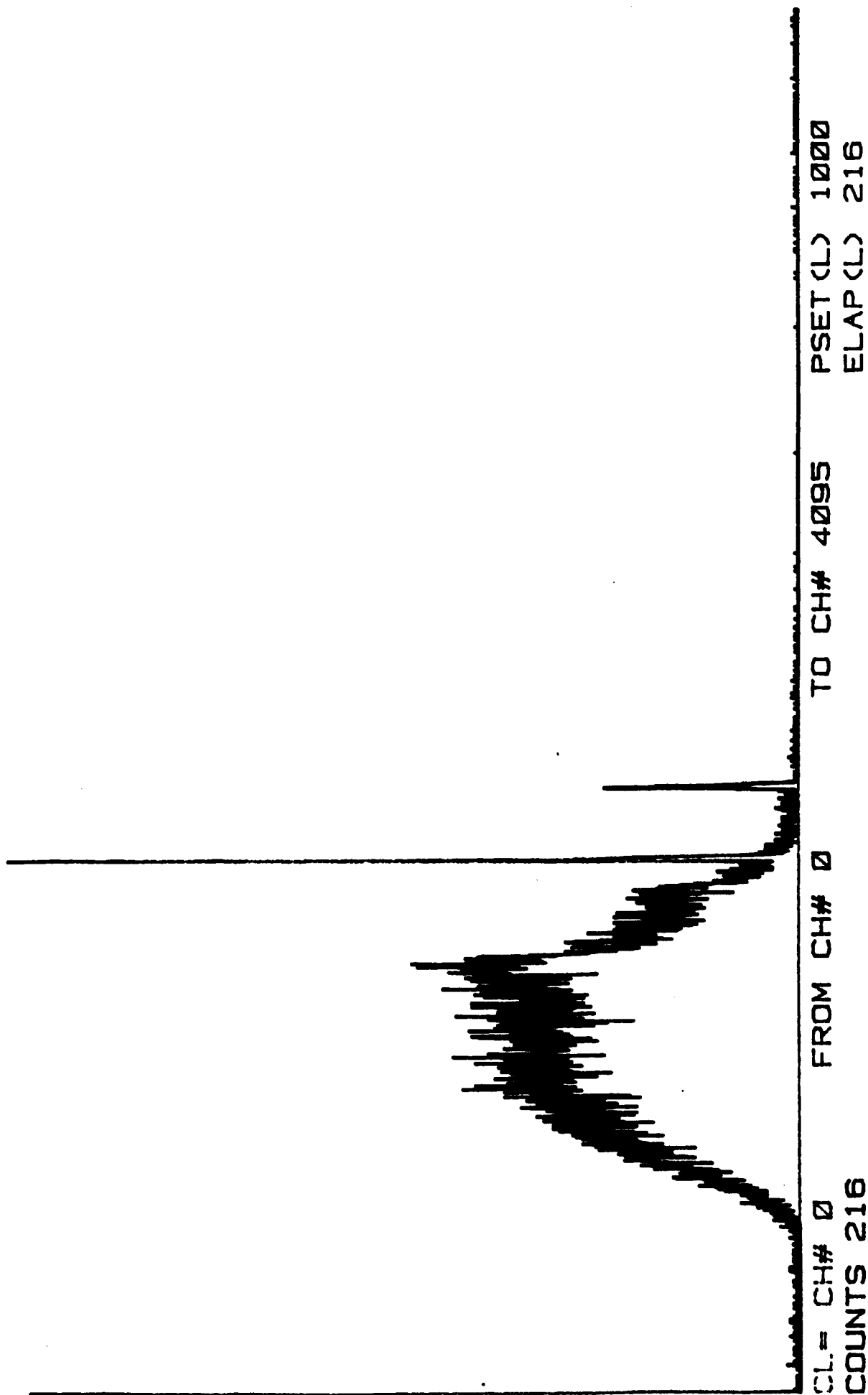
Figure 8.2.2 Cobalt60 spectrum produced by the digital pulse processor (used with an analogue trigger channel shaping of 22nS and a trigger threshold of 350mV).
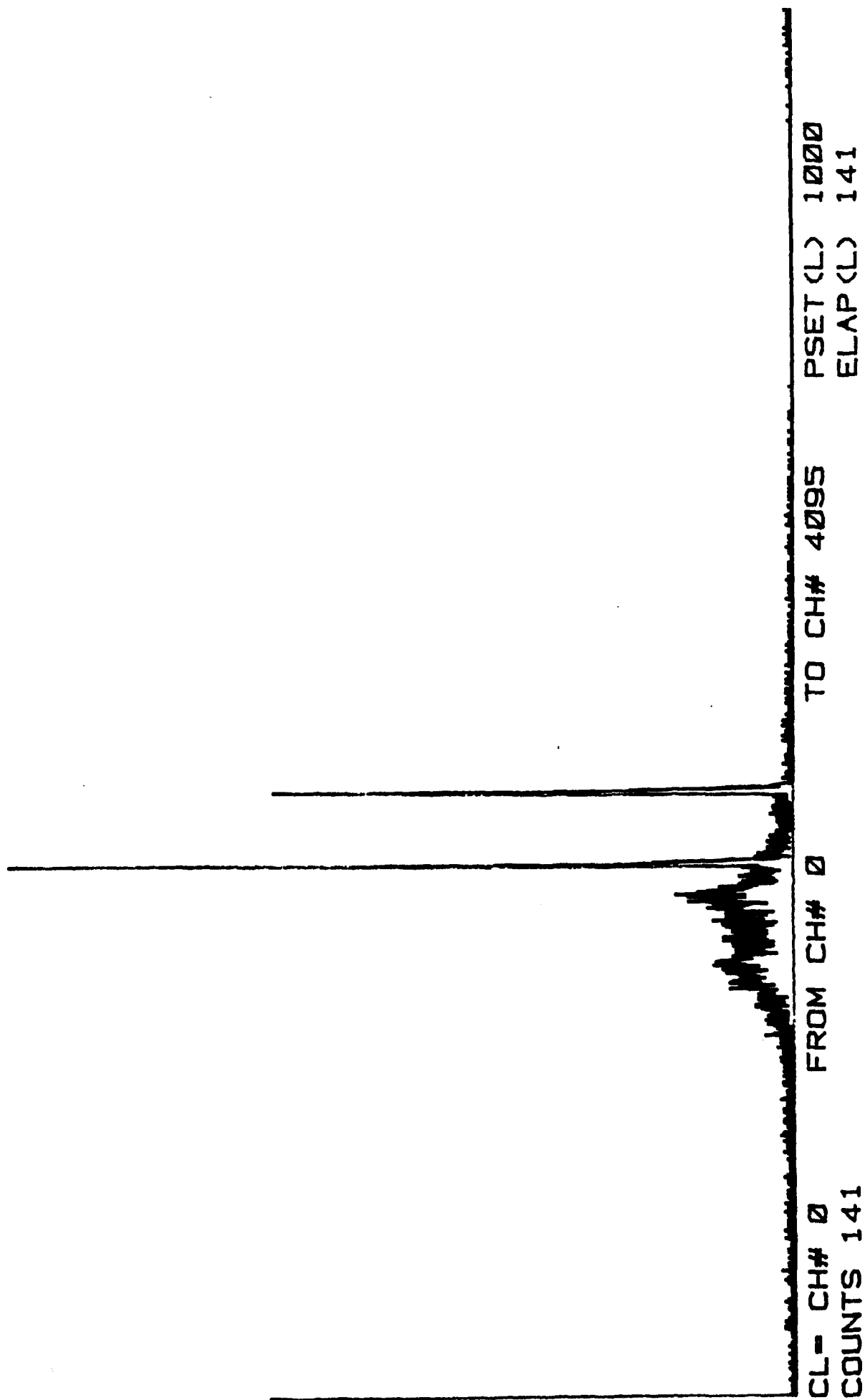
Figure 8.2.3   Cobalt60 spectrum produced by the digital pulse processor (used with an analogue trigger channel shaping of 220nS).

TAG NO. = Ø

CH# Ø

SERIES 4Ø V- 2.2

MEMORY = 1/2

VFS = 4K

Ø3:56   9 APR 1981

CH# 4Ø95

CANBERRA

CL= CH# Ø

COUNTS 542

FROM CH# Ø

INT 695149

TO CH# 4Ø95

PSET (L) 1ØØØ

ELAP (L) 542

Figure 8.2.4 Cobalt60 spectrum produced by the digital pulse processor using a filter length of 64 in the signal estimation interval, and a rise-time delay of 1.2µs.

Figure 8.2.5   Cobalt60 spectrum produced by the digital pulse processor using a
filter length of 32 in the signal estimation interval, and a rise-time
delay of 1.2µs.
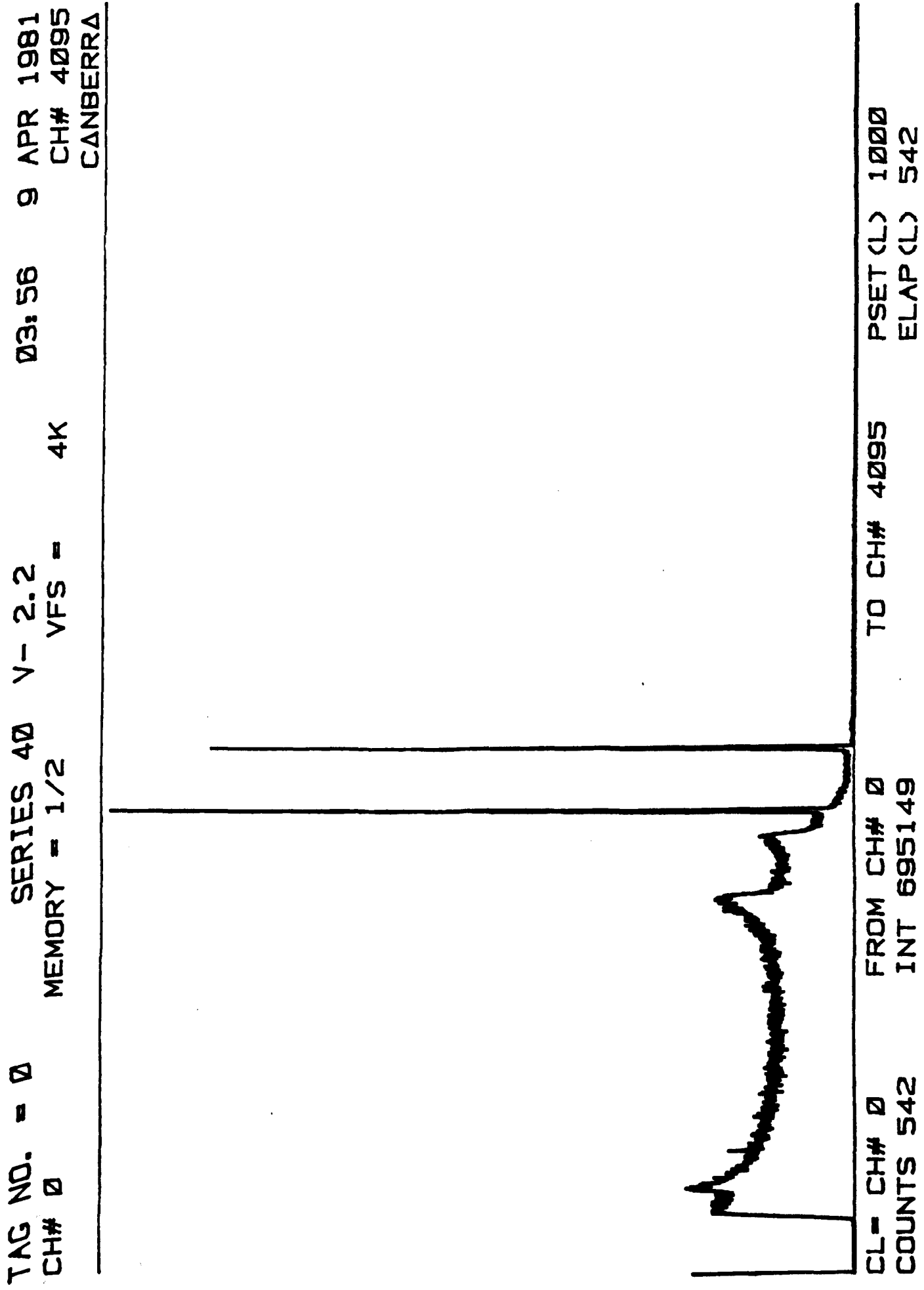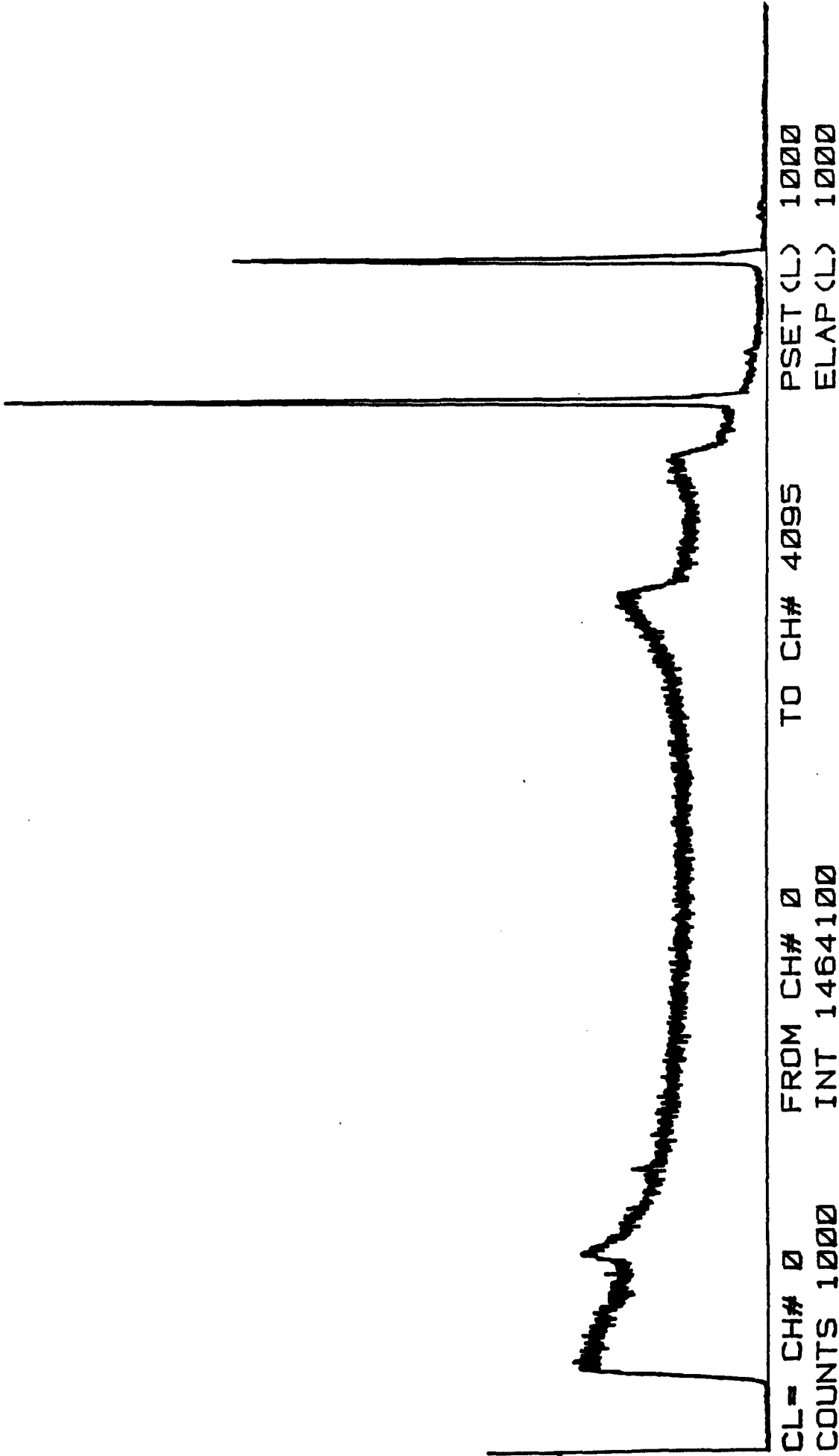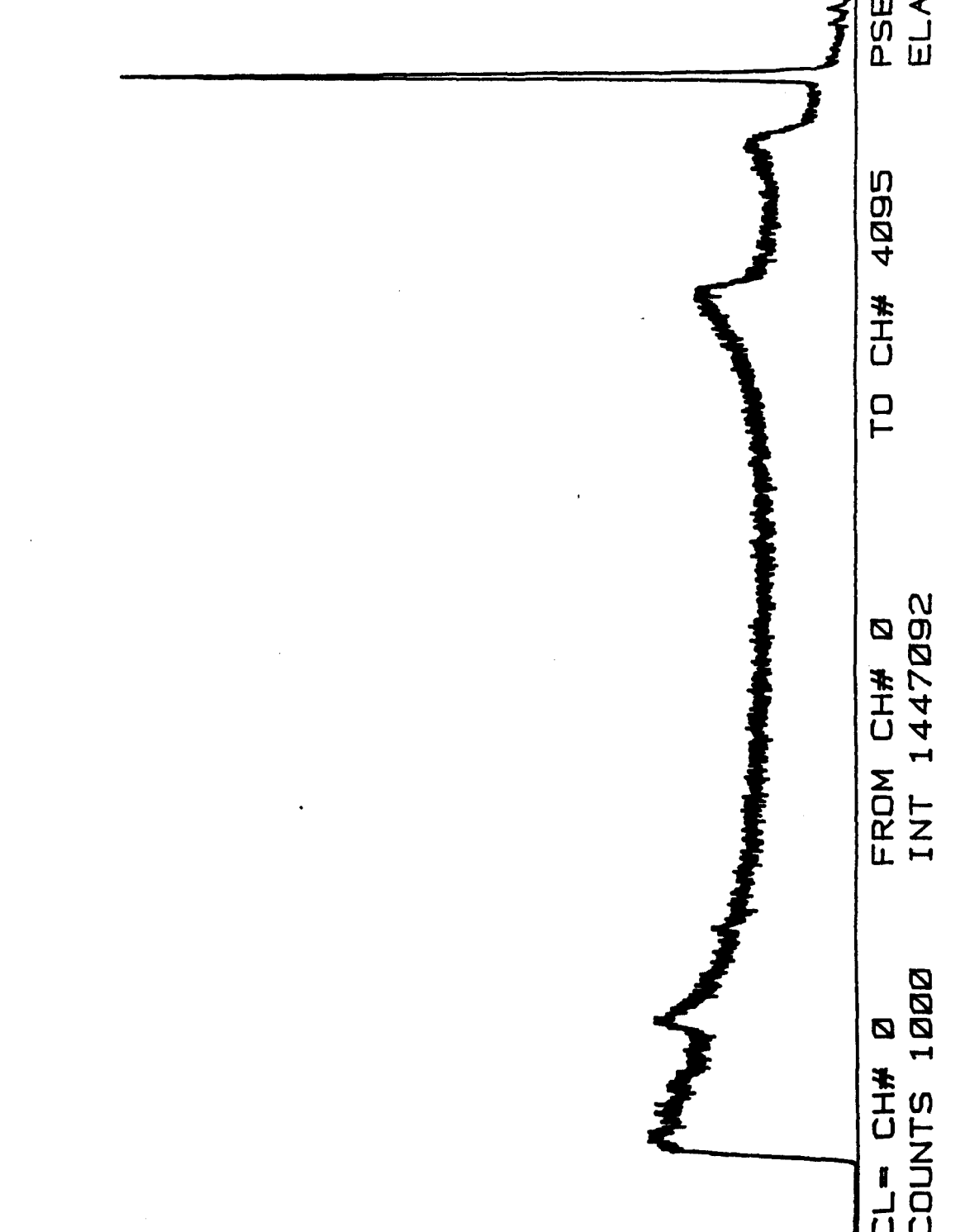
Figure 8.2.6 Cobalt60 spectrum produced by the digital pulse processor using a filter length of 8 in the signal estimation interval, and a rise-time delay of 1.2µs.
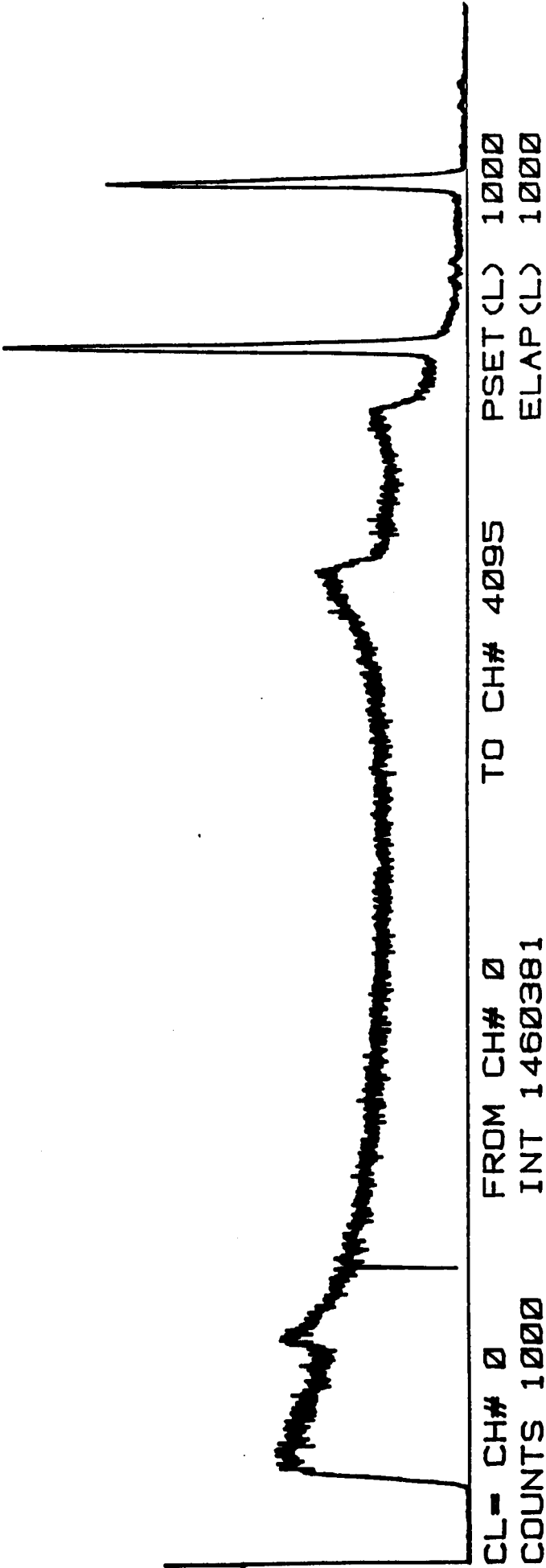
CONCLUSIONS

It is clear from a review of the theory that the 'Harwell' or 'Kandiah' processor has great potential as a high performance spectroscopy amplifier. Its use in the past, however, has been limited to rather specialist applications. Versatility in a spectroscopy amplifier has always been a strong selling point; even the highest grade amplifiers are advertised as being 'able to meet most detector applications'. This research work has shown that modern electronic components and innovative circuit techniques can be used to build a commercially viable time-variant processor.

In the longer term, digital signal processing techniques will be adopted in the design of the next generation of spectroscopy electronics; the rapid development of the technology means that this may happen sooner rather than later. It has been shown in this work that a simple running average digital filter can be used as a pulse processor and that its performance, theoretically, is as good as a trapezoidal shaper. Further, it has been shown how a digital filter with a cusp response can be constructed. Such a filter would have even better noise reducing properties at the cost of some extra complexity.

The problematic areas in the development of an all digital pulse processor would seem to be the front-end converter and the trigger channel. This work shows that an ADC of at least 12 bits and a conversion rate of at least 20MHz is needed. Such devices are still relatively expensive and power hungry. It is also apparent that some means of linearising the ADC is required. A limit restore charge amplifier would work, but resolution would be compromised.

Digital pulse processors of the type described here are time-variant and a trigger pulse is needed to initiate the processing sequence. The problem of establishing a good pile-up resolving ability whilst maintaining good noise discrimination appears to be a challenging one if a digital trigger channel is to be used.

The traditional analysis of analogue pulse shaping for spectroscopy assumes that the noise generated by the spectrometer is stationary; Campbell's theorem and the theory of matched filters can then be readily applied. When digital filters are considered, this assumption cannot be made, and a different approach to the theory has to be taken. It is shown, however, that in a practical case, where the sum of the filter coefficients has

to made zero, the traditional method of calculating the noise indices from the weighting function can still be applied, and the weighting function is derived from the impulse response defined by the filter coefficients.

REFERENCES

1: G.F.Knoll, 'Radiation Detection and Measurement', Second Edition, Wiley, p340.

2: J.W.Haslett and E.J.M.Kendall, IEEE Trans. Electron Devices, Vol ED-19, N^{O}8, Aug 1972.

3: A. Van Der Ziel, Proc. I.R.E., 50, 1808, 1962.

4: A. Van Der Ziel, Proc. I.R.E., 51, 461, 1963.

5: F.S.Goulding, J.T.Walton and R.H.Pehl, IEEE Trans. Nucl. Sci., NS-17, Feb 1970, pp218-225.

6: D.A.Landis, F.S.Gouiding, R.H.Pehl and J.T.Walton, IEEE Trans Nucl. Sci., NS-18, Feb 1971, p115.

7: D.A.Landis, C.P.Cork, N.W.Madden and F.S.Goulding, IEEE Trans Nucl. Sci., NS-29, Feb 1982, p619.

8: J.M.McKenzie and L.J.Witt, IEEE Trans. Nucl. Sci., NS-21, Feb 1974, pp794-797.

9: T.Nashashibi and G.White, IEEE Trans. Nucl. Sci., NS-37, Oct 1990, p452.

10: C.Cottini, E.Gatti and V.Svelto, Nucl. Inst. and Meth., 24 (1963), pp241-242.

11: E.Fairstein, IEEE Trans. Nucl. Sci., NS-37, April 1990, pp382-397.

12: M.O.Deighton, Harwell Laboratory Report, AERE-R5439, May 1967.

13: A Papoulis, 'Probability, Random Variables, and Stochastic Processes', Second Edition, McGraw-Hill, p237.

14: J.G.Melbert, IEEE Trans. Nucl. Sci., NS-29, Feb. 1982, pp614-618.

15: A.Papoulis, 'Probability, Random Variables, and Stochastic Processes', op.cit., p285.

16: T.Nashashibi and P.Sanssingkeow, IEEE Trans. Nucl. Sci., NS-38, April 1991, pp77-82.

17: F.S.Goulding, Nucl. Inst. and Meth., 100 (1972), pp493-504.

18: F.S.Goulding and D.A.Landis, IEEE Trans. Nucl. Sci., NS-29, June 1982, pp1125-1141.

19: A.B.Gillespie, 'Signal Noise and Resolution in Nuclear Counter Amplifiers', Pergamon Press, 1953.

20: M Konrad, IEEE Trans. Nucl. Sci., NS-15 (1968), pp268-282.

21: W.Potzel and N.Halders, Nucl. Inst. and Meth., 226 (1984), pp418-420.

22: F.S.Goulding, D.A.Landis and N.W.Madden, Trans. Nucl. Sci., NS-30, Feb 1983, pp301-310.

23: V.Radeka, Nucl. Inst. and Meth., 99 (1972), pp525-539.

24: C.L.Britton, T.H.Becker, T.J.Paulus and R.C.Trammell, IEEE Trans. Nucl. Sci., NS-31 Feb 1984, pp455-460.

25: K.Husimi, S.Ohkawa, IEEE Trans. Nucl. Sci., NS-36, Feb 1989, pp346-400.

26: M.L.Simpson, T.H.Becker, R.D.Bingham and R.C.Trammell, IEEE Trans. Nucl. Sci., NS-38, April 1991, pp89-96.

27: K.Kandiah, Harwell Laboratory Report AERE-R5019 (1965).

28: M.O.Deighton, Harwell Laboratory Report AERE-R5021 (1967).

29: P.W.Nicholson, 'Nuclear Electronics', Wiley, p144.

30: M.O.Deighton, Nucl. Inst. and Meth., 58 (1968), pp201-212.

31: K.Kandiah "Semiconductor Nuclear Particle Detectors and Circuits", p 544 US National Academy of Sciences Publication 1593 (1969) [Proc. of Gatlingburg Conference, 1967].

32: K.Kandiah, A.Stirling, D.L.Trotman and G.White, Intern. Symp. Nuclear Electronics (Versailles, 1968).

33: K.Kandiah, Nucl. Instr. and Meth., 95 (1971), pp289-300.

34: M.O.Deighton, Nucl. Instr. and Meth., 103 (1972), pp1-12.

35: K.Kandiah, A.J.Smith and G .White, Proc. 2nd ISPRA Nuclear Electronics Symp., Stresa (1975).

36: K.Kandiah and G.White, IEEE Trans. Nucl. Sci., NS-28, Feb1981, pp613-620.

37: G.White, UK Patent 1359883; US Patent 3792255.

38: G.White, Harwell Laboratory Report AERE-R11241, Aug. 1984.

39: 'Standard Nuclear Instrument Modules', Report No TID20893, U.S. Atomic Energy Commission.

40: 'An Introduction to Spectroscopy Amplifiers', Silena Application Note, 1982.

41: E.V.Evans and A.R.Owens, 'CMOS Analog Switches in Time-Variant Circuits', Internal Report, School of Electronic Engineering Science, University of Wales, Bangor, Dec 1990.

42: C.H.Nowlin and J.L.Blankenship, Rev. Sci. Instr., 36, 1830 (1965).

43: P.W.Nicholson, op.cit., p191.

44: 'Current-Feedback Amplifiers', Comlinear Application Note, 1993.

45: A.R.Owens, 'Production of a Breadboard Model of Electronic Circuits', Internal Report, School of Electronic Engineering Science, University of Wales, Bangor, March 1989.

46: A.R.Owens, private communication.

47: K.Steiglitz, Information and Control 8, 455 (1965).

48: H.Koeman, Nucl. Instr. and Meth., 123 (1975), p161.

49: H.Koeman, Nucl. Instr. and Meth., 123 (1975), p169.

50: H.Koeman, Nucl. Instr. and Meth., 123 (1975), p181.

51: G.L.Miller and D.A.H.Robinson, IEEE Trans. Nucl. Sci., NS-22 (1975), p9.

52: R.D.Baertsch, IEEE Trans. Nucl. Sci., NS-24 (1977), p312.

53: J.G.Melbert, IEEE Trans. Nucl. Sci., NS-30 (1983), p314.

54: F.Hilsenrath, H.D.Voss and J.C.Bakke, IEEE Trans. Nucl. Sci., NS-32 (1985), p145.

55: J.S.Karp, G.Muehllehner, D.Beerbohhm, D.Mankoff, IEEE Trans. Nucl. Sci., Vol.33 (1986), p550.

56: R.E.Chrien and R.J.Sutter, Nucl. Instr. and Meth., A249 (1986), p421.

57: H.G.Ortlepp and A.Romaguera, Nucl. Instr. and Meth., A276 (1989), p500.

58: V.Jordanov and G.F.Knoll, IEEE Trans. Nucl. Sci., Vol.40, Aug 1993, pp764-769.

59: N.Bingefors et al., Nucl. Instr. and Meth., A326 (1993) p112.

60: G.Ripamonti, A.Castoldi, R.Spigarlo and E.Gatti, IEEE Trans. Nucl. Sci., Vol.41, Aug 1994, pp1109-1115.

61: V.Drndarevic, P.Ryge and T.Gozani, Nucl. Instr. and Meth., A277 (1989), p532.

62: A.Georgiev and W.Gast, IEEE Trans. Nucl. Sci., Vol.40, Aug 1993, pp770-779.

63: E.Cosulich and F.Gatti, Nucl. Instr. and Meth., A321 (1992), p211.

64: H.Takahashi et al., IEEE Trans. Nucl. Sci, Vol.40, Aug 1993, pp626-629.

65: J.M.Los-Arcos and E.Garcia-Torano, Nucl. Instr. and Meth., A339 (1994), p99.

66: J.M.Los-Arcos, E.Garcia-Torano, P.Olmos and J.Marin, Proc. of 1994 Symp. on Radiation Measurements and Applications, Michigan 1994.

67: G.Bertuccio, E.Gatti and M.Sampietro, Nucl. Instr. and Meth., A322 (1992), p271.

68: G.Bertuccio, A.Fazzi, A.Geraci and M.Sampietro, Proc. of 1994 Symp. on Radiation Measurements and Applications, Michigan 1994.

69: T.Lakatos, Nucl. Instr. and Meth., B47 (1990), p307.

70: T.Lakatos, Nucl. Instr. and Meth., B62 (1991), p289.

71: V.T.Jordanov and G.F.Knoll, Nucl. Instr. and Meth., A345 (1994), p337.

72: V.T.Jordanov, G.F.Knoll, A.C.Huber and J.A.Pantazis, Proc. of 1994 Symp. on Radiation Measurements and Applications, Michigan 1994.

73: A.R.Owens, Harwell Laboratory Report, AERE-R12928 (1987).

74: M.O.Deighton, Harwell Laboratory Report, AERE-R12046 (1986).

75: A.R.Owens, private communication.

76: A.Papoulis, 'Probability, Random Variables, and Stochastic Processes', op.cit., p225.

77: A.Papoulis, 'Signal Analysis', McGraw-Hill, p303.

78: C.W. Therrien, 'Discrete Random Signals and Statistical Signal Processing', Prentice-Hall, p201.

79: A.Papoulis, 'Probability, Random Variables, and Stochastic Processes', op.cit., p344.

80: A.R.Owens, private communication.

81: P.W.Nicholson, op.cit., p146.

APPENDIX 1 : RESPONSE OF A PULSE PROCESSOR SYSTEM WITH AN AMPLIFIER OF LIMITED BANDWIDTH FOLLOWING THE DETECTOR CHARGE AMPLIFIER.

1: Specification of input waveform (rising edge):

$$m := 1..100$$

$$v_m := if\left[m<11, \left(\frac{m-.5}{10}\right), 1\right]$$

2: Amplifier response specification

$$M := 1..3 \qquad Tc := 10$$

$$MM_M := if(M=3, 5, M)$$

$$To_M := \left(\frac{MM_M}{100}\right) \cdot Tc \qquad \text{Amplifier time constant in terms of collection time of detector}$$

The corresponding amplifier bandwidths are given by fo = 1/(2.π.To);
for example, if Tc = 500ns, the bandwidths considered are: 32MHz, 16MHz, 6.4MHz

Impulse response of first order system:

$$k := 0..100 \qquad h_{k,M} := exp\left(\frac{-k}{To_M}\right) \cdot \left(1 - exp\left(\frac{-1}{To_M}\right)\right)$$

(Includes correction factor for zero-order-hold in the representation)

3: Convolution to calculate effect of amplifier on detector pulse.

$$n := 0..100 \qquad x := 0..100$$

$$g_{n,M} := \sum_x v_x \cdot \left[if\left[n \geq x, h_{(n-x),M}, 0\right]\right]$$

4: Effect of switched time constant filter

$ng := NG \cdot Tc$ Series switch time in relation to collection time

$gg_{n,M} := if\left(n > ng, g_{n,M}, 0\right)$ Gated waveform from post-detector amplifier

$vg_n := if\left(n > ng, v_n, 0\right)$ Gated version of input waveform for reference

$k := 0 .. 100$ $Ti2 := 2 \cdot Tc$ Filter time-constant in relation to collection time; two time-constants are considered.

$Ti1 := 0.5 \cdot Tc$

$H2_k := exp\left(\dfrac{-k}{Ti2}\right) \cdot \left(1 - exp\left(\dfrac{-1}{Ti2}\right)\right)$ Impulse response of the gated filter for the two time-constants.

$H1_k := exp\left(\dfrac{-k}{Ti1}\right) \cdot \left(1 - exp\left(\dfrac{-1}{Ti1}\right)\right)$

$G2_{n,M} := \displaystyle\sum_x gg_{x,M} \cdot \left(if\left(n \geq x, H2_{n-x}, 0\right)\right)$ Convolution of filter response with gated waveform from post-detector amplifier

$G1_{n,M} := \displaystyle\sum_x gg_{x,M} \cdot \left(if\left(n \geq x, H1_{n-x}, 0\right)\right)$

$G2_{n,0} := \displaystyle\sum_x vg_x \cdot \left(if\left(n \geq x, H2_{n-x}, 0\right)\right)$ Convolution of filter response with gated reference input waveform, representing the infinite bandwidth case

$G1_{n,0} := \displaystyle\sum_x vg_x \cdot \left(if\left(n \geq x, H1_{n-x}, 0\right)\right)$

$NG \equiv 1$ Gate time in relation to collection time at the detector.

5: Effect of gated integrator

$$F2_{n,M} = \sum_{x=ng}^{2 \cdot Ti2 + ng} if\left(n \geq x, G2_{x,M}, 0\right)$$

Output of gated integrator integrating for twice the circuit time constant.

Practical Amplifier

$$F2_{n,0} = \sum_{x=ng}^{2 \cdot Ti2 + ng} if\left(n \geq x, G2_{x,0}, 0\right)$$

Ideal Amplifier

$$F1_{n,M} = \sum_{x=ng}^{2 \cdot Ti1 + ng} if\left(n \geq x, G1_{x,M}, 0\right)$$

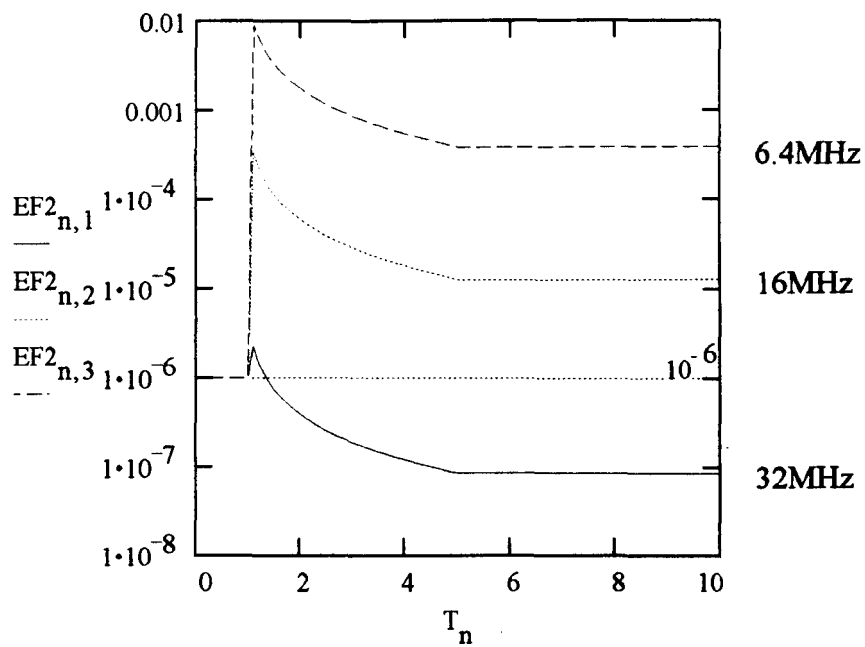$$F1_{n,0} = \sum_{x=ng}^{2 \cdot Ti1 + ng} if\left(n \geq x, G1_{x,0}, 0\right)$$

$$EF2_{n,M} = 1 - \frac{F2_{n,M} + 0.999999 \cdot 10^{-8}}{F2_{n,0} + 10^{-8}}$$

Normalised error in amplitude of output pulse.

$$EF1_{n,M} = 1 - \frac{F1_{n,M} + 0.999999 \cdot 10^{-8}}{F1_{n,0} + 10^{-8}}$$

$$T_n = \frac{n}{Tc}$$

Top figure

Amplitude error with 2 micro sec. processing.

$EF2_{n,1}$ ——

$EF2_{n,2}$ ·········

$EF2_{n,3}$ — —

6.4MHz

16MHz

10^{-6}

32MHz

T_n

Time measured in relation to collection time.

Bottom figure

Amplitude error with 500 nano sec. processing.

$EF1_{n,1}$ ——

$EF1_{n,2}$ ·········

$EF1_{n,3}$ — —

6.4MHz

16MHz

10^{-6}

32MHZ

T_n
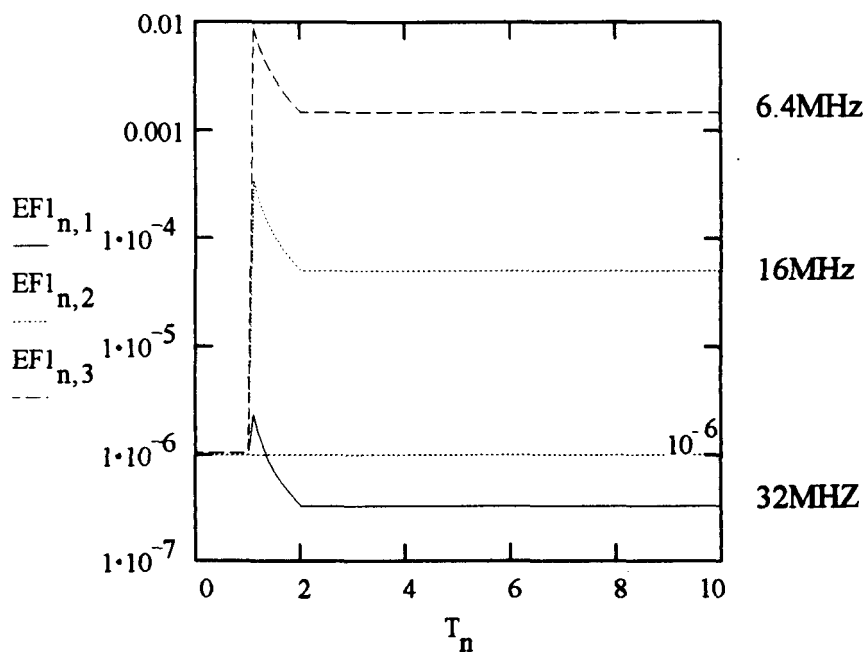
Time measured in relation to collection time.

APPENDIX 2 : COARSE GAIN STAGE FREQUENCY RESPONSE

Coarse gain amplifier frequency response:-
frequency definitions:

$$f = 0..25 \qquad F_f = 10^4 \cdot 10^{\frac{f}{3}} \qquad W_f = 2 \cdot \pi \cdot F_f \qquad s_f = W_f j$$

amplifier parameters:

$Zo = 63 \cdot 10^4$ dc open-loop transimpedance gain

$Ta = 3 \cdot 10^{-6}$ 50kHz bandwidth

$Rf = 250$ feedback resistance
$Ri = 32$ inv. input output impedance

$Cs = 2.75 \cdot 10^{-12}$ relay capacitance

$g = 0..3$

$$R_g = \frac{Rf}{2^{g-1}} \qquad R_0 = 10^9 \quad \text{gain setting resistors} \qquad R_g$$

R_g
$1 \cdot 10^9$
250
125
62.5

$$Yo_{f,g} = \frac{s_f Cs}{1 + R_g \cdot s_f Cs} \qquad \text{admittance of arm with relay open}$$

$$Yc_g = \frac{1}{R_g} \qquad \text{admittance of arm with relay closed}$$

$$Y_{f,0} = Yo_{f,1} + Yo_{f,2} + Yo_{f,3} \qquad \text{total admittance equations}$$

$$Y_{f,1} = Yc_1 + Yo_{f,2} + Yo_{f,3}$$

$$Y_{f,2} = Yc_1 + Yc_2 + Yo_{f,3}$$

$$Y_{f,3} = Yc_1 + Yc_2 + Yc_3$$

$$D_{f,g} := 1 + Rf \cdot Y_{f,g}$$ demanded gain

$$Z_f := \frac{Zo}{1 + s_f \cdot Ta}$$ freq dependent open-loop transimpedance gain

$$Zt_{f,g} := Rf + Ri \cdot \left(1 + Rf \cdot Y_{f,g}\right)$$ feedback transimpedance

$$L_{f,g} := \frac{Z_f}{Zt_{f,g}}$$ loop gain

$$G_{f,g} := \frac{D_{f,g}}{1 + \dfrac{1}{L_{f,g}}}$$ closed loop gain

frequency compensation network parameters:-

$$Cp := 8.25 \cdot 10^{-12}$$ parallel capacitor value

$$Rs := 250$$ series resistor value

$$T_f := \frac{1}{1 + Rs \cdot Cp \cdot s_f}$$ transfer function

$$Gc_{f,g} := G_{f,g} \cdot T_f$$ compensated gain

$$Ddb_{f,g} := 20 \cdot \log\left(D_{f,g}\right)$$

$$Zdb_f := 20 \cdot \log\left(Z_f\right)$$

$$Gdb_{f,g} := 20 \cdot \log\left(G_{f,g}\right)$$

$$Gcdb_{f,g} := 20 \cdot \log\left(Gc_{f,g}\right)$$

$$Ztdb_{f,g} := 20 \cdot \log\left(Zt_{f,g}\right)$$
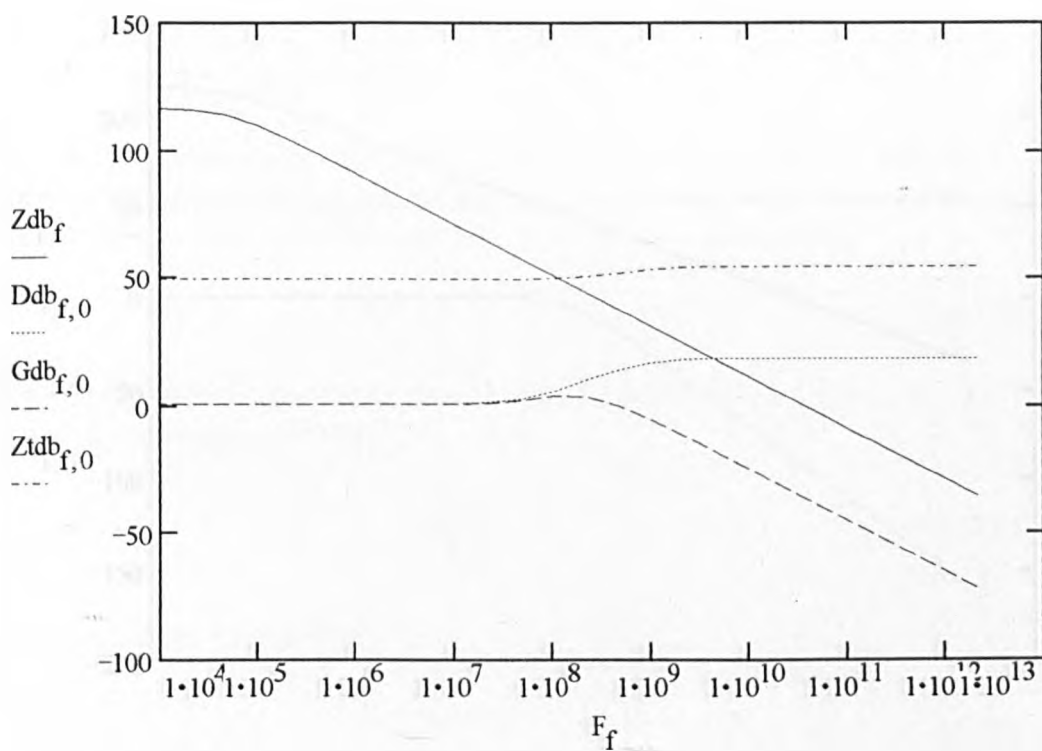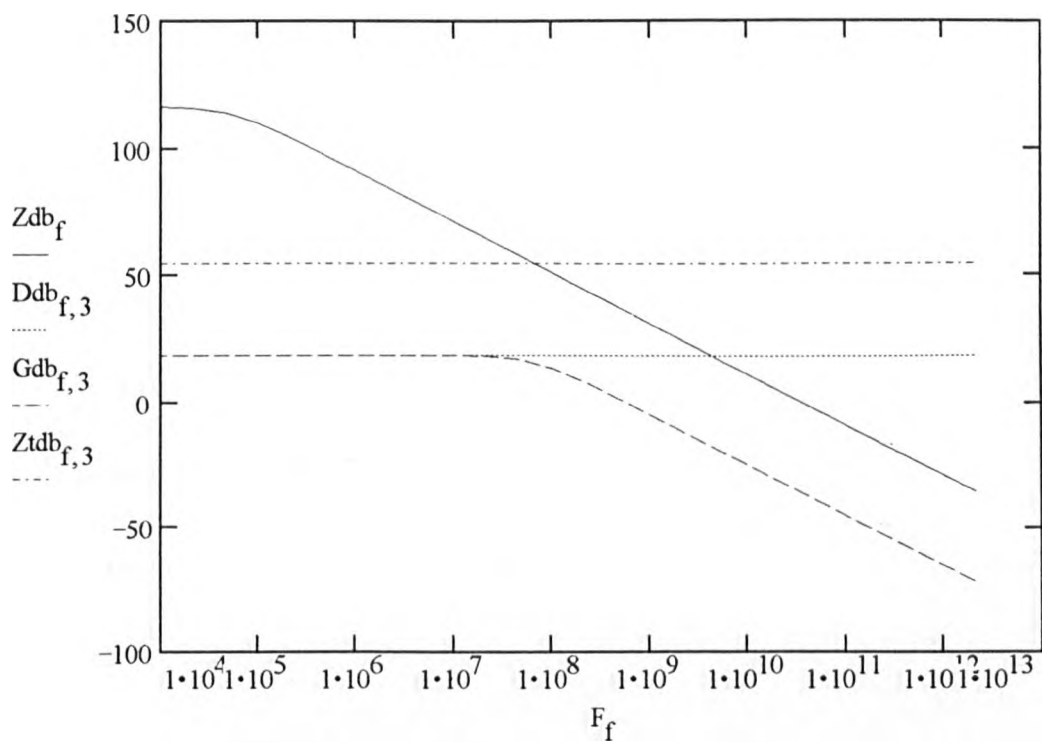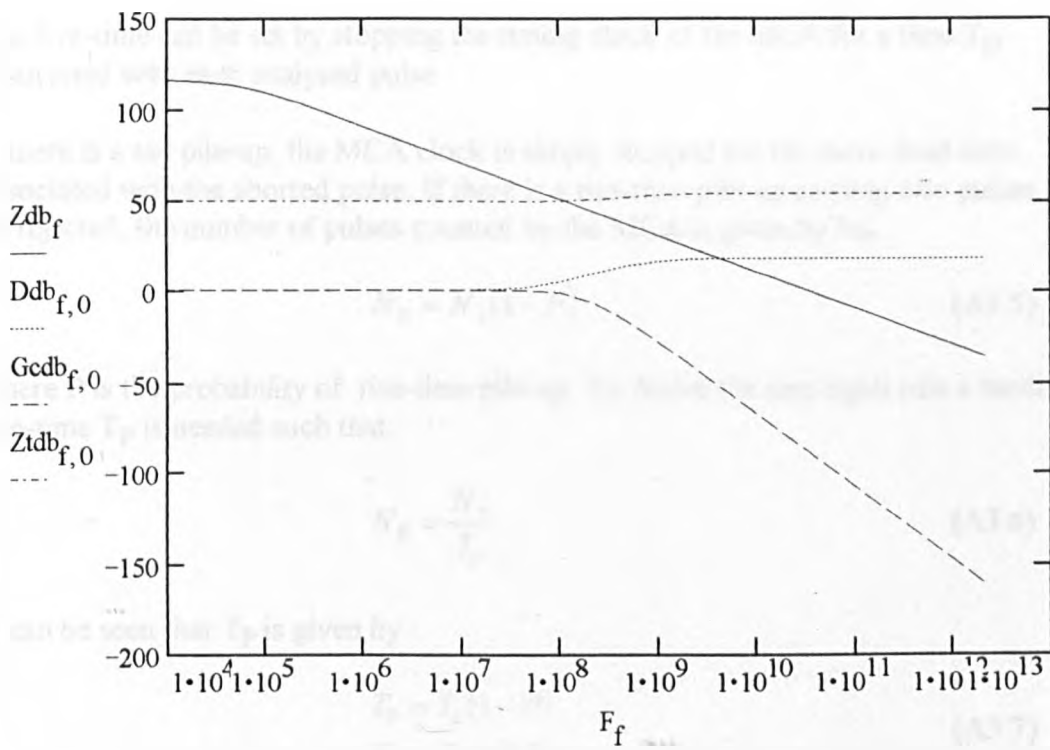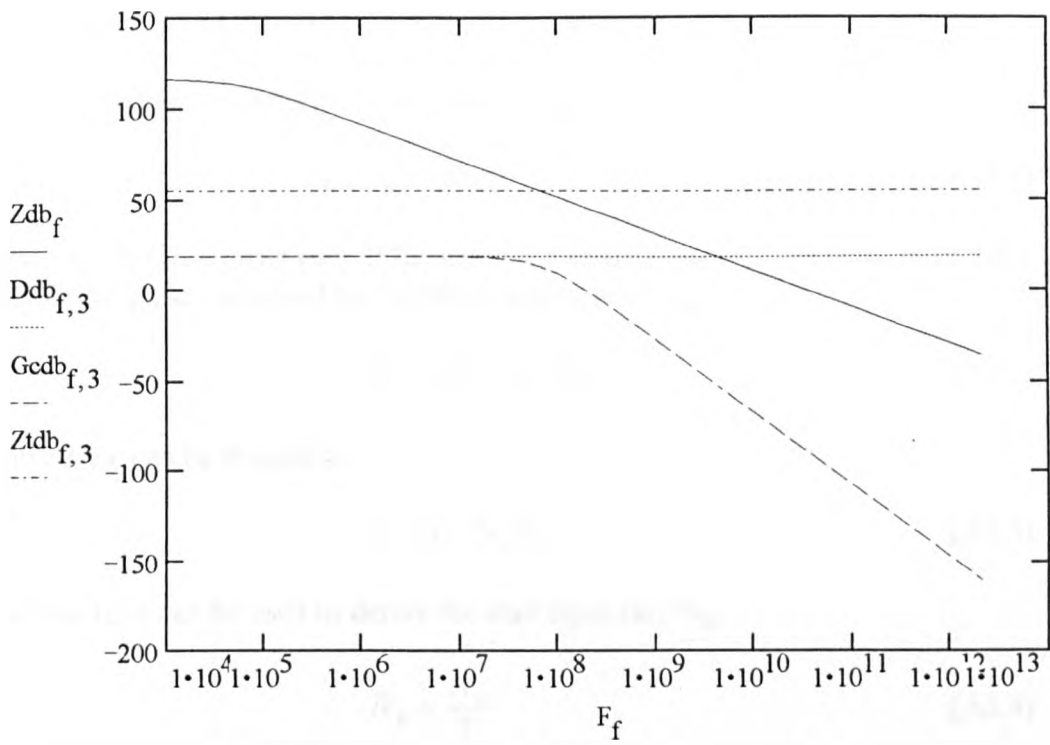
APPENDIX 3 : LIVE-TIME CORRECTION

The true number of pulses N_R in a time t is given by:

$$N_R = r \times t \tag{A3.1}$$

where r is the true mean rate. If the deadtime associated with one pulse is T_D then the number of pulses counted by the MCA is given by N_A.

$$N_A = r(t - N_A T_D) \tag{A3.2}$$

A live-time can be defined as :

$$T_L = t - N_A T_D \tag{A3.3}$$

The live-time can be used to derive the true input rate N_R.

$$N_R = \frac{N_A}{T_L} \tag{A3.4}$$

The live-time can be set by stopping the timing clock of the MCA for a time T_D associated with each analysed pulse.

If there is a tail pile-up, the MCA clock is simply stopped for the extra dead-time associated with the aborted pulse. If there is a rise-time pile-up causing two pulses to be rejected, the number of pulses counted by the MCA is given by N_P.

$$N_P = N_A(1 - P) \tag{A3.5}$$

where P is the probability of rise-time pile-up. To derive the true input rate a modified live-time T_P is needed such that:

$$N_R = \frac{N_P}{T_P} \tag{A3.6}$$

It can be seen that T_P is given by :

$$\begin{aligned} T_P &= T_L(1 - P) \\ T_P &= T_L - T_L P \end{aligned} \tag{A3.7}$$

The number of pulses rejected because of rise-time pile-up is given by :

$$N_A P = N_R T_L P \tag{A3.8}$$

If, for each of these occurrences, the MCA clock is stopped until the arrival of the next valid event, the total extra dead-time is given by :

$$N_R T_L P \times \frac{1}{N_R} = T_L P \qquad\qquad (A3.9)$$

where $\dfrac{1}{N_R}$ is the mean time interval between pulses.

The modified live-time is therefore given by :

$$T_P = T_L - T_L P \qquad\qquad (A3.10)$$

as required by the derivation above.

APPENDIX 4 : POLE-ZERO COMPENSATION CONTROL

If the charge-amplifier decay time-constant is given by $T_a = CR$, and suppose the basic time-constant in the compensating circuit to be $T_c = \dfrac{CR}{a}$, then the multiplication constant K needs to be $K = \dfrac{1}{a}$ such that

$$\frac{1 + \dfrac{sT_c}{K}}{\dfrac{sT_c}{K}} = \frac{1 + sT_m}{sT_m} \qquad (A4.1)$$

If the over-compensated situation is considered, in the worst case :

$$K = \frac{1}{a} + \Delta K \qquad (A4.2)$$

where ΔK is the minimum change in K allowed by the control. Figure A4.1 shows the pole-zero circuit output waveform.
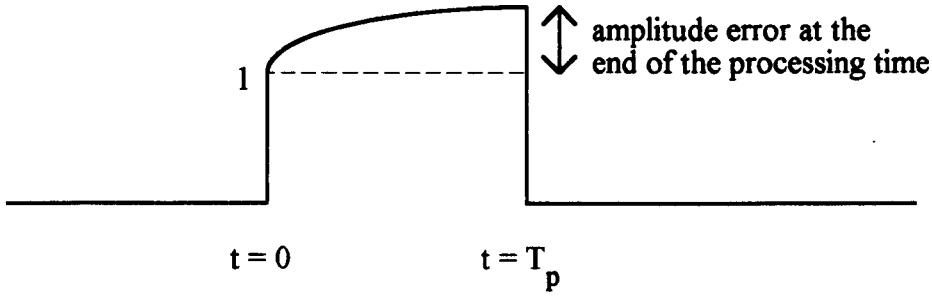
Fig A4.1

The inverse Laplace Transform gives an output waveform defined by :

$$V_o = 1 + \left(\frac{T_a - T_m}{T_m}\right)\left(1 - \exp\left(\frac{-t}{T_a}\right)\right) \qquad (A4.3)$$

The percentage error in amplitude is given by :

$$E = \left(\frac{T_a - T_m}{T_m}\right)\left(1 - \exp\left(\frac{-t}{T_a}\right)\right) \times 100\% \qquad (A4.4)$$

$$\text{but } T_m = \frac{\dfrac{CR}{a}}{\dfrac{1}{a} + \Delta K} = \frac{CR}{a} \times \frac{a}{(1 + a\Delta K)} \qquad (A4.5)$$

$$\text{therefore } E_{t=\infty} = \frac{CR - \dfrac{CR}{(1+a\Delta K)}}{\dfrac{CR}{(1+a\Delta K)}} \times 100\% = a\Delta K \times 100\% \qquad (A4.6)$$

$$\text{and } E_{t=T_p} \approx a\Delta K \left(1 - \exp\left(\frac{-T_p}{T_a}\right)\right) \times 100\% \qquad (A4.7)$$

If a 12bit, 5V DAC is used to generate K, and the control resolution on the front-panel is 1:128, then $\Delta K = 12 \times 10^{-3}$. Assuming $T_c = 60\mu s$ and $T_p = 32\mu s$, then:

if $T_a = 50\mu s$ then $a = 0.83$ and $E = 0.46\%$
if $T_a = 500\mu s$ then $a = 8.53$ and $E = 0.60\%$.

The amplitude error at the end of a long processing time is less than 1%.

APPENDIX 5 : CALCULATION OF COEFFICIENTS

In Section 5.4 the z-transform of a combined whitening/matched filter was given as:

$$H(z) = \sum_{r=0}^{2N-2} C_1(r)z^{-r} - \sum_{r=1}^{2N-1} C_0(r)z^{-r} \qquad \text{(A5.1)}$$

From the definitions of C_1 and C_0 given in Section5.4, the expression may be re-written as:

$$H(z) = \sum_{r=0}^{N-1}\sum_{q=0}^{r} A^r A^{-2q}z^{-r} + \sum_{r=N}^{(2N-2)}\sum_{q=0}^{(2N-2-r)} A^{2N-2-r}A^{-2q}z^{-r}$$
$$- \sum_{r=1}^{N-1}\sum_{q=0}^{r-1} A^{r-1}A^{-2q}z^{-r} - \sum_{r=N}^{(2N-1)}\sum_{q=0}^{(2N-1-r)} A^{2N-1-r}A^{-2q}z^{-r} \qquad \text{(A5.2)}$$

The first N coefficients are given by:

$$H(z) = 1 + \sum_{r=1}^{N-1}\left(\sum_{q=0}^{r} A^r A^{-2q} - \sum_{q=0}^{r-1} A^{r-1}A^{-2q}\right)z^{-r} \qquad \text{(A5.3)}$$

The sum of a geometric series $\sum_{k=0}^{N} x^k = \dfrac{1-x^{N+1}}{1-x}$ is used to simplify the equation:

$$H(z) = 1 + \sum_{r=1}^{N-1}\left[A^r\left(\frac{1-A^{-2(r+1)}}{1-A^{-2}}\right) - A^{r-1}\left(\frac{1-A^{-2r}}{1-A^{-2}}\right)\right]z^{-r}$$

$$H(z) = 1 + \sum_{r=1}^{N-1} \frac{A^r - A^{-r-2} - A^{r-1}+A^{-r-1}}{(1-A^{-1})(1+A^{-1})}z^{-r}$$

$$H(z) = 1 + \sum_{r=1}^{N-1} \frac{A^r + A^{-r-1}}{1+A^{-1}}z^{-r}$$

$$H(z) = \sum_{r=0}^{N-1} \frac{A^r + A^{-r-1}}{1+A^{-1}}z^{-r} \qquad \text{(A5.4)}$$

But $A = \exp(aT)$, therefore the positive coefficients can be defined by:

$$C_2(r) = \frac{\cosh\left(\left(r+\frac{1}{2}\right)aT\right)}{\cosh\left(\frac{aT}{2}\right)} \qquad \text{(A5.5)}$$

The last N coefficients are given by:

169

$$H(z) = \sum_{r=N}^{2N-2} \left(\sum_{q=0}^{(2N-2-r)} A^{(2N-2-r)} A^{-2q} - \sum_{q=0}^{(2N-1-r)} A^{(2N-1-r)} A^{-2q} \right) z^{-r} - z^{-(2N-1)} \quad (A5.6)$$

Developing the equation as shown above:

$$H(z) = \sum_{r=N}^{2N-2} \frac{A^{2N-2-r} - A^{-2N+r} - A^{2N-1-r} + A^{-2N-1+r}}{\left(1 - A^{-1}\right)\left(1 + A^{-1}\right)} z^{-r} - z^{-(2N-1)}$$

$$H(z) = \sum_{r=N}^{2N-2} \frac{\left(-A^{2N-1-r} - A^{-2N+r}\right)}{\left(1 + A^{-1}\right)} z^{-r} - z^{-(2N-1)} \quad (A5.7)$$

The next term in the geometric series(ie r = 2N-1) is $-z^{-(2N-1)}$, therefore:

$$H(z) = \sum_{r=N}^{2N-1} - 1 \times \frac{\left(A^{2N-1-r} + A^{-2N+r}\right)}{\left(1 + A^{-1}\right)} z^{-r} \quad (A5.8)$$

The negative coefficients are therefore given by:

$$C_2(r) = - 1 \times \frac{\cosh\left(\left(2N - \frac{1}{2} - r\right)aT\right)}{\cosh\left(\frac{aT}{2}\right)} \quad (A5.9)$$

APPENDIX 6 : FILTER GAIN AND MAXIMUM COEFFICIENT

define shaping time

$k := 0..2 \qquad T := 0.05$

$$a_k := \frac{1}{0.25 \cdot 4^k}$$

$$aT_k := a_k \cdot T$$

aT_k

0.2
0.05
0.0125

define filter length

$j := 0..2$

$$N_j := 16 \cdot 2^j$$

define filter gain

$$A_k := \exp\left(aT_k\right)$$

$$Gs_{k,j} := \frac{\left(A_k\right)^{N_j} - \left(A_k\right)^{-N_j}}{A_k - \left(A_k\right)^{-1}}$$

define maximum coefficient

$$C2_{k,j} := \frac{\left(A_k\right)^{(N_j - 0.5)} + \left(A_k\right)^{-(N_j - 0.5)}}{\left(A_k\right)^{0.5} + \left(A_k\right)^{-0.5}}$$

unscaled filter gain

$Gs_{k,0}$	$Gs_{k,1}$	$Gs_{k,2}$	
60.823	$1.495 \cdot 10^3$	$8.995 \cdot 10^5$	Ts = 0.25 microsec
17.755	47.492	244.816	Ts = 1 microsec
16.106	32.859	71.047	Ts = 4 microsec

16	32	64

unscaled coefficients

$C2_{k,0}$	$C2_{k,1}$	$C2_{k,2}$	
11.066	270.931	$1.631 \cdot 10^5$	Ts = 0.25 microsec
1.315	2.518	11.981	Ts = 1 microsec
1.019	1.079	1.332	Ts = 4 microsec
16	32	64	

scale coefficients such that Gs is 64

$$CS2_{k,j} = \frac{C2_{k,j}}{Gs_{k,j}} \cdot 64$$

$CS2_{k,0}$	$CS2_{k,1}$	$CS2_{k,2}$	
11.644	11.601	11.601	Ts = 0.25 microsec
4.741	3.393	3.132	Ts = 1 microsec
4.048	2.101	1.2	Ts = 4 microsec
16	32	64	

scale coefficients such that Gs is 8

$$CS2_{k,j} = \frac{C2_{k,j}}{Gs_{k,j}} \cdot 8$$

$CS2_{k,0}$	$CS2_{k,1}$	$CS2_{k,2}$	
1.456	1.45	1.45	Ts = 0.25 microsec
0.593	0.424	0.391	Ts = 1 microsec
0.506	0.263	0.15	Ts = 4 microsec
16	32	64	

Only coefficients < 1 can be represented by the 16bit input.
If Gs is set to 8, the ADC code has to be left-shifted by three bits.

APPENDIX 7 : OUTPUT OF DIGITAL TRIGGER CIRCUIT

define first input pulse

$i := 0..9$

$a_i := 0$

$i := 10..19$

$a_i := (i - 9) \cdot 25$

$i := 20..29$

$a_i := 250$

define second input pulse

$i := 0..14$

$b_i := 0$

$i := 15..24$

$b_i := (i - 14) \cdot 25$

$i := 25..29$

$b_i := 250$

define input

$i := 0..29$

$ab_i := a_i + b_i$

calculate output of first differentiator (with delay set to one clock period)

$j := 1..29$

$d1_j := ab_j - ab_{j-1}$

calculate output of second differentiator (with delay set to one clock period)

$k := 2..29$

$d2_k := d1_k - d1_{k-1}$

calculate output of first differentiator (with delay set to five clock periods)

$l := 5..29$

$del_l := ab_l - ab_{l-5}$

calculate output of second differentiator (with delay set to five clock periods)

$m := 10..29$

$de2_m := del_m - del_{m-5}$